The Dissertation Committee for Carla Maria Sanchez Certifies that this is the approved version of the following dissertation:

Controls on Sedimentary Processes and 3D Stratigraphic Architecture of a Mid-Miocene to Recent, Mixed Carbonate-Siliciclastic Continental Margin: Northwest Shelf of Australia

Committee:

Ronald Steel, Supervisor

Craig Fulthorpe, Co-Supervisor

James Austin, Jr.

Charles Kerans

David Mohrig

Xavier Janson

Controls on Sedimentary Processes and 3D Stratigraphic Architecture of a Mid-Miocene to Recent, Mixed Carbonate-Siliciclastic Continental Margin: Northwest Shelf of Australia

by

Carla Maria Sanchez, B.E., M.Sc.

Dissertation

Presented to the Faculty of the Graduate School of

The University of Texas at Austin

in Partial Fulfillment

of the Requirements

for the Degree of

Doctor of Philosophy

The University of Texas at Austin

May 2011

Dedication

To my parents, Morelia and Carlos, and Ryan for their love and support.

Acknowledgements

During my time as a Ph.D. student at UT I received support in a variety of ways, here I want to express my sincere gratitude to all people and institutions that provided such support. First, I would like to acknowledge the guidance, time, and dedication provided by Dr. Craig Fulthorpe, Dr. Ronald Steel, and Dr. James A. Austin, Jr. during my time as a Ph.D. student. Since I arrived to Austin to start my graduate education, Dr. William Fisher has offered advice and friendship that, without a doubt, helped me go through the journey of a Master and, later on, a Doctorate. I am also grateful to the rest of my committee: Dr. Charles Kerans, Dr. David Mohrig, and Dr. Xavier Janson for very helpful ideas and constructive criticism of my research.

Special thanks to the Jackson School of Geosciences, the UT Institute for Geophysics, the National Science Foundation, ConocoPhillips SPIRIT Scholars Program, and the AAPG Grants-in-Aid for financial support provided for my Ph.D. The project documented here would not exist without the data contributions from Woodside Petroleum, Geoscience Australia, and OCCAM Technology and the computing resources from the UT Institute for Geophysics and Bureau of Economic Geology. Dallas Dunlap, Reuben Reyes, Mark Wiederspahn, and Steffen Saustrup provide invaluable technical support. Lorena Moscardelli and Xavier Janson generously allowed me to use their workstations for interpretation of the 3D data used in this project.

I want to thank my parents for the personal education they have lovingly given me, especially for the motivation to move forward. And to Ryan: you have been the most important source of love, support, and motivation for me during these four years.

Controls on Sedimentary Processes and 3D Stratigraphic Architecture of a Mid-Miocene to Recent, Mixed Carbonate-Siliciclastic Continental Margin: Northwest Shelf of Australia

Publication No._____

Carla Maria Sanchez Ph.D.

The University of Texas at Austin, 2011

Supervisors: Ronald Steel and Craig Fulthorpe

Determining the relative importance of processes that control the generation and preservation of continental margin stratigraphy is fundamental to deciphering the history of geologic, climatic and oceanographic forcing imprinted on their sedimentary record. The Northern Carnarvon Basin (NCB) of the North West Shelf of Australia has been a site of passive margin sedimentation throughout the Neogene. Cool-water carbonate sedimentation dominated during the early-middle Miocene, quartz-rich siliciclastics prograded over the shelf during the late-middle Miocene, and carbonate sedimentation resumed in the Pliocene. Middle Miocene to Pliocene siliciclastics were deposited as clinoform sets interpreted as delta lobes primarily based on their plan-view morphology and their relief of 40-100 m. Shelf-edge trajectory analysis suggests that part of this stratigraphic succession was built during a long-term, third order, regressive phase, producing shelf-edge deltas, followed by an aggradational episode. These trends appear to correlate with third-order global eustatic cycles. Slope incisions were already

conspicuous on the slope before deltas reached the shelf-break. Nevertheless, slope gullies immediately downdip from the shelf-edge deltas are wider and deeper (>1 km wide, ~100 m deep) than coeval incisions that are laterally displaced from the deltaic depocenter (~0.7 km wide, ~25 m deep). This change in gully morphology is likely the result of greater erosion by sediment gravity flows sourced from shelf-edge deltas. Total late-middle to late Miocene margin progradation increased almost three times from 13 km in the southwest to 34 km in the northeast, where shelf-edge deltas were concentrated.

Flat-topped carbonate platforms seem to have initiated on subtle antecedent topographic highs resulting from these deltaic lobes. A reduction of siliciclastic supply to the outer paleo-shelf during the Pliocene combined with the onset of a southwestward-flowing, warm-water Leeuwin Current (LC) most likely controlled the initiation of these carbonate platforms. These platforms display marked asymmetry, likely caused by an ancestral LC, which created higher-angle, upcurrent platform margins, and lower-angle, downcurrent clinoforms. The along-strike long-term migration trend of the platforms could be the result of differential subsidence. These platforms constitute the first widespread accumulation of photozoan carbonates in the Northern Carnarvon Basin. They became extinct after the mid-Pleistocene when the LC weakened or became more seasonal.

Table of Contents

List of Figures

Chapter 1: Introduction and Dissertation Overview

1.1. INTRODUCTION

Deciphering what processes, global versus regional or local, control the stratigraphic record of continental margins has been a matter of debate among geologists for decades. A number of studies have claimed that the stratigraphic architecture of continental margins represents a record of the interplay among three main processes: (1) eustasy, (2) tectonism, and (3) climatic fluctuations (Vail et al., 1977; Kendall and Schlager, 1981; Haq et al., 1987; Vail, 1987; Bartek et al., 1991; Schlager, 1991; Vail et al., 1991; Abreu and Anderson, 1998). Some have claimed that eustatic variations constitute the dominant control on stratigraphy, in particular that of Icehouse/Neogene passive margins (Abreu and Anderson, 1998; Haq et al., 1987; Kendall and Schlager, 1981; Miller et al., 1991; Vail, 1987; Vail et al., 1991; Vail et al., 1977).

Other studies have proposed that regional/local processes such as ocean currents can also cause environmental stresses affecting sequence development, for example through changes in carbonate sediment productivity (Isern et al., 2004; Schlager, 1991), which in turn result in profound effects on stratigraphy. For instance, Schlager (1991) has argued that changes in temperature, salinity, and nutrient concentrations, caused by oceanographic variations, are possible factors controlling sequence development on carbonate-prone continental margins. Isern et al. (2004) have illustrated how ocean currents can control platform morphology (Schlager, 1991), the growth potential of

carbonate platforms, and the final location of sediment produced in platform tops in the Marion Plateau of Northeast Australia.

Existing sequence stratigraphic models predict sequence development and architecture as the result of the interplay between changes in accommodation, caused by the combined effect of eustasy, tectonism, and sediment supply in depositional dip-oriented cross-sections (Martinsen and Helland-Hansen, 1995). A significant limitation of the classic sequence stratigraphy approach is that clastic depositional systems (e.g., lobate delta systems) can be highly variable along-strike. The spatial variability of depositional systems, and therefore of sediment supply, can result in coeval but opposing stacking patterns on different dip-oriented cross-sections (Martinsen and Helland-Hansen, 1995; Church and Gawthorpe, 1997). This variation of stacking patterns within contemporaneous stratigraphic units represents a major limitation for system tract interpretation as defined by Van Wagoner et al. (1988), in particular if changes in accommodation are to be inferred from stacking patterns. Along-strike variability of larger-scale, shelf-edge trajectories have also been suggested by Henriksen et al. (2009) but have not been yet documented. I document in this dissertation this kind of along-strike variability using both dip-oriented seismic profiles and detailed mapping of deltaic depocenters.

This dissertation is an effort to address the larger scale, along-strike variability of stratigraphic sequences using a large 3D seismic volume combined with a dense 2D seismic grid that allows for detailed mapping of key stratigraphic surfaces, identification of depositional systems through the application of seismic geomorphology, and selection of several dip-oriented cross-sections that allow the comparison of opposing but coeval stratigraphic architectures. The results I include in this study highlight the importance of spatial variations of siliciclastic sediment supply for along-strike margin growth and its

resulting architecture. Existing stratigraphic methods should be preferably used on a regional scale if interpretations of changes in accommodation and/or sediment supply are to be made.

1.2. PREVIOUS WORK

The along-strike variation of contemporaneous stacking patterns has been previously documented as the result of variable sediment supply on a few basins. For instance, different dip-oriented cross-sections intersecting the Mississippi delta lobes developed since the Last Glacial Maximum show the lateral change from a retrogradational lobe-staking pattern (apparent transgression, but in fact part of the highstand) to a progradational pattern in another cross-section located to the east (Martinsen and Helland-Hansen, 1995). A similar lateral variation of coeval stacking patterns observed in outcrops has been documented in the Carboniferous of northern England (Church & Gawthorpe, 1997) and of forced-regressive stratigraphic architecture of the Quaternary in Greece (McMurray and Gawthorpe, 2000).

Some delta systems seem to be more spatially variable than others; the degree of variability depends on several factors, such as the competition between the energy of the fluvial feeder and marine processes acting on the receiving basin (Martinsen and Helland-Hansen, 1995). For instance, fluvial-dominated deltas tend to show more lateral shifting than wave-dominated deltas. The resulting spatial variations in sediment supply at any given time will result in different stratal architectures from one area to another, which complicates the interpretation of stratigraphic successions. Martinsen and Helland-Hansen (1995) also proposed that the variation of sediment supply along a coast can

result in coeval but opposing types of depositional systems, and therefore contrasting stacking patterns. They referred in particular to the Gironde Estuary in the Bay of Biscay, which is constructing a highstand delta, whereas to the south the coast is sediment starved and undergoing erosion that is resulting in a transgressive succession.

An additional along-strike change observed in sequences that has been attributed to spatial changes in sediment supply is thickness change. Examples of such lateral thickness changes in Miocene sequences on the New Jersey shelf have been documented using high-resolution, dense seismic data by Fulthorpe and Austin (2008) and Monteverde et al. (2009).

The term clinoform is commonly used to describe the topset-foreset-bottomset depositional profile (Rich, 1951; Steel and Olsen, 2002) and can be observed at multiple scales (Figure 1.1). The shelf-slope-basin profile corresponds to a clinoform profile that is hundreds to thousands of meters high (Steel et al., 2008; Helland-Hansen and Hampson, 2009). Successive positions of the shelf-edge (also called the shelf-slope break, rollover, offlap break, or shelf-margin) through time form a path that has been referred as the shelf-edge trajectory (Steel and Olsen, 2002; Figure 1.1). Typically, these shelf margin clinoforms accrete at rates of 1-10's km/my (the approximate scale for this trajectory analysis) in response to changing rates of relative sea level and sediment supply (Steel and Olsen, 2002; Helland-Hansen and Hampson, 2009).

Carvajal et al. (2009) reviewed and compared shelf-margin aggradation and progradation rates from different margins that have grown mainly by sediment supplied by shelf-edge deltas; they concluded that these deltas are the most efficient system for delivering sediment into the deep water and drive shelf-margin progradation. Other processes, such as contour currents, are less effective and therefore produce lower margin progradation rates. Areas with high sediment supply exhibit a wider shelf topset than

margins with lower sediment supply (Carvajal et al., 2009); for this reason, shelf-edge deltas create protuberances in the shelf edge in plan view (Suter and Berryhill, 1985; Olariu and Steel, 2009).

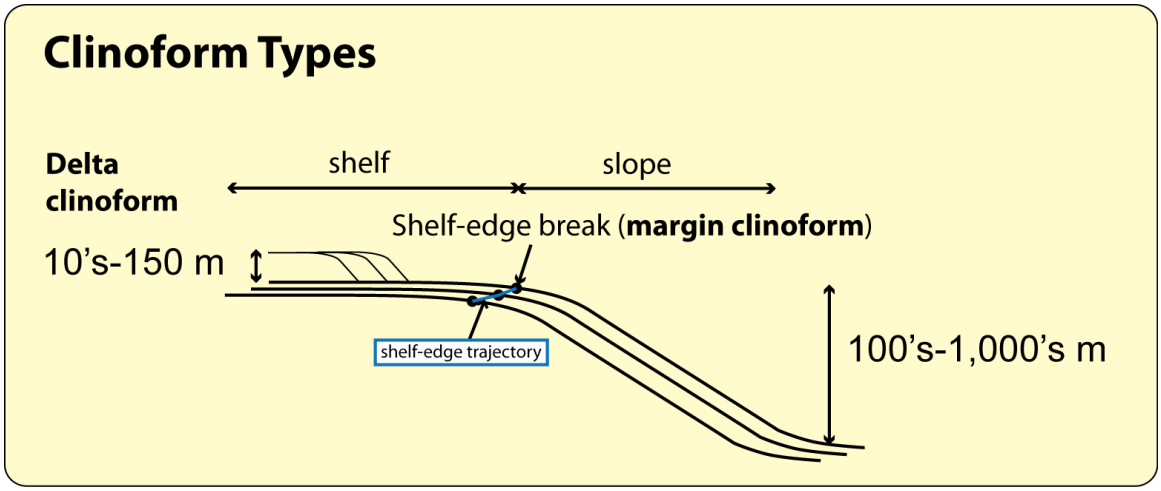

Figure 1.1: Delta vs. shelf-margin clinoforms and the shelf-edge trajectory. Based on Steel and Olsen (2002) and Helland-Hansen and Hampson (2009).

High-resolution seismic data has been previously used to map late Quaternary shelf-margin deltas on the Gulf of Mexico (Suter and Berryhill, 1985; Sydow et al., 1992). These studies have imaged these deltaic wedges as clinoform sets in dip-oriented seismic profiles; they also show the complex, multilobate character of these shelf-edge deltas that seems to be a result of delta shifting and relative sea level fluctuations.

1.4. DATA AND GENERAL METHODOLOGY

This study was based on seismic stratigraphic interpretation of 3D and 2D seismic reflection data, integrated with wireline log data and well completion reports. Seismic data were collected for various oil exploration projects on the NCB (Figures 1.2 and 1.3) and made available to the Institute for Geophysics by Woodside and Geoscience Australia. The total area covered by 2-D seismic data (total of 55,700 line-km) is approximately 31,000 square-kilometers (km^2). The area covered by 3-D seismic data is ~7,500 km^2.

Central frequencies of seismic data for the interval containing the siliciclastics of the Bare Formation are 32-44 Hz, which result in a theoretical vertical resolution of 12-15 m (Sheriff, 1985) using an average velocity of 2,000 m/s (from sonic logs). On the other hand, the central frequency for the seismic interval that contains interpreted Plio-Pleistocene tropical carbonates is ~55 Hz, which results in a theoretical vertical resolution of ~18m, assuming an average velocity of 4,000 m/s for carbonate lithology (Schlager, 2005).

The database also includes wireline-log suites and completion reports from five exploration wells distributed across the NCB. These well wireline logs and reports have been donated to the Institute for Geophysics by OCCAM Technology and Geoscience Australia. The wireline suites include the following logs: gamma ray, sonic, and density. The well completion reports include lithology (Figure 1.4), age tops, and checkshot surveys for the Pliocene and older section. These reports allowed seismic facies to lithology correlation for the middle-Miocene to Pliocene interval containing interpreted deltas, but did not provide any lithology control for the shallower section that includes interpreted tropical carbonate accumulations.

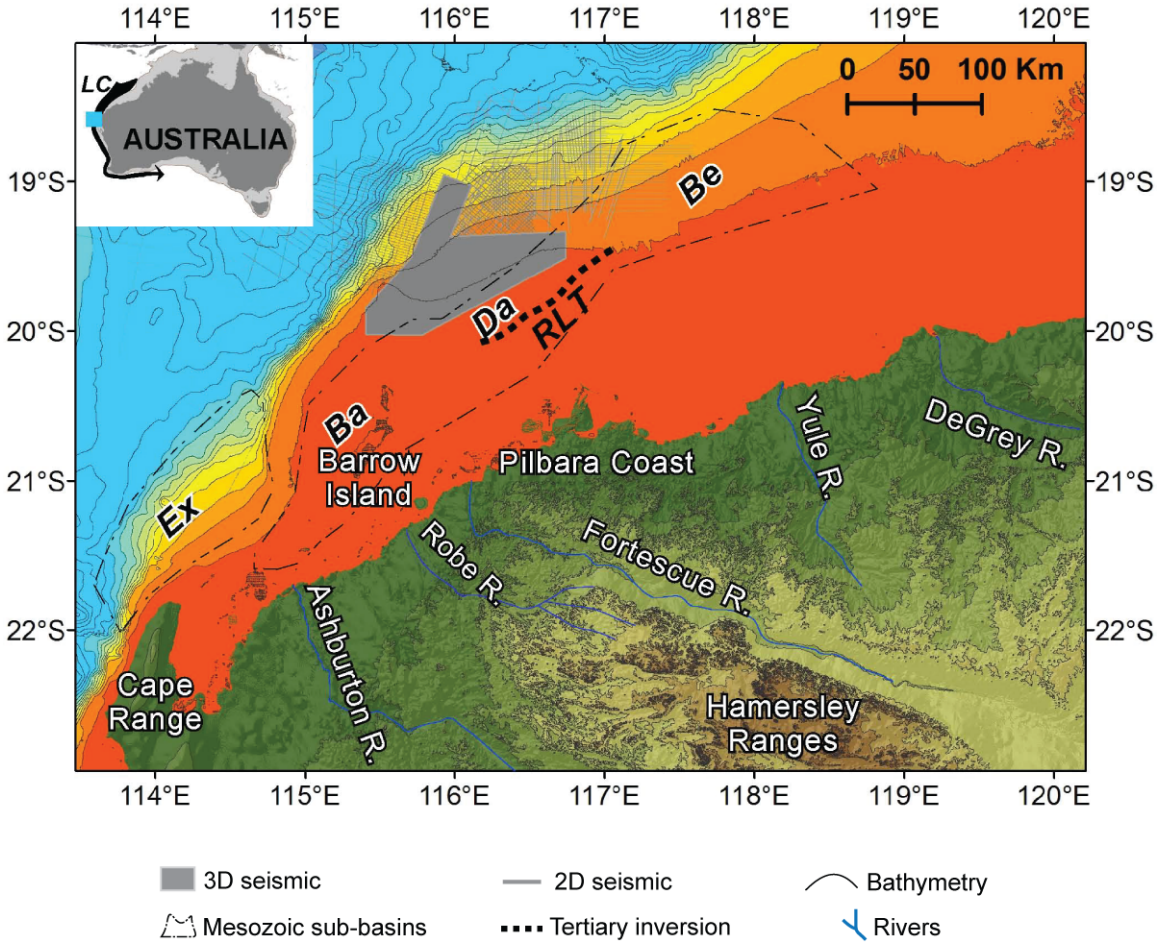

Figure 1.2: Available seismic data, Mesozoic sub-basins of the Northern Carnarvon Basin (Ex=Exmouth, Ba=Barrow, Da=Dampier, Be=Beagle; Stagg and Colwell, 1994; Cathro et al., 2003), and modern rivers draining the Hamersley Ranges (Semeniuk, 1996). Bathymetric contours are at 100 m intervals. Inset map shows a box with the location of the study area respect to the Australian continent and the Leeuwin Current (LC), which flows along the Western Australia shelf edge (Tomczac and Godfrey, 1994).

The large area covered by 3D and dense 2D seismic data allowed detailed mapping of seismic unconformities such as sequence boundaries (Figure 1.4), and delta lobe and carbonate platform top boundaries. Other seismic horizons were mapped within

the defined sequences within the seismic volume in order to generate attribute (seismic amplitude and spectral decomposition) maps, allowing recognition of depositional systems such as channels. Seismic facies were identified and correlated to lithology from well completion reports. The detailed methodology is described in chapters 2-4.

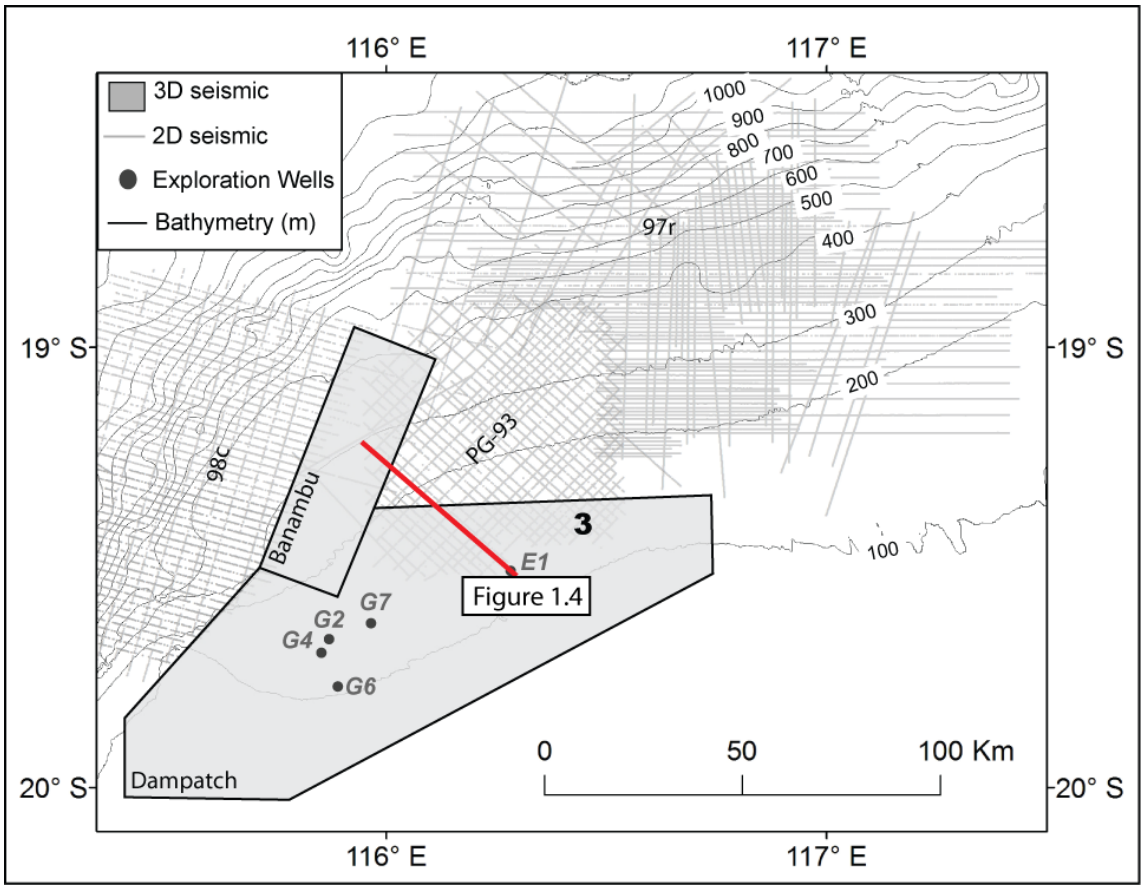

Figure 1.3: 3D and 2D seismic data used in this study. Exploration wells (G2=Goodwyn_2, G4=Goodwyn_4, G6=Goodwyn_6, and G7=Goodwyn_7, E1=Eaglehawk_1) were used to obtain age estimates and for seismic facies correlation to lithostratigraphy.

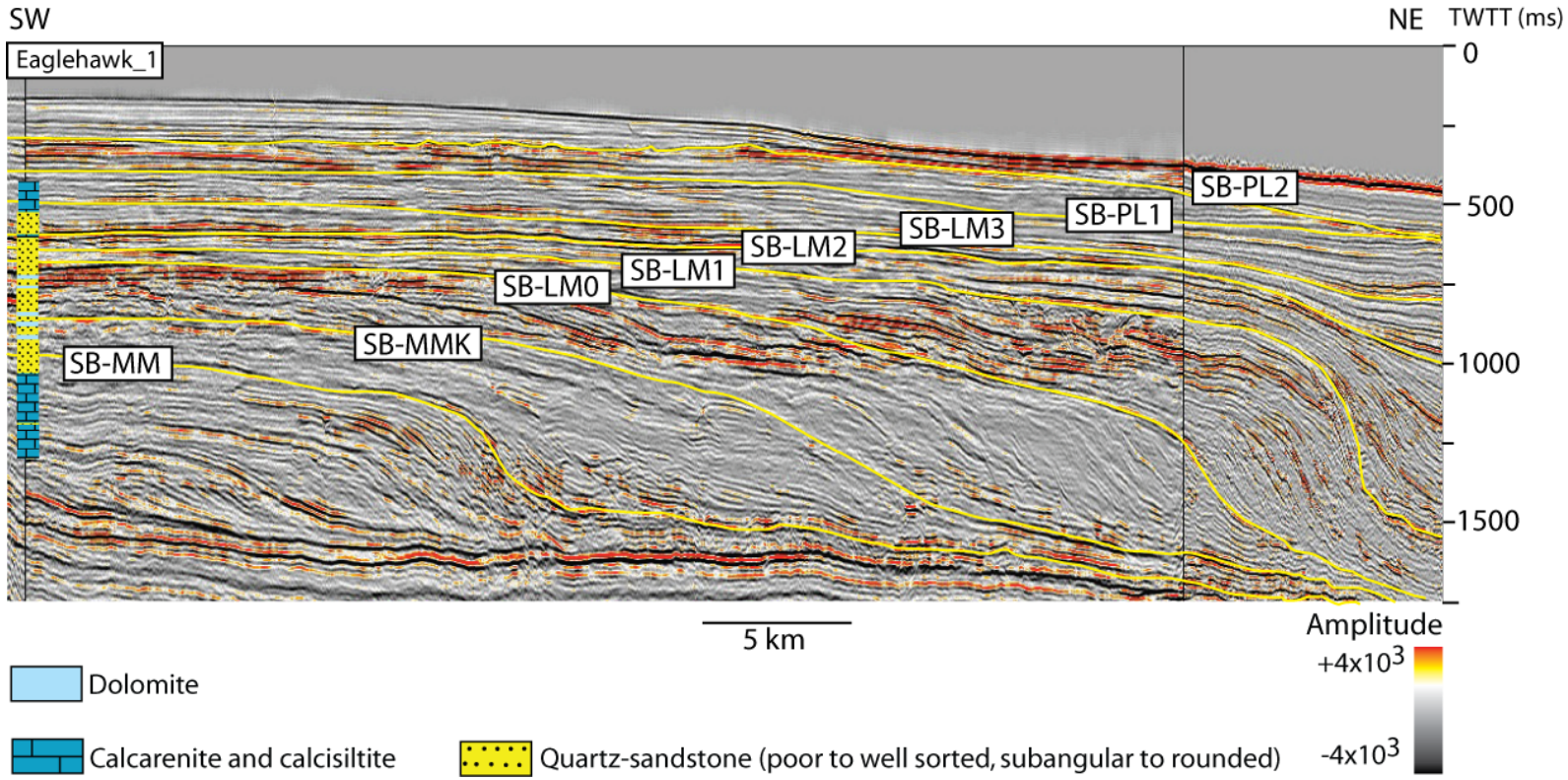

Figure 1.4: Dip-oriented seismic profile showing correlation between seismic facies and lithology. Well-completion report from industry well Eaglehawk_1 and Moss et al. (2004) confirm the presence of quartz sandstones in this high-amplitude seismic package, characterized by oblique and mounded reflection geometries. See Figure 1.3 for location.

1.5. SIGNIFICANCE

This study will contribute to the still limited understanding of the influence of relative sea level on the stratigraphic record of continental margins relative to sediment supply, in particular for those margins with mixed carbonate-siliciclastic systems. This study will also provide insights concerning the variability and complexity of 3-D sequence development on a passive continental margin through the investigation of stratigraphic architecture. Documenting this spatial complexity is relevant to understanding the relationship between the stratigraphic record of continental margins and global processes (e.g. sea level and climatic fluctuations) and highlights the need for 3-D seismic data to conduct investigations of this kind. In addition, the results presented here highlight the impact of lobate shelf-edge deltaic systems on a passive margin's long-term growth. Results from this work will ultimately be used to select drill site locations in support of an existing, highly ranked IODP (Integrated Ocean Drilling Program) proposal (Proposal 667-Full; Fulthorpe et al.) designed to contribute to global sea level studies.

Significant lateral variability of lithology, a result of the spatial variability of depositional systems (siliciclastics and carbonates), seems to cause complex lateral acoustic velocity changes in the Tertiary section of the NCB. This complex velocity structure affects seismic imaging of Mesozoic and Paleogene hydrocarbon reservoirs. Therefore, a better understanding of the mid-Miocene to Recent NCB stratigraphy should allow reprocessing seismic data in that area for a better imaging and interpretation of the prospective/producing interval.

Finally, the hydrocarbon reservoir potential of the middle-Miocene and younger succession of the NCB is poorly known. This study shows a direct link between sands

sourced from late-middle Miocene and Pliocene deltas and the deep-water slope and basin. Therefore, this study opens new possible prospective intervals for hydrocarbon accumulations on the NCB if migration pathways from older source rocks to these deep-water sands can be identified.

1.6. OBJECTIVES

This dissertation intends to contribute to a better understanding of the influence of local/regional factors, such as the 3D variability of depositional systems, and therefore of sediment supply, on the stratigraphic architecture of a passive margin. I used detailed seismic mapping to assess the spatial and temporal variability of depositional systems and how that variability can impact the stratigraphic architecture of the shelf margin.

This study addresses two main questions: 1) what processes can significantly influence the 3D stratigraphic architecture of a mixed carbonate-siliciclastic passive margin; and 2) how much variability can be observed along-strike as the result of local sedimentary processes?

The Neogene NCB of the NWS provides an excellent study area to address these questions because of the extensive, high-quality 3D seismic coverage that allows detailed mapping of stratigraphic surfaces, selection of several dip- or strike-oriented cross sections, and the application of seismic geomorphology that provides map view images of depositional systems within interpreted sequences.

1.7. ORGANIZATION OF CHAPTERS

The main results of this dissertation are condensed in three chapters (Chapters 2-4). Each one of these three main chapters has been written with the objective to be submitted for publication. A summary of the content of each of these follows:

- Chapter 2: This chapter presents results of the detailed seismic mapping of the interval containing the sandstones of the Bare Formation. The main results are:
  - Mapping of 40-100 m clinoform sets revealed strike- and dip-elongated features on the shelf that I interpret as delta lobes based on their plan-view morphology, clinoform dimensions and their correlation with sandstones.
  - These deltas prograded across a preexisting carbonate shelf as the result of climatic change or deterioration that seems to have caused a global pulse of clastic sediment supply and relative sea level that helped this delta system reach the shelf edge.
  - These delta lobes seem to migrate greater distances along strike during relative sea-level rises than during interpreted falls. These features also exhibit long-term northeastward migration, likely as a result of localized uplift in the south portion of the study area. An inversion anticline probably steered the fluvial feeder for this delta system through time as it grew during continued collision of Australia and the Banda Arc that started in the late Miocene.

- Chapter 3: The main topics discussed in this section are:

- Deltas can be a major contributor to shelf margin growth. I quantified the along-strike increase in margin progradation from areas where deltas were absent to the region where these shelf-margin deltas were concentrated.
- Along-strike variability of depositional systems near the shelf edge cause dramatic changes in the shelf-edge trajectory. These results confirm that shelf-edge trajectory results from the complex interaction of relative sea-level change and sediment supply, and that because the latter can be highly variable in space, opposing but contemporaneous trajectory patterns can develop under the same accommodation change regime.
- Shelf-edge deltas can deliver sediment to the deep-water slope and beyond effectively using preexisting slope incisions. My results show morphologic and stratigraphic evidence that these incisions, which already existed along the slope probably as a result of slope oversteepening, served as conduits for sediment gravity flows sourced from the deltas that were near or at the shelf edge.
- Miocene-Pliocene deltas mapped for this study reached the shelf edge influencing margin growth in a localized manner by creating a high sediment supply fairway that was basically absent along strike (away from the delta system). Since shelf-edge trajectory is dependent on changes of accommodation and sediment supply, areas that have very low sediment supply can not fully record the history of accommodation changes

- Chapter 4:
  - This chapter focuses on the controls on initiation, distribution, and termination of broad, tropical carbonate platforms on the shelf of the

NCB, which is otherwise dominated by heterozoan carbonates during the Neogene (with the exception of the late-middle Miocene to Pliocene when siliciclastics prograded across the shelf as discussed in Chapters 2 and 3).

- Carbonate sedimentation resumed after the deltas that delivered siliciclastics to the outer shelf of the NCB retreated in the Pliocene (the end of the clastic pulse in this region of the NWS). Therefore a combination of transgression and decrease in siliciclastic supply (probably due to increasing aridity in the western Australian area) allowed carbonate production to resume.
- My results suggest that the mid-Miocene to Pliocene outer-shelf and shelf-edge deltas (Chapters 2 and 3) created subtle topographic highs that favored the development of these extensive platforms controlling their distribution. However, along-strike pulses of migration of these tropical carbonate systems suggest that differential subsidence along-strike also influenced the location of these platforms.
- My results in Chapter 4 show the along-strike shifting of tropical carbonate platforms, which could also be a source of variability of margin stratigraphic architecture on different dip-oriented cross-sections. These platforms had not been previously identified in the NCB. Interpretation of the high-quality, extensive seismic data available for my dissertation has allowed me to identify the first occurrence of such broad tropical carbonate platforms. The modern Rowley Shoals, which are isolated platforms in the NWS that have been studied using high-resolution boomer data, show a decreasing amount of lagoon infill from southwest to northeast (general along-strike direction for the NWS) that has been

interpreted to be the result of increasing rates of tectonic subsidence in the same direction under the effect of the collision between the Banda Arc and Australia (Collins, 2002). In the case of the Plio-Pleistocene NCB platforms, now extinct, either differential rates of tectonic subsidence along depositional strike, or differential compaction of the underlying clastic depocenters, have caused the general northeast to southwest migration of the platforms.

Chapter 2: Mid-Miocene Siliciclastic Sediment Influx Across a Carbonate Shelf and Influence of Delta Type on Shelf Construction, Northern Carnarvon Basin, Northwest Shelf of Australia

2.1. INTRODUCTION

Understanding the occurrence and progradation history of late-middle Miocene siliciclastics across the preexisting Miocene carbonate shelf of the Northern Carnarvon Basin (NCB), Northwest Shelf of Australia (NWS), is key to deciphering the Neogene stratigraphic architecture of this margin (Figure 2.1A). The Neogene siliciclastic sediments have been identified previously as the Bare Formation in at least 13 industry wells and on reflection seismic data (Cathro et al., 2003; Wallace et al., 2003). Based on well data and observations of progradational style and a partially mounded geometry along a single strike-oriented regional 2D seismic profile, Cathro et al. (2003) have interpreted this quartz-sandstone rich succession as a shelf-restricted, clastic wedge that was reworked by a shelf-parallel, northeastward-flowing ocean current. This current has been proposed to be the cause for the interpreted along-strike progradation of the clastic wedge (Cathro 2002, Cathro et al., 2003).

The late-middle Miocene influx of siliciclastic sediment to the NCB raises three main questions of broad importance:

1. What is the architecture of this siliciclastic unit?

2. What are sedimentary processes controlling the occurrence of this siliciclastic interval in an otherwise carbonate-dominated setting?

3. What is the mechanism causing increased clastic sediment flux into the NCB during the middle and late Miocene and why are these sediment volumes so effectively spread across the shelf and to the shelf edge?

Analysis of 3D and dense 2D seismic data suggests that the Upper-Middle Miocene to Pliocene siliciclastic strata of the NCB formed from multiple phases of Neogene deltaic progradation across the preexisting carbonate shelf. The mapped deltas achieved a maximum progradation distance of 77 km, and many reached the shelf-edge, likely in response to both relative sea-level fall and climatic forcing during the late-middle Miocene (Haq et al., 1987; Zachos et al, 2001; Molnar, 2004). The long-lived and repeated sand delivery to the shelf edge by delta systems was likely also the source for redeposited deep-water sands in the NCB. The 2D/3D seismic data provided an exceptional opportunity to reconstruct the distribution of delta lobes as the system prograded to the shelf edge and later retreated landwards. The NCB was largely an undisturbed passive margin during the Neogene, only a few localized inversion structures have been proposed for this area (Cathro and Karner, 2006), so tectonic disturbances on subsidence could be excluded from the seismic stratigraphic analysis.

This study of deltas deposited on the outer shelf and shelf edge, in common with areas like the Cretaceous West Siberia Basin (Pinous et al., 2001), should help provide analog models for shelf-edge hydrocarbon plays. In addition, the coexistence of siliciclastic (delta and shoreface) and carbonate (shelf) depositional systems have a significant impact on acoustic velocity models in this kind of mixed carbonate-siliciclastic margin. This variability should be accounted for when building velocity models for data processing to image hydrocarbon plays in the underlying, prospective Cretaceous-Paleogene section of the NCB.

2.2. GEOLOGIC SETTING: NORTHERN CARNARVON BASIN, NORTHWEST SHELF, AUSTRALIA

2.2.1. Tectonic History

The NCB, which is composed of the Exmouth, Barrow, Dampier and Beagle sub-basins (Figure 2.1A), has been formed and reactivated as the result of three phases of rifting that affected the NWS. The oldest rifting phase was in the Late Permian (Baillie et al., 1994; Bradshaw et al., 1988) and the most recent rifting occurred in the Late Jurassic (Baillie et al., 1994; Bradshaw et al., 1988; Veevers et al., 1991). The dominant tectonic control since the Early Cretaceous in the NCB has been subsidence during thermal-cooling (Veevers et al., 1991; Baillie et al., 1994; Driscoll and Karner, 1998; Cathro and Karner, 2006). Several studies have suggested an interruption of such thermal subsidence in the NWS because of collision between the Banda Arc and Australia beginning in the late Miocene (Veevers et al., 1991; Baillie et al., 1994; Lee and Lawver, 1995; Driscoll and Karner, 1998; Hull and Griffiths, 2002; Pryer et al., 2002; Cathro and Karner, 2006). However, the impact of this collision on the NCB has been limited to localized uplift (up to 75 m) at the northwest end of the Rosemary-Legendre structural trend during the Miocene, inferred from seismic stratigraphy integrated with kinematic and flexural modeling in the Dampier sub-basin (Figure 2.1A; Cathro and Karner, 2006).

2.2.2. Stratigraphy

A change in the dominant sediment type in the NCB from siliciclastics in the Mesozoic to largely carbonates in the Cenozoic (Apthorpe, 1988; Romine et al., 1997)

has been interpreted as the result of the northward drift of the Australian Plate that initiated in the Mesozoic (Baillie et al., 1994; Bradshaw et al., 1988). The Eocene to Recent strata in the NCB forms an impressive progradational succession of shelf-margin scale clinoforms (heights up to 900 m) recognizable in seismic data (Romine et al., 1997; Cathro et al., 2003). Oligocene to mid-Miocene clinoforms within this northwesterly prograding interval are dominated by heterozoan carbonate sediments (Cathro et al., 2003).

Previous well-data studies have divided the middle-upper Miocene stratigraphy of the NCB into (1) middle Miocene carbonates, the Trealla Limestone (Figure 2.2, Hocking et al., 1987), that are predominantly skeletal packstones to grainstones which transition offshore into pelagic marls and (2) late-middle to late Miocene-age Bare Formation (Apthorpe, 1988; Figure 2.2), consisting of well-sorted, medium-grained mature quartz sandstones interbedded with fine-grained calcarenites and dolomites that include scattered traces of quartz grains throughout (Heath and Apthorpe, 1984). Heath and Apthorpe (1984) have interpreted the Bare Formation as coastal, based on the: 1) near absence of fauna, 2) presence of interbedded dolomites, and 3) occurrence of mature, quartz-rich sandstones. Wallace et al. (2003) have documented the presence of evaporite cements at the base of these sandstones, in addition to the occurrence of interbedded dolomites, which further support the interpretation of nearshore depositional environment for the Bare Formation.

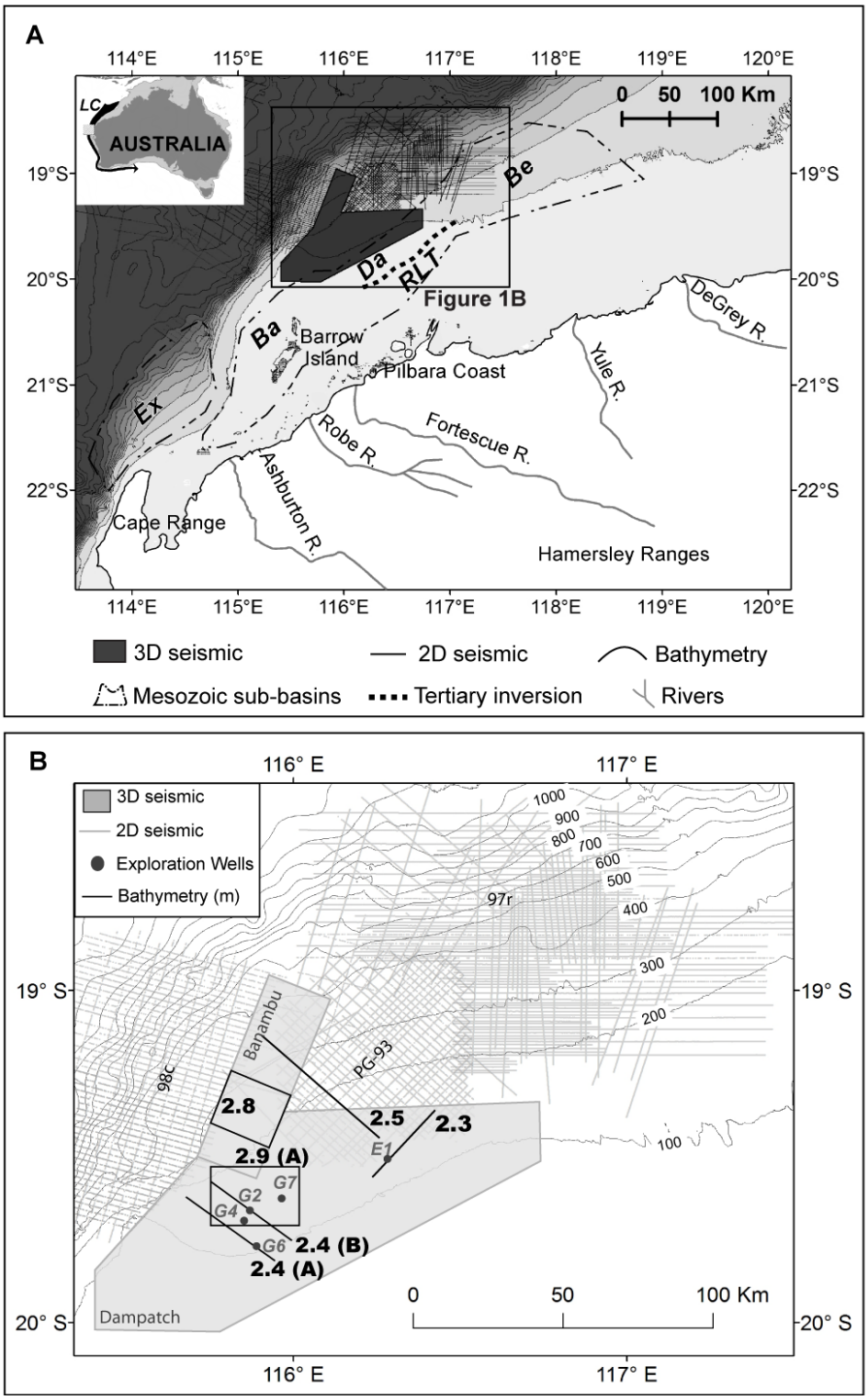

Figure 2.1: (A) Map showing location of study area, available seismic data, Mesozoic

sub-basins of the NCB (Ex=Exmouth, Ba=Barrow, Da=Dampier, Be=Beagle; Stagg and Colwell, 1994; Romine et al., 1997; Cathro et al., 2003), and modern rivers draining the Hamersley Ranges (Semeniuk, 1996). Bathymetric contours are at 100 m intervals. Inset map shows a box with the location of the study area respect with the Australian continent and the Leeuwin Current (LC), which flows along the western Australia shelf edge (Tomczac and Godfrey, 1994). (B) Area covered by 3D and 2D seismic data used in this study. Industry wells specifically referenced in this study: G2=Goodwyn_2; G4=Goodwyn_4; G6=Goodwyn_6; G7=Goodwyn_7; E1=Eaglehawk_1; L1=Lacerta_1; B1=Brigadier_1.

Modern sedimentation in the NCB is influenced by the arid climate of northwest Australia, resulting in a low terrigenous input to the shelf (Semeniuk, 1996). On the modern Pilbara coast (Figure 2.1A), siliciclastics are deposited mainly along barrier islands, whereas carbonates and evaporites occur in tidal flats and as foreshore skeletal calcarenite sheets (Semeniuk, 1996). Farthest offshore, modern shelf sedimentation is dominated by skeletal calcarenites (James et al., 2004).

2.2.3. Modern Environmental Conditions

Cyclonic storms, strong winds and wind-driven waves all influence the modern NWS, making it a generally high-energy depositional setting (Dix et al., 2005; James, 2004; Semeniuk, 1996). Waves impinging on the NCB portion of the shelf are divided into three frequency bands which originate from: a) long-period, 12-20 s, swells caused by weather fronts from the southwest, occurring at intervals of 2-4 days mostly between May and October; b) 8-12 s storm swells generated by episodic summer cyclones, from February to April; and c) 4-8 s waves caused by sea breezes and local winds (Hamilton, 1997). These three bands of waves result in three wave-base levels: a) swell wave base at ~300 mbsl; b) storm wave base at ~115 mbsl; and c) fairweather wave base at ~50 mbsl

(James et al., 2004). Similar high-energy conditions likely dominated the NWS during the Miocene and Pliocene.

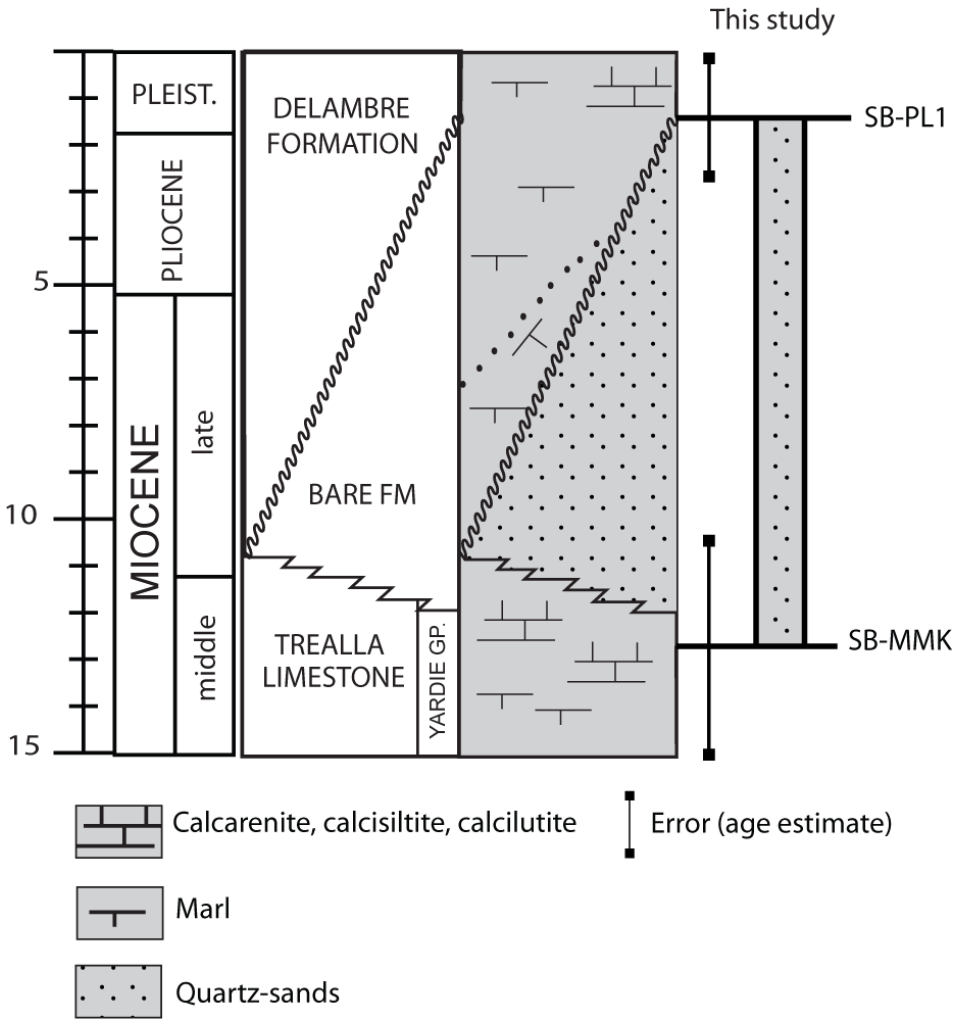

Figure 2.2: Generalized Miocene-Pleistocene stratigraphy of the NCB. Sequence boundaries derived from this study are calibrated to the Berggren et al. (1995) timescale. Two sequence boundaries from this study, SB-MMK and SB-PL1, represent the base and top, respectively, of siliciclastic progradation in the NCB (Bare Formation). Vertical bars represent errors for estimated ages. Modified from Cathro (2002).

2.3. DATA

This study makes use of industry-acquired subsurface data. Both 3D and 2D multichannel seismic data (Figure 2.1B) were donated to the University of Texas Institute for Geophysics (UTIG) by Woodside Petroleum, Ltd and Geoscience Australia. Exploration well data (Figure 2.1B), including wireline log suites, checkshot surveys, and well completion reports from 16 wells on the modern outer shelf and upper slope, were donated to UTIG by OCCAM Technology and Geoscience Australia.

The areal extent and resolution of the available 3D seismic make these data ideally suited for 3D mapping and sequence stratigraphic analysis of the targeted Tertiary clinoformal succession. The 3-D seismic covers 7,500 km^2; the total area covered by 2D and 3D seismic data combined is ~31,000 km^2 (Figure 2.1B). Central frequencies for the seismic reflection data range from 32 to 50 Hz, which result in a theoretical vertical resolution of 15 to 10 m, assuming an average velocity of 2,000 m/s. This average velocity, estimated from sonic logs, is representative of the uppermost second of two-way travel-time (twtt) sub-seafloor, the interval containing the mapped clinoforms. Offshore bathymetry data (Figure 2.1A) have been purchased from Geoscience Australia (originally compiled by Webster and Petkovic, 2005).

2.4. METHODOLOGY

I subdivided the upper-middle Miocene to Pliocene stratigraphy of the NCB into six mappable stratal packages bounded by seven unconformities (Table 2.1; Figure 2.3). I mapped these unconformities using GeoFrame® and Seisworks® at a 125-140 m profile spacing within the 3D volumes and on every 2D profile shown in Figure 2.1B. I could not

map these surfaces in the southwest portion of the study area because of poor data quality there, possibly because of acoustic interference from an overlying reef present on the modern sea floor (Collins, 2002).

Observations of toplap, truncation, and onlap seismic terminations were used to interpret seismic unconformities as sequence boundaries (Vail, 1987). In instances where 3D seismic coverage allowed it, flat or falling shelf-edge trajectories (stable to falling relative sea-level; Steel and Olsen, 2002) in dip-oriented profiles, and basinward shifts of facies and depocenters, were used to confirm sequence boundary interpretations. Sequence boundaries were labeled using estimated ages; for example SB-MM corresponds to a sequence boundary of middle Miocene age. Mapped surfaces were then tied to well data using synthetic seismograms generated in Geoframe®, using density and acoustic velocity (sonic) logs from wireline data and calibrated using checkshot surveys where available.

Age control for the Miocene-Pliocene stratigraphic interval (Figure 2.2) is based on the work of Cathro (2002) and Moss et al. (2004). These studies included defined foraminiferal zones in four exploration wells within the study area. Using these zones, I defined minimum and maximum ages for mapped unconformities in each of the four wells used by Moss et al. (2004). The ages (given in Figure 2.2 and Table 2.1) are averages of these maximum and minimum ages. Notice that error bars are on the order of 10^6 years.

Distinct seismic facies correlate with siliciclastic and carbonate facies reported in well completion reports. Siliciclastic intervals generally exhibit higher seismic amplitudes, continuous, oblique reflections (northwest-dipping clinoforms) on dip-oriented seismic sections, and oblique (northeast-dipping) to subtly mounded (bidirectional downlap) reflections on strike-oriented sections (Figure 2.3). In contrast,

carbonates that are known to result from heterozoan production (Moss et al., 2004) show generally lower amplitudes, continuous, parallel reflections on strike-oriented sections (Figure 2.3). These correlations between seismic facies and lithologies are confirmed using descriptions of cuttings included in industry well completion reports.

Siliciclastic intervals correlate with groups of clinoforms that are 40-100 m high (Figures 2.4 and 2.5). These clinoform sets are bounded by a toplap surface above and a downlap surface below (Figures 2.4 and 2.5). I have mapped the toplap surfaces that overlie these clinoform sets and have defined their areal extent using the rollover of the most recent clinoform in each group. Time and horizon slices through a conventional seismic amplitude volume have been generated to examine the geomorphologies of depositional systems in the studied interval.

The distance between the narrowest and most basinward point of successive siliciclastic clinoform sets along depositional strike and dip was measured using their mapped extent. These measurements were plotted to examine the variability of these migration distances and to compare them with inferred relative sea level change from shelf-edge trajectory (Figure 2.6; Johannessen and Steel, 2005). These plots include relative distance between successive clinoform sets and cumulative distance. The oldest set has been used as the initial reference point, except in our estimated cumulative progradation plot.

The shelf-edge trajectory (Steel and Olsen, 2002; Johannessen and Steel, 2005) has been interpreted for part of the studied interval using a dip-oriented profile that intersects numerous siliciclastic clinoform sets (Figure 2.6). Paleo-shelf edges were picked visually using the first major basinward change in shelf gradient (Wear et al., 1974; Southard & Stanley, 1976; Olariu and Steel, 2009) that correlates to the end of deposition of individual, or groups of, siliciclastic clinoform sets. The vertical and

horizontal changes of the shelf-edge position were quantified, i.e. aggradation/ degradation and progradation/ backstepping respectively, in this profile (Table 2.2). Vertical changes of the shelf-edge position through the period of deposition of mapped delta lobes 1-20 were compared to a global sea level curve (Haq et al., 1987) using available age control to evaluate the possible role of eustasy on the progradation of the Bare Formation sandstones.

Two-way-travel time structure maps of sequence boundaries were created in order to document variations in shelf-edge morphology. These surfaces define larger clinoforms, with a relief of up to 900 m, which form a shelf-slope-basin system along depositional dip. Shelf-edges were traced on these maps in order to indicate the positions of the siliciclastic clinoform sets relative to paleoshelf-edges.

Sequence Boundary	Seismic terminations	Estimated age (Ma)
SB-PL1	Below: toplap, Above: onlap, downlap	1.5 +/- 1.5
SB-LM3	Below: truncation, toplap Above: onlap, downlap	6.1 +/- 4.2
SB-LM2	Below: toplap, Above: onlap, downlap	7.1 +/- 4.1
SB-LM1	Below: truncation, toplap Above: onlap, downlap	9.8 +/- 6.8
SB-LM0	Below: truncation Above: onlap, downlap	9.8 +/- 6.8
SB-MMK	Below: truncation, Above: onlap, downlap	12.7 +/- 2.5
SB-MM	Below: toplap Above: onlap, downlap	12.7 +/- 2.5

Table 2.1: Interpreted sequence boundaries, characteristic seismic terminations observed above and/or below these surfaces, and estimated ages (based on Moss et al., 2004). The available age control does not allow separation of the estimated ages for SB-MMK (base of siliciclastic progradation) and SB-MM.

Shelf Break Point (lobe)	Relative Progradation (km)	Relative Aggradation (m)	Cumulative Progradation (km)	Cumulative Aggradation (m)	Trajectory
SB-MMK*	0	0	0	0	-
1-6	2	11	2	11	rising
7	12	-61	14	-50	falling
8	2	-18	16	-67	falling
9	3	-24	19	-92	falling
10	4	-38	23	-130	falling
11-12	6	-143	29	-274	falling
13-14	1	48	30	-226	rising
15	2	-56	32	-282	falling
16-17	0	32	32	-250	rising
18	1	105	33	-145	rising
19	1	72	34	-73	rising
20	0	100	34	27	aggradational

Table 2.2: Summary of shelf-edge relative and cumulative progradation and aggradation, and trajectory measured in the profile shown in Figure 2.6. SB-MMK is at the top of the carbonate shelf preceding siliciclastic progradation. (*) reference point for measurements.

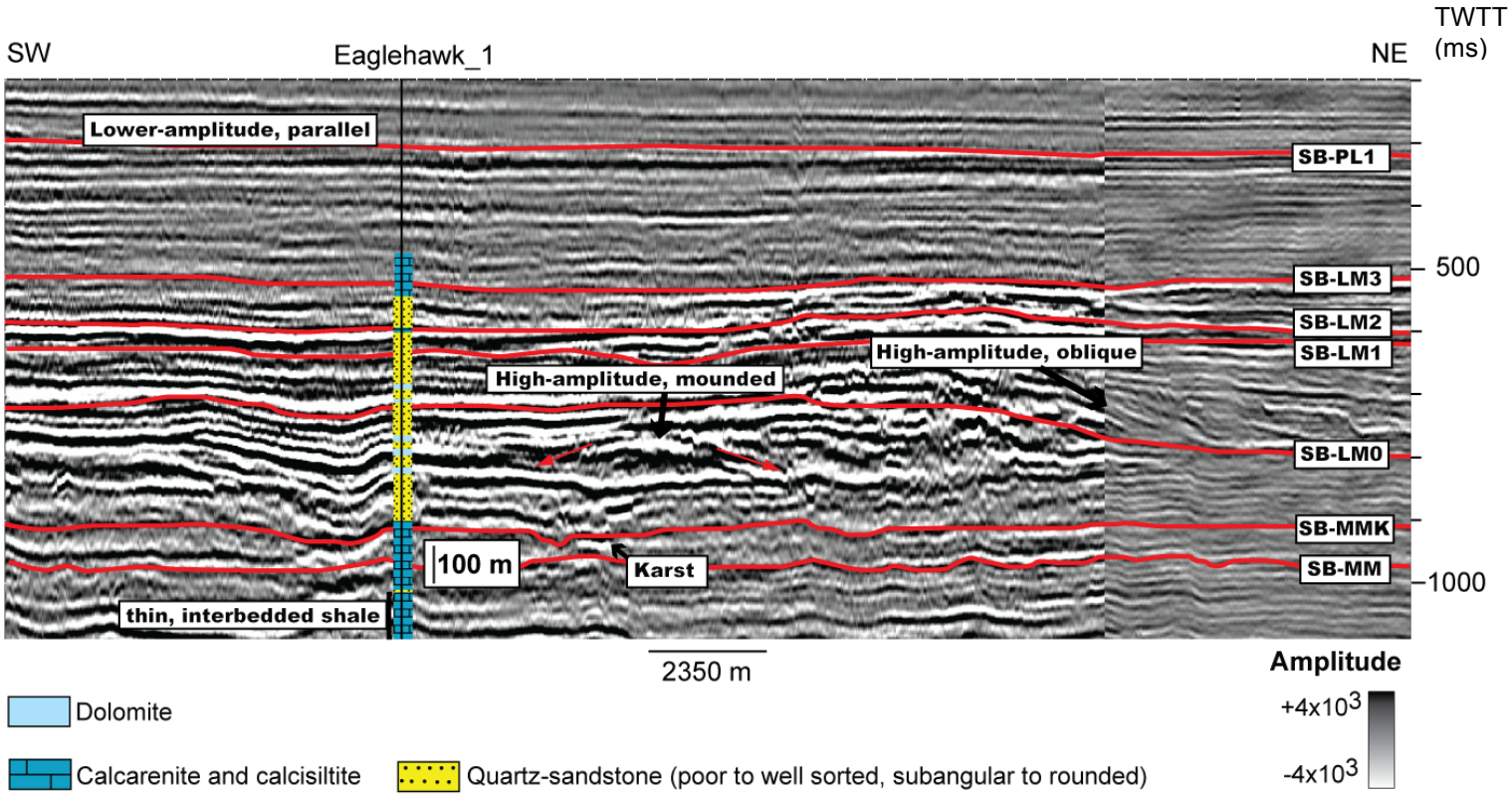

Figure 2.3. Strike-oriented (northeast-southwest) seismic profile showing correlation between seismic facies and lithology. Well completion report from industry well Eaglehawk_1 and Moss et al. (2004) confirm the presence of quartz sandstones in this high-amplitude seismic package, characterized by oblique and mounded reflection geometries. See Figure 2.1B for location.

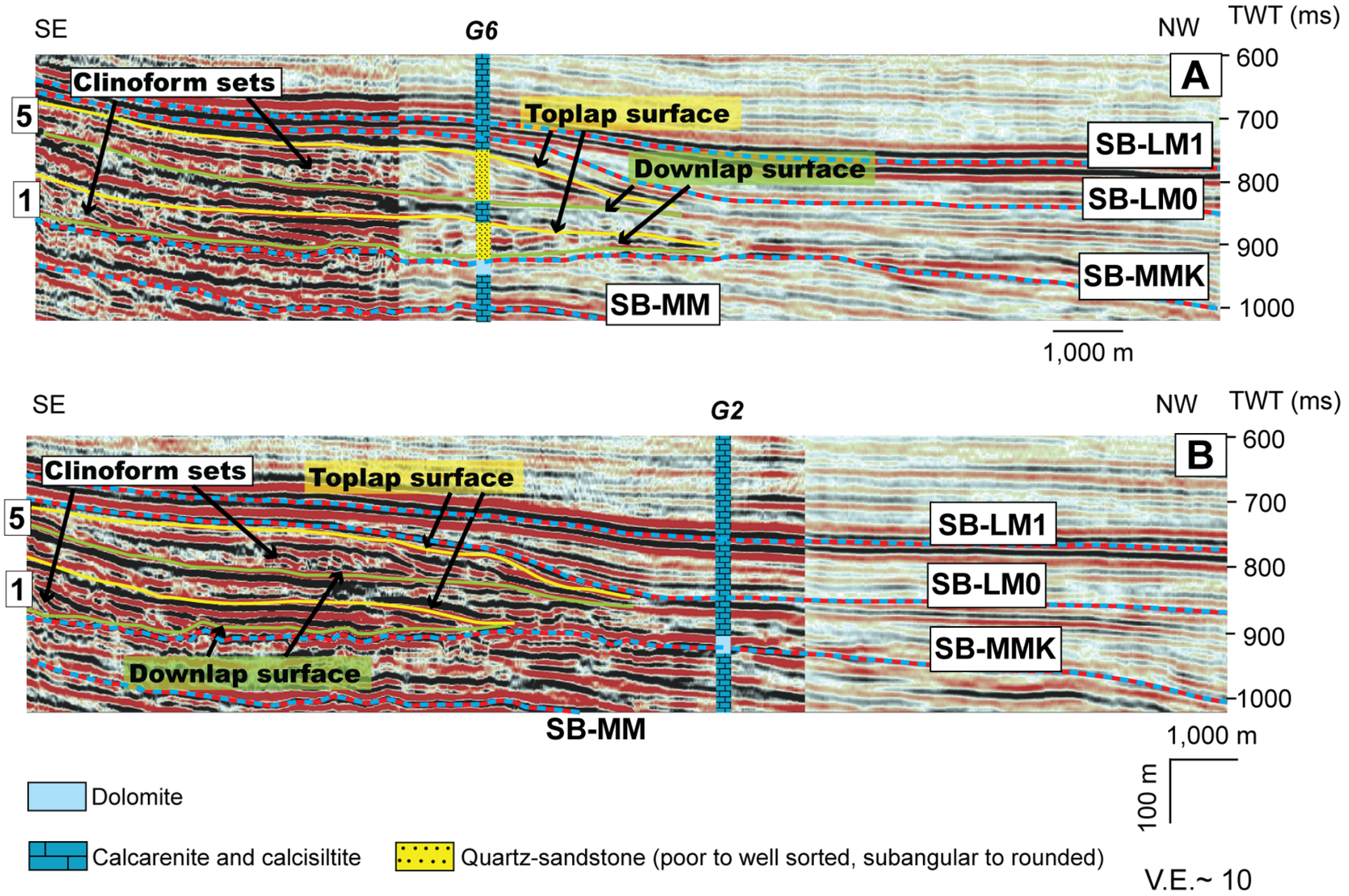

Figure 2.4. Dip-oriented (northwest-southeast) seismic profiles showing examples of mapped clinoform sets, four sequence boundaries, and lithology from industry well completion reports. (A) Clinoform sets between SB-MMK and SB-LM1 intersected by Goodwyn_6 (G6) in the paleo-outer shelf. Observe quartz-sand intervals associated with these sets. These clinoform heights are mostly ~40-50 m. (B) Sets between SB-MMK and SB-LM1 adjacent to Goodwyn_2 (G2). These sets are the same shown in I. Note absence of quartz-sands in Goodwyn_2 (G2). See Figure 2.1B for location of these profiles.

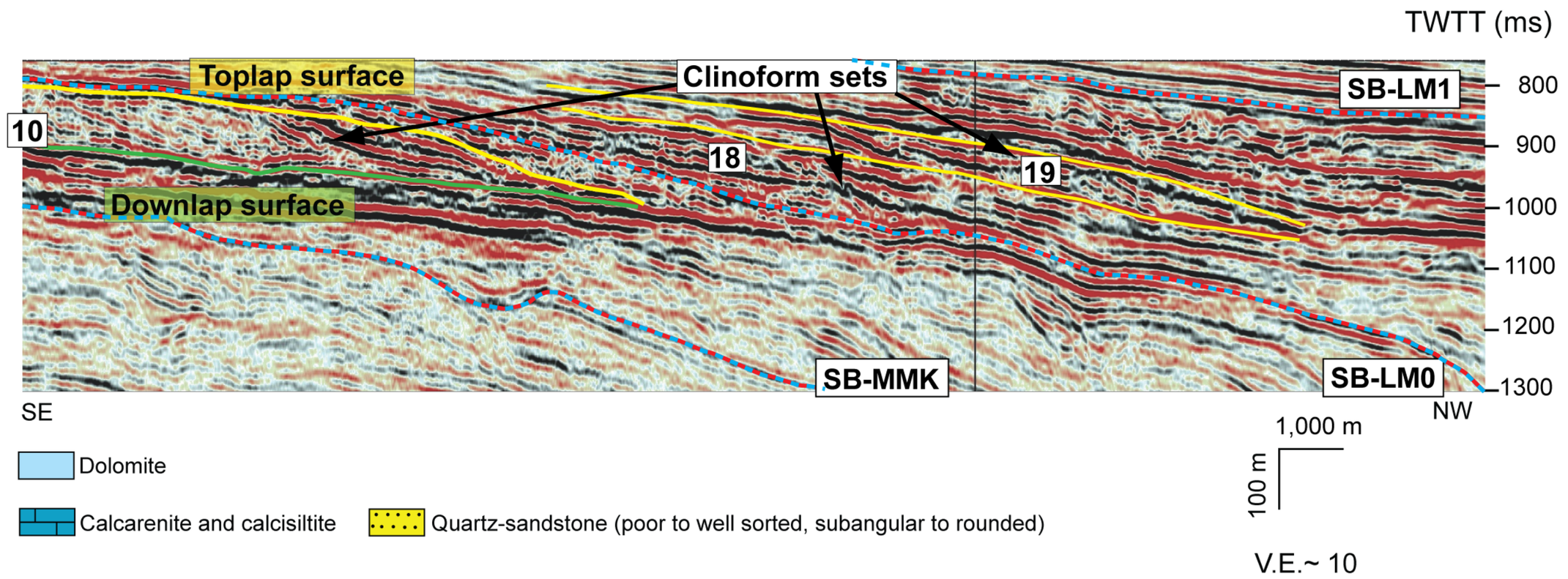

Figure 2.5. Dip-oriented (northwest-southeast) seismic profile showing examples of mapped clinoform sets, sequence boundaries. These sets, between SB-MMK and SB-LM1, were deposited closer to the shelf-edge. Their clinoforms show greater heights (up to ~100 m) than the sets shown in Figure 2.4. See Figure 2.1B for location.

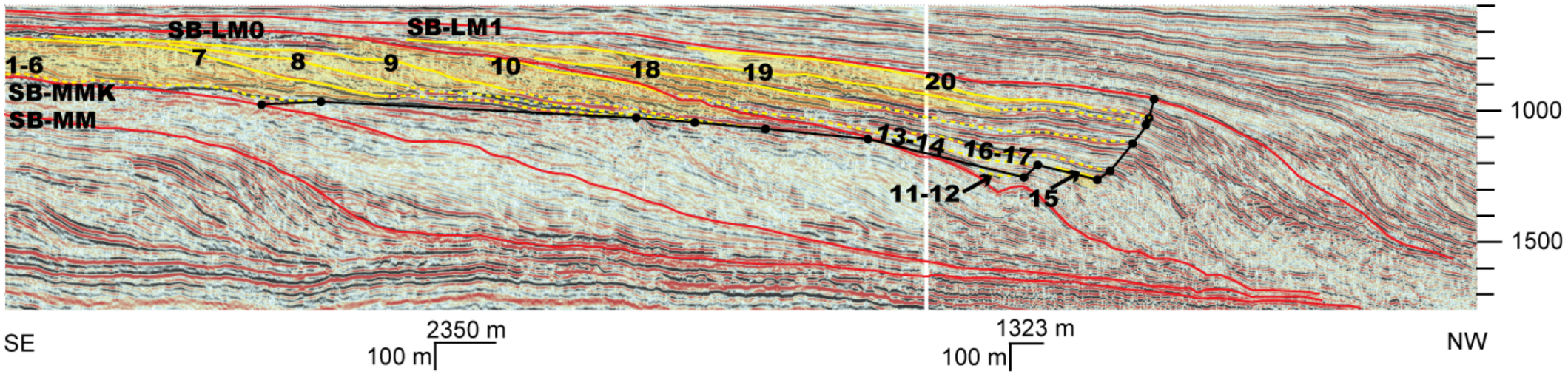

Figure 2.6. Dip-oriented seismic profile showing delta lobes (yellow) or time lines corresponding to lobes outside the plane of this profile and connecting lobe or groups of lobes to their coeval shelf-edge (dashed yellow), shelf-edge positions relative to time of deposition of lobes (or groups of lobes if several merge on one reflection), and shelf-edge trajectory. Numbering represents lobe upper boundary). Shelf-edge trajectory is quantitatively summarized in Table 2.2. See location in Figure 2.7.

2.5. RESULTS

2.5.1. Sequence Boundaries

Seven sequence boundaries SB-MM, SB-MMK, SB-LM0, SB-LM1, SB-LM2, SB-LM3, and SB-PL1 (Figure 2.3, Table 2.1), subdivide the upper middle Miocene to Pliocene NCB stratigraphy. Five sequences between SB-MMK and SB-PL1 contain the siliciclastic-dominated interval that is the focus of this investigation.

SB-MMK, which underlies the quartz-sands in Goodwyn-6 (Figure 2.4A), shows significant truncation of underlying reflections (with up to 60 m of relief) and higher seismic amplitudes. This sequence boundary correlates with ~20 m of dolomite at Goodwyn-2 and ~70 m of the same material at Goodwyn-6 (Figure 4) according to well completion reports. Wallace et al. (2003) have identified interbedded limestones within this dolomitized interval, with abundant anhydrite and gypsum.

2.5.2. Clinoform Sets

The Bare Formation sandstones have been reported in some industry wells that intersect the middle to late Miocene outer paleoshelves of the NCB (Moss et al., 2004); however, these sandstones are absent in other wells in the area. The current study shows that these sandstones occur within areas of high seismic-amplitude clinoform packages. For example, clinoforms 40-50 m high coincide with quartz-sandstone intervals in Goodwyn_6 (Figure 2.4A). In contrast, Goodwyn_2 (located southeast of Goodwyn_7) does not intersect these clinoform features and there are no reported quartz-sandstone

intervals of the Bare Formation reported from that well (Figure 2.4B). Quartz-sandstones grade southwestward along strike, and northwestward down dip (Figure 2.4) to calcarenites, suggesting the coeval development of siliciclastic and carbonate deposits beginning in the late middle Miocene in the NCB.

A clinoform set is here defined as a prograding stratigraphic unit containing a series of broadly conformable clinoform surfaces. Clinoform sets are bounded by a toplap surface above and a downlap surface at the bottom. Twenty-seven clinoform sets (Figure 2.7) have been identified within the interpreted succession, all presumably of siliciclastic composition based on the correlation of clinoform sets to lithology from well reports (Figures 2.3 and 2.4). Numbers were assigned to these clinoform sets in their order of occurrence, i.e. clinoform set "1" was deposited first and therefore is the oldest clinoform set; higher set numbers are progressively younger. Individual clinoform heights within these mapped sets range from 40 to 100 m (Figures 2.4 and 2.5). Their foreset inclination ranges from 2.2˚ to 2.8˚. These clinoform sets, located on the paleo outer-shelf and shelf-edge, are key elements of the NCB middle Miocene-Pliocene siliciclastic Bare Formation.

2.5.2.1. Clinoform set morphology and migration patterns

Most clinoform sets are elongated along strike (southwest-northeast) in map view (Figure 2.7); however, some display a slightly more dip-elongated planview morphology (e.g. lobe 14 in figures 2.7 and 2.8). A time slice that intersects clinoform set 5 (Figure 2.9) displays gentle convex-outward lineations generally oriented east-west. The clinoforms that comprise sets 1-6 are 40-50 m high and were deposited on the paleo-outer

shelf the coeval shelf edge can be identified some 15-22 km basinwards (Figure 2.4). These sets migrate along strike (Figure 2.10) distances between 70 km southwest (shifts relative to the apex of the preceding set) and 50 km northeast. The changes in position along dip (either progradation or backstepping, Figure 2.11) range between 4 km of backstepping and 5 km of progradation. There is some vertical stacking of these sets (Figure 2.4). A dip-oriented profile shows that the shelf-edge trajectory during deposition of sets 1-6 was rising (Figure 2.6).

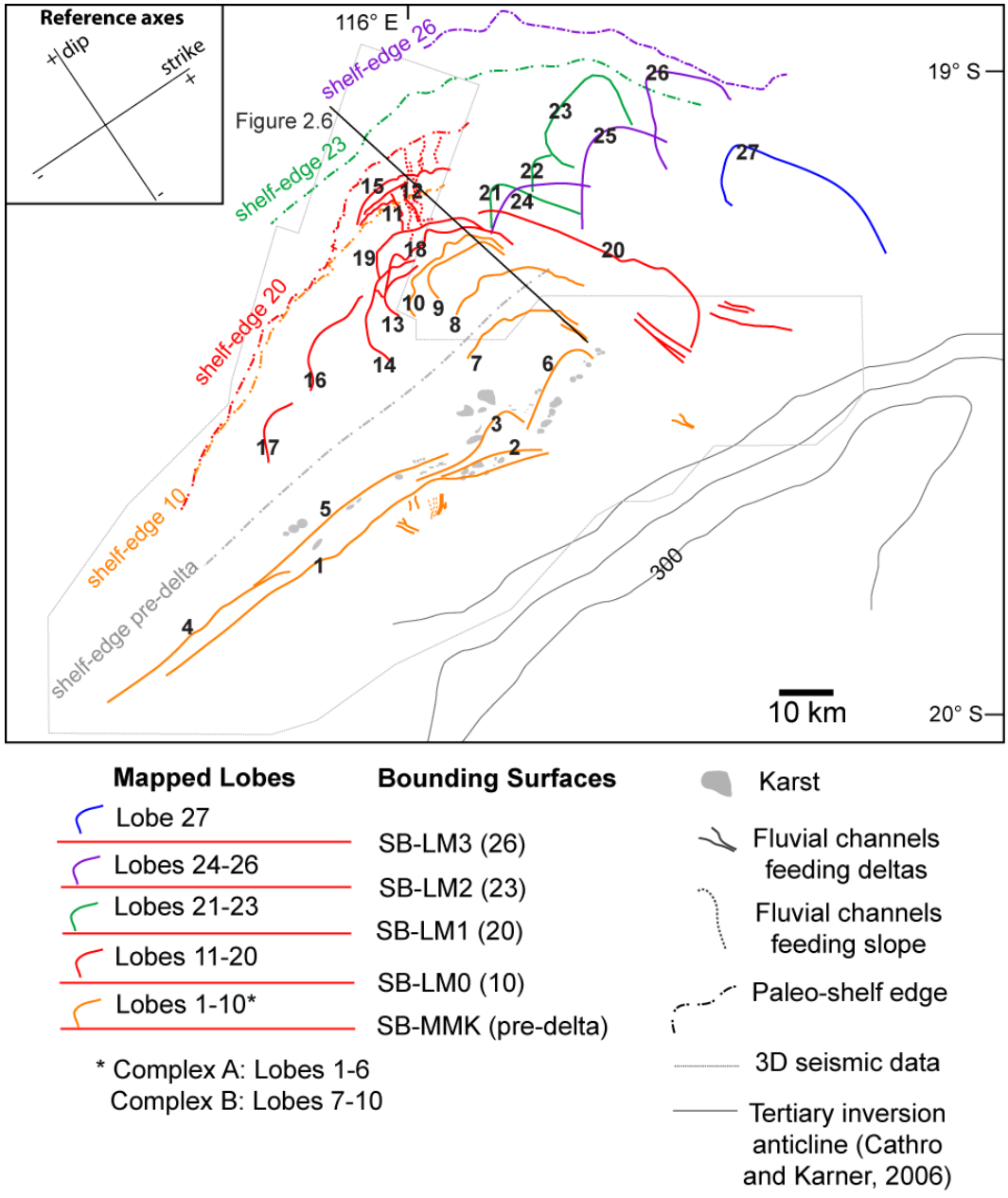

Figure 2.7. Mapped delta lobes and paleo shelf-edges at the end of deltaic progradation pulses between SB-MMK and SB-LM3. The outline of the lobes corresponds to the rollover of the last clinoform, or the top-bounding unconformity, of the respective mapped clinoform set (Figures 2.4 and 2.5). The paleo-shelf edges are numbered according to the last lobe deposited under that paleo-shelf profile, to associate the shelf-edge geometry with delta progradation. Note Tertiary inversion anticline in the southwest

(Cathro and Karner, 2006). Karst underlies lobes 1-6. Interpreted fluvial channels within the siliciclastic interval are shown in colors corresponding to the interval where they occurred. Inset show reference axes for changes in position of delta lobes along-strike and dip.

Clinoform sets 7-27 (Figure 2.7) are 40-100 high (Figure 2.5) and were deposited near or at the paleoshelf edge. These sets show shifts in position along strike of up to 45 km (Figure 2.10). These sets shift along dip by distances up to 16 km (Figure 2.11). In comparison to sets 1-6, the sets 7-27 show less migration along strike and more progradation and backstepping through time.

2.5.3. Long-term Progradation Patterns of Clinoform Sets

Successive clinoform sets shows displacements both along strike and along dip (progradation and backstepping). I observed long-term trends in along-strike migration and progradation of these sets using cumulative plots of these displacements (Figures 2.12 and 2.13).

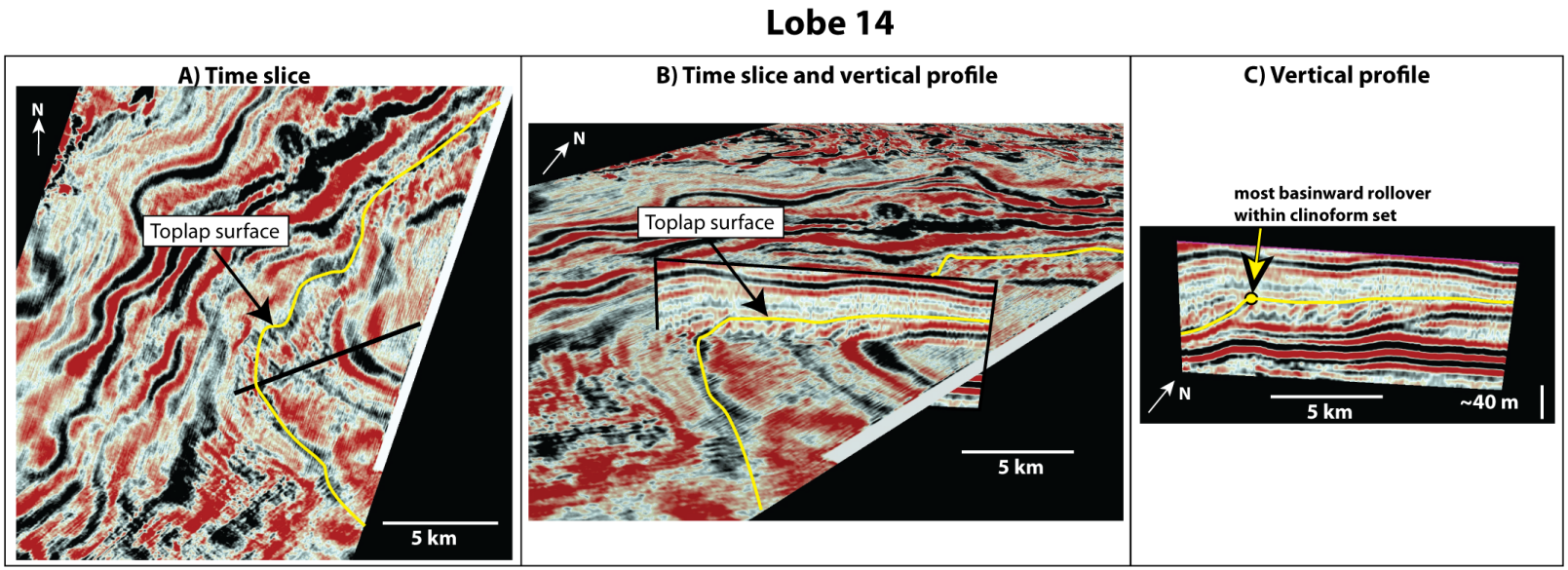

Figure 2.8. A) Time slice through seismic volume showing convex planview morphology exhibited by several clinoform sets (Figure 2.7). B) Vertical profile intersecting the time slice shown in (A); notice the mapped toplap surface (yellow) both in the vertical profile and the intersected time slice. B) Vertical profile displaying the clinoform set that composes lobe 14 (Figure 2.7).

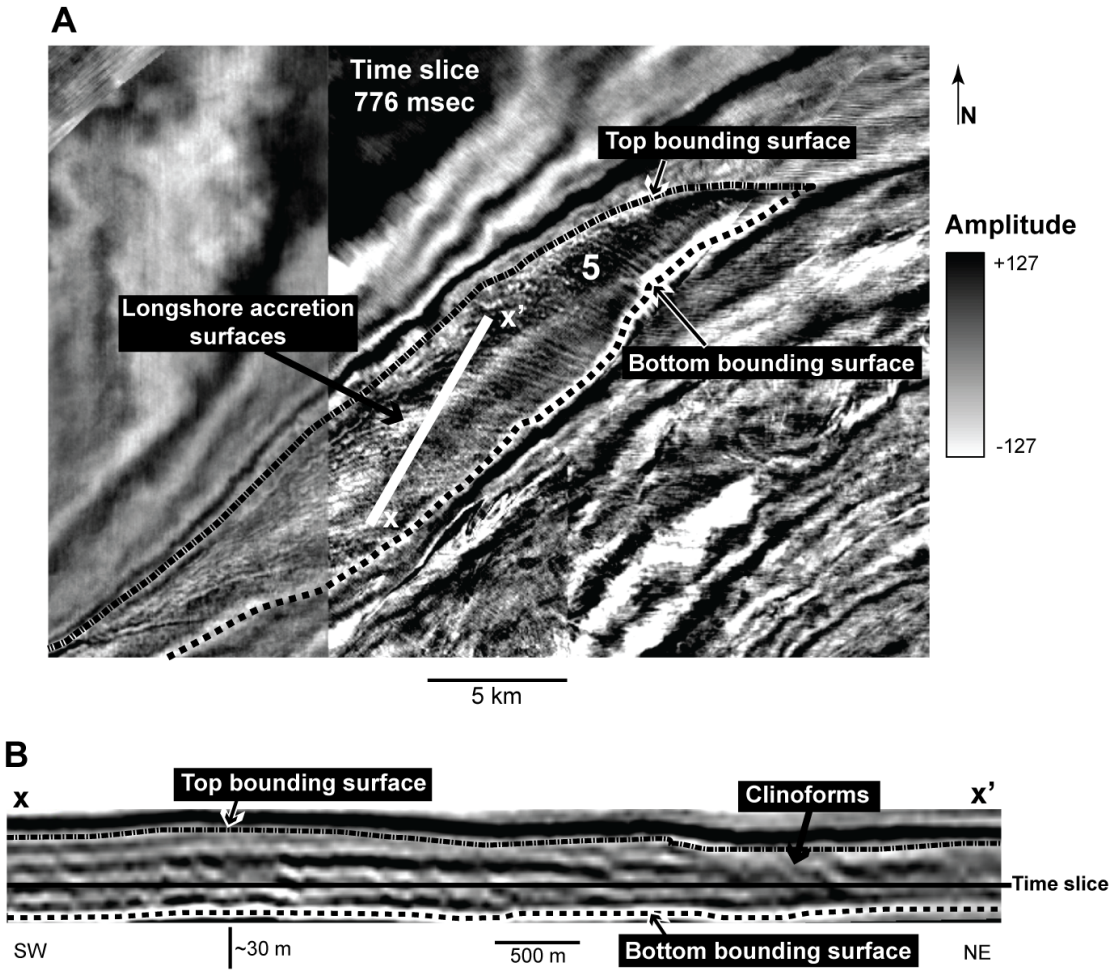

Figure 2.9. A) Time slice through seismic amplitude volume. Top and a bottom unconformity bound convex-outward lineations are interpreted as surfaces created by longshore accretion. B) Strike-oriented (southeast-northwest) seismic profile showing the clinoforms that correspond to the lineations and the bounding unconformities observed in the time slice in A. See Figure 2.1B for location of time slice.

The long-term migration along strike is to the northeast if the positions of the younger clinoform sets (25-27, Figure 2.12) are compared to the reference clinoform set (1, Figure 2.12). Total migration is 91 km to the northeast relative to the position of the reference clinoform set 1 (Figure 2.12). In terms of long-term progradation pattern, the

maximum overall long-term progradation distance is 77 km; this distance is reached with clinoform set 15 (Figure 2.13). Subsequent sets show a long-term backstepping trend. A progradation value of 30 km is assigned for clinoform set 1. No similar clinoforms are observed below set 1. Therefore, I suggest that the initial progradation pulse that caused the occurrence of set 1 would have been at least of 30 km (Figure 2.7), which is the along-dip distance between clinoform set 1 and the edge of the 3D seismic coverage.

2.5.4. Shelf-edge trajectory

I have examined the shelf-edge trajectory in a dip-oriented profile between SB-MMK and SB-LM1 (Figure 2.6 and Table 2.2). This trajectory rises stratigraphically basinward (i.e., aggradational and progradational simultaneously) during the growth of clinoform sets 1-6 (Table 2.2). The trajectory then falls basinwards during deposition of clinoform sets 7 to 12, and then rises during deposition of sets 13 and 14. Trajectory falls again during deposition of set 15 and rises during deposition of set 16 through 19. The trajectory becomes aggradational (i.e., near vertical) during deposition of set 20.

2.6. INTERPRETATION

2.6.1. Delta lobes

Upper-middle Miocene siliciclastics of the Bare Formation (Figure 2.14) are interpreted as the result of deltaic progradation onto the middle-outer reaches of the preexisting carbonate shelf, perhaps driven by an antecedent of the modern Fortescue

River situated on the Pilbara Coast (Figure 2.1A). Our interpretation of the deltaic system is based on common lobate morphologies revealed by detailed mapping of seismic data (Figures 2.4, 2.5, 2.8, and 2.9) and the correlation between the Bare Formation sandstones and the 40-100 m-high clinoforms created as these delta lobes prograded towards the deeper-water reaches of the outer shelf (Figure 2.4). Observed clinoforms heights are within the characteristic range for shelf deltas (10s of m) to shelf-edge deltas (up to ~150 m; Steel et al., 2008). A few elongated incisions, likely the fluvial feeders, associated to these lobes have been mapped (Figures 2.7 and 2.14).

It is suggested that each of the observed clinoform sets corresponds to a delta lobe (Figures 2.4, 2.5, 2.7, 2.8, and 2.9). Sydow et al. (1992) described similar morphologic features in the Pleistocene section in the Gulf of Mexico to represent subdivisions of a larger deltaic clinoform wedge. Their sets comprise many individual clinoforms, each interpreted as the position of the delta front at a given time, and are bounded by unconformities above and below. Those bounding unconformities exhibit toplap terminations below and downlap terminations above. Although the NCB clinoform sets have similar bounding unconformities, our seismic data have lower vertical seismic resolution (10-15 m) than the sub-meter vertical resolution of the boomer data used by Sydow et al. (1992). Therefore, individual clinoforms in the NCB seismic data represent stratigraphic units that are thicker than the individual deltas identified by Sydow et al. (1992). The bounding surfaces of the NCB clinoform sets likely represent the limits of delta lobes, sensu Coleman and Roberts (1991). The mounded reflections (Figure 2.3) within this siliciclastic interval would then correspond to the progradation centers of delta lobes (Sydow and Roberts, 1994).

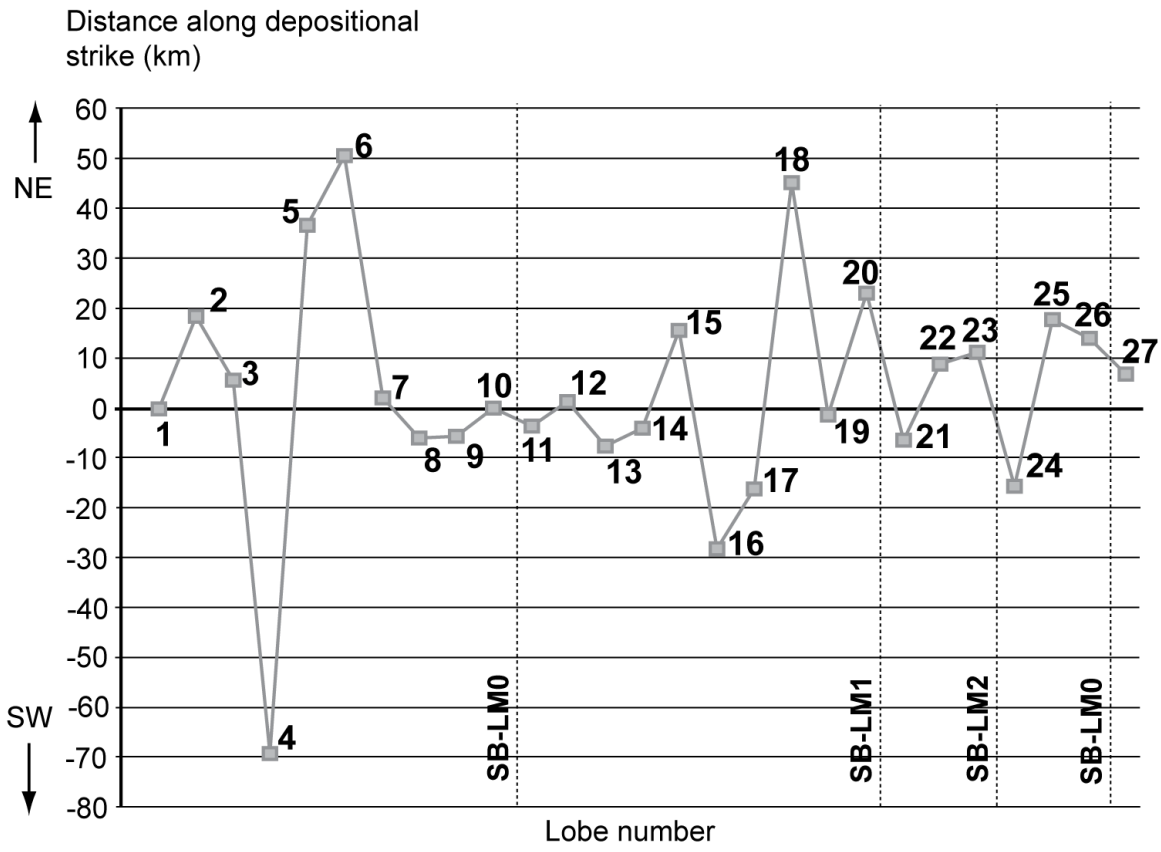

Figure 2.10. Plot of lobe migration along strike, relative to preceding lobe (Figure 2.7). Positive values refer to northeastward shifts relative to apex of preceding set, negative values to southwestward shifts. Note higher shift distances for lobes 1 to 6 and lobes 16 to 20.

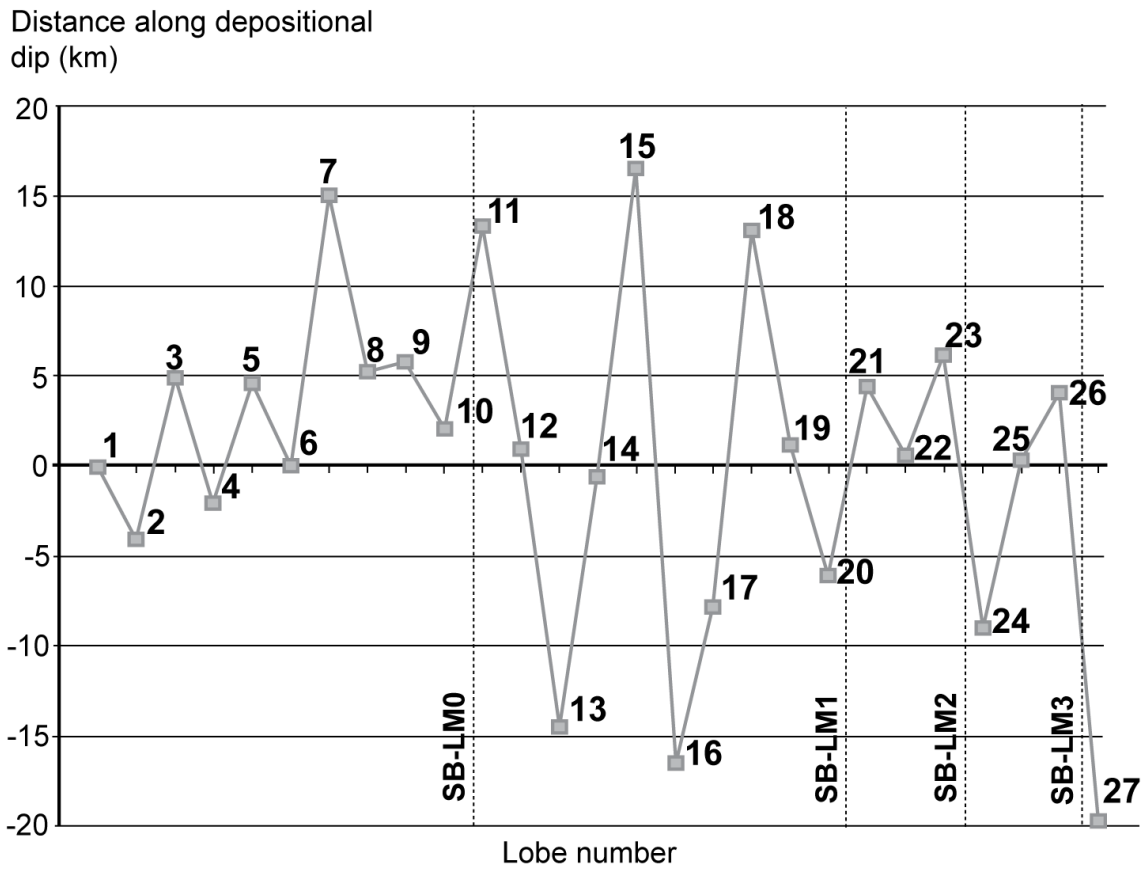

Figure 2.11. Plot of lobe progradation (positive values) and backstepping (negative values) relative to preceding lobe (Figure 2.7). Highest variability occurs between lobes 11 and 19.

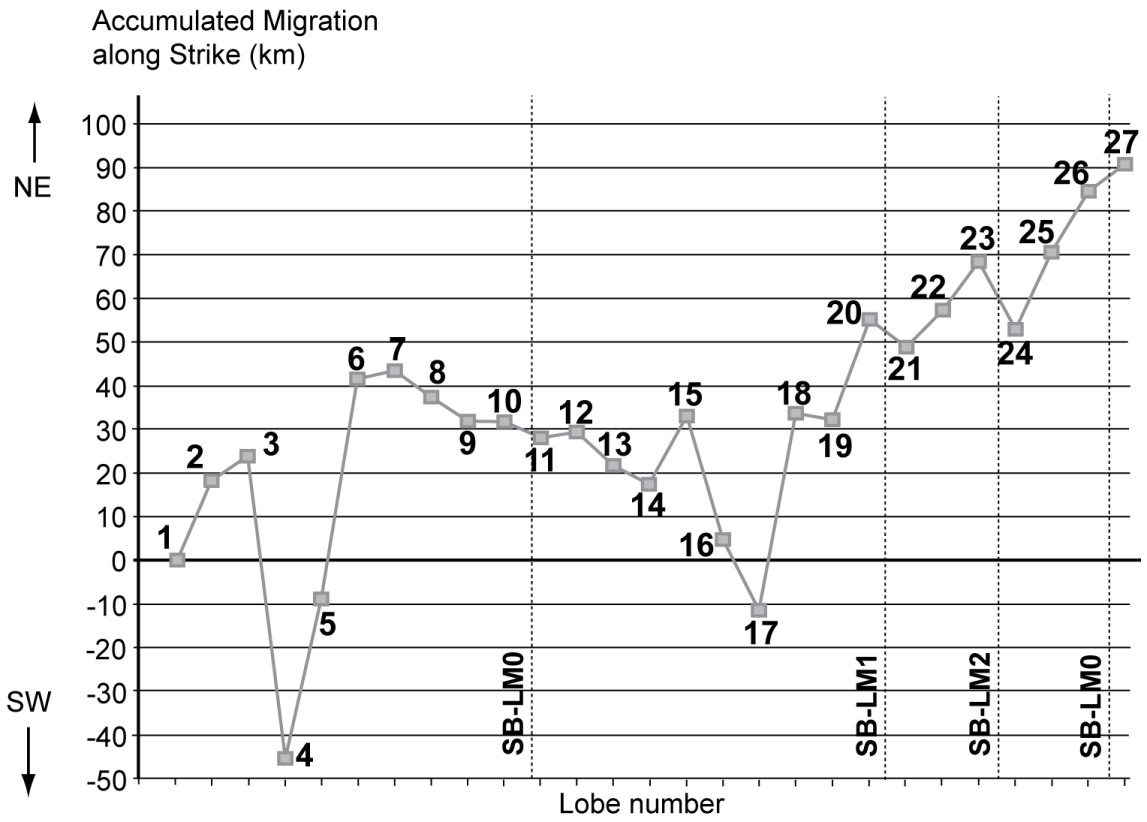

Figure 2.12. Cumulative lobe migration along strike. Higher positive values correspond to northeastward migration while higher negative values correspond to southwestward migration. Notice that the long-term trend is northeastward migration.

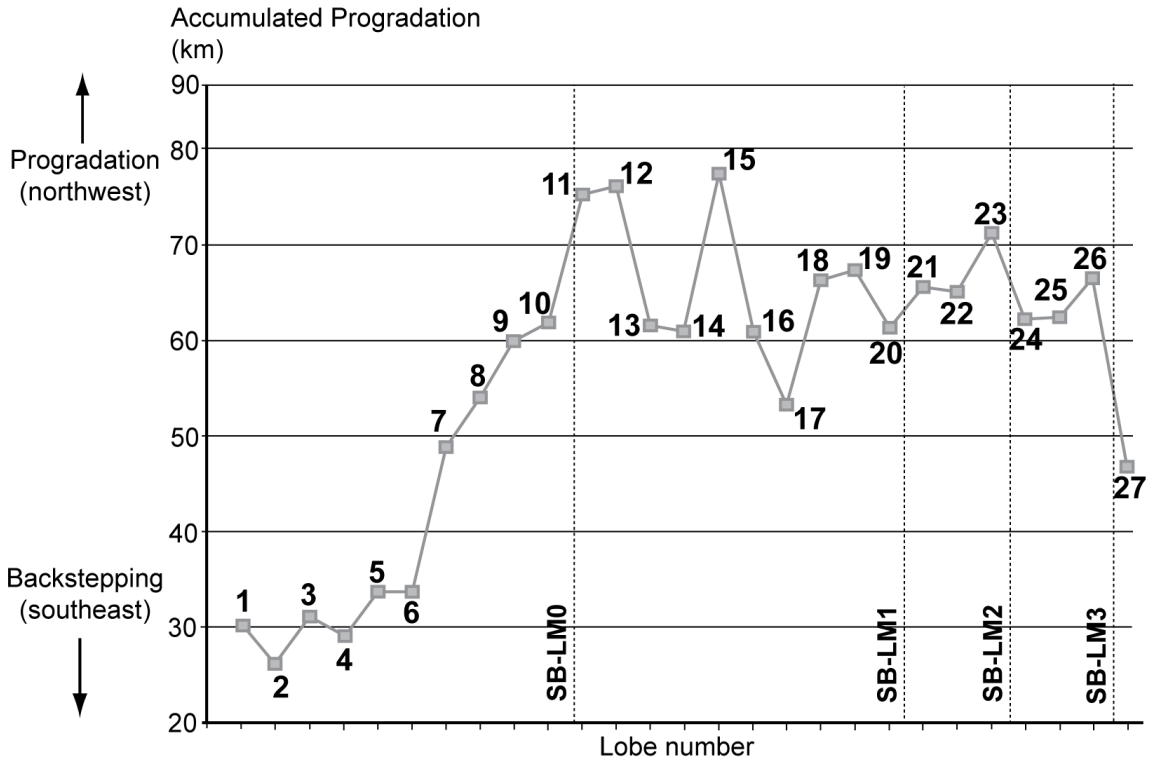

Figure 2.13. Cumulative lobe progradation. Progradation values start at 30 km, which comes from the assumption that the preexisting shoreline must have been outside our study area (≥30 km southeast of lobe 1). Notice long-term progradation from lobes 1 to 15, and subsequent long-term backstepping from lobes 16-27.

2.6.1.1. Wave-dominated delta lobes

The strike-elongated morphology of the majority of the mapped lobes suggests significant syn-depositional wave reworking with strike feeding of sands (Bhattacharya and Walker, 1992), therefore I interpret them as wave-dominated delta lobes. The width of these wave-dominated lobes (1-6) ranges between 7 and 80 km, which is comparable to the wave-influenced lobes of the modern Danube (Bhattacharya and Giosan, 2003) and Rhone deltas (Bhattacharya and Walker, 1992). The gently convex-outward lineations observed in a time slice (Figure 2.8) are interpreted as accretion beach-ridge surfaces caused by longshore sediment transport to the northeast. The marked asymmetry of lobes 1, 3, and 6 also suggests strong influence of northeastward-flowing longshore currents. Clinoform sets 7-27 are located basinward from lobes 1-6, near or at the shelf-edge. Their greater height (40-100 m) is consistent with this interpretation as water depth increases at the shelf edge.

The clean quartz-sand lithology associated with lobes 1-6 is known from the more proximal set of industry wells (e.g. Goodwyn_6 and Eaglehwak_1; Figure 2.4). Such mature quartz-sands are characteristic accumulations in high-energy, storm-wave dominated shoreface environments adjacent to fluvial feeders draining terrigenous hinterlands (Bhattacharya and Walker, 1992). The modern Pilbara Coast is a high-energy setting, dominated by waves and swells, and a similar high-energy setting probably prevailed along this paleo-coast and shelf during the middle and late Miocene. The modern Lacepede Shelf in Southern Australia offers an excellent example of clean

quartz-sands being deposited in a wave-dominated delta next to a high-energy, cool-water mixed carbonate-siliciclastic shelf (James et al., 1992).

2.6.2. Lobe migration and relative sea level

Integrating the evidence of lobe migration along-strike (Figure 2.10) with shelf-edge trajectory (Figure 2.6, Table 2.2) allows an estimate of how much how much these lobes shift along strike during relative sea level rise (i.e., rising shelf-edge trajectory) or fall (falling shelf-edge trajectory).

Lobes show greater degree of migration along strike during relative sea level rise. For instance, lobes 1-6 show lateral migration distances between 5 and 70 km (Figure 2.10). Lobes 13 and 14 and 16 to 20 migrate distances between 4 and 45 km (Figure 2.10). In contrast, during periods of relative sea-level fall, lobes 7-12 and 15 show smaller migration distances, between 0 and 15 km. The smallest amount of observed lateral migration is associated with lobes 7-12 (0-6 km). This relatively straight fairway of delta progradation (Figure 2.7) could have been caused by an absence of marine reworking or progradational confinement during the relative sea-level fall. However, I have not been able to map a valley system associated with or containing lobes 7 through 10. Nevertheless, these lobes were mapped using 2D seismic data and incised valleys may be below data resolution or missed because of the profile spacing (2 km along strike, 4 km along dip).

The long-term migration trend of lobes 1-27 is to the northeast (Figures 2.12 and 2.14). The ongoing collision between the Banda Arc and Australia since the late Miocene (Veevers et al., 1991) has caused several uplift/inversion pulses in the NCB since ~17 Ma

(Figure 2.1A; Cathro and Karner, 2006). Each one of these pulses created relief up to 75 m on an anticline (Figure 2.7) along the western end of the Rosemary-Legendre Trend (Cathro and Karner, 2006; Figure 2.1A). The uplift of this anticline concomitant with deposition of lobes 1-27 likely caused the long-term northeastward migration trend (Figures 2.12 and 2.14).

Another possible cause for a unidirectional long-term migration trend is differential subsidence of the margin. This alternative model would require greater subsidence in the northeast area of the NCB relative to that in the southeast. This northeastern area of enhanced subsidence would create accommodation space at a faster rate favoring northeastward migration of depocenters through time. However, subsidence curves from several industry wells in the NCB indicate only localized Miocene uplift, which did not interrupt the simple thermal subsidence pattern across the basin (Kaiko and Tait, 2001). Since the Bare Formation was presumably deposited at an approximately constant water depth through time, subsidence rate can be estimated using its thickness and the available age control. In the Eaglehawk_1 well (Figures 2.1 and 2.3) the formation is 590 m thick and was deposited over a time interval of approximately 2.9 My. The subsidence rate can then be estimated to be around 0.2 mm/yr and therefore lies within the range for thermal cooling subsidence typical of passive margins (Watts and Ryan, 1976).

2.6.3. Lobe progradation

I assume an initial delta progradation distance of at least 30 km (Figure 2.13), the distance from lobe 1 to the landward boundary of our seismic coverage (Figure 2.7). No

older lobes are observed within this zone, but the delta/shoreface siliciclastic facies must have persisted some distance landward from the limit of our data coverage.

Progradation/backstepping distances for lobes 1-6 range up to 5 km (excluding the initial pulse of siliciclastic progradation of at least 30 km). Regressive distance for lobe 7 shows a significant increase to 15 km across the platform (Figure 2.11), with a subsequent backstepping of 10 km. This increase in the progradational/retrogradational character of the deltas coincides with a relative sea level fall interpreted from the flat to downward trend of the shelf-edge trajectory (Figure 2.6, Table 2.2). The onset of high amplitude and frequency glacioeustatic sea-level changes during the late Miocene, caused by growth of the Antarctic Ice Sheet (Shackleton and Kennett, 1975; Zachos et al., 2001), is a possible cause for this dramatic increase in progradation and backstepping distances.

The mapped lobes also show a longer-term progradation/backstepping trend (Figures 2.13 and 2.14). After an initial period of limited progradation/backstepping on the shelf (lobes 1-6), there is a period of significant deltaic progradation (lobes 7-15) of at least 77 km (Figures 2.7 and 2.13). After this maximum progradation, lobes 16-27 (Figures 2.7 and 2.13) exhibit a long-term backstepping trend of almost 30 km.

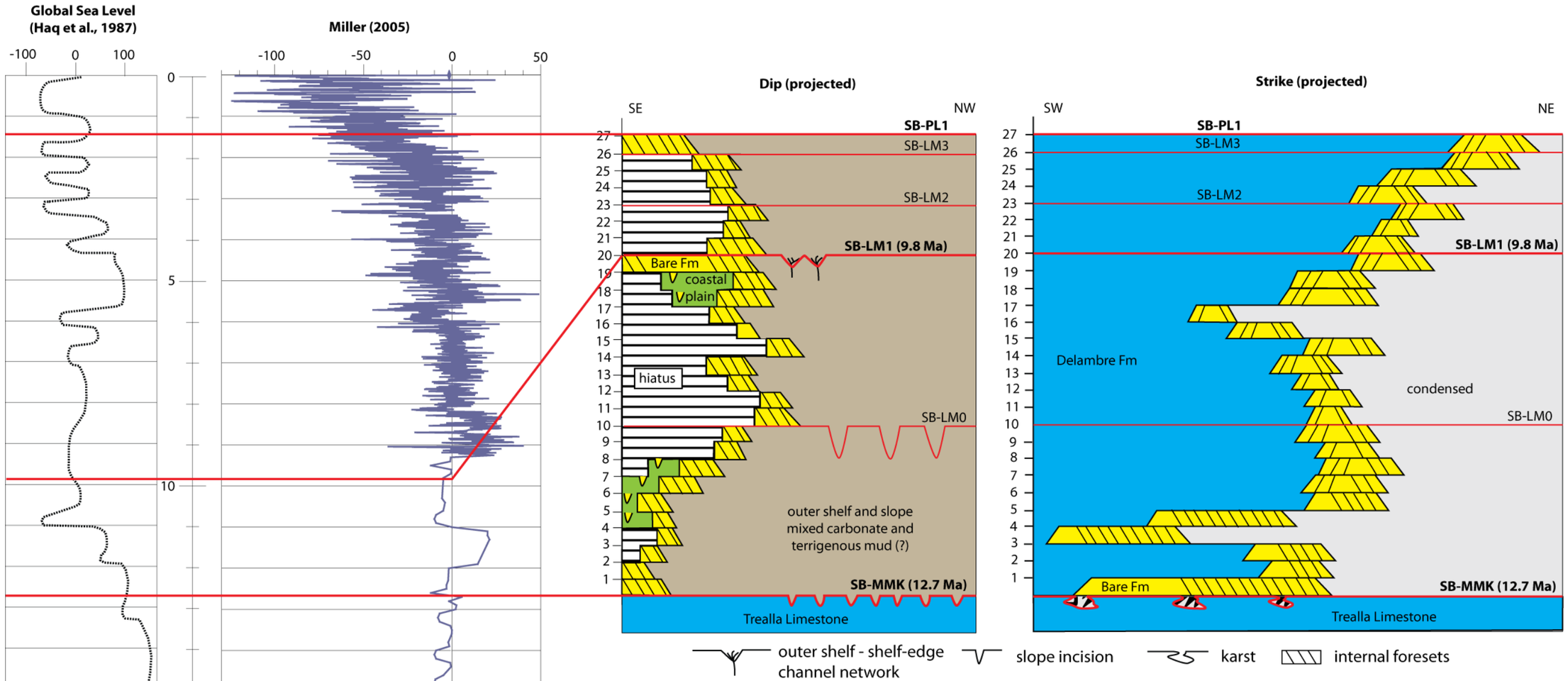

Figure 2.14. Stratigraphic chart reflecting dip- and strike-oriented deposition of the siliciclastics composing the Bare Formation in the NCB. Ages have been estimated using results from Moss et al. (2004), error bars for these ages are shown in Table 2.1.

2.7. DISCUSSION

2.7.1. Origins of Late-Middle Miocene Siliciclastic Influx to the NCB

The presence of subordinate quartz sands within the carbonate-dominated facies of the Trealla and Delambre formations suggests a continuing supply of siliciclastics to the NCB from the middle Miocene to the Recent, presumably from an arid onshore source, both preceding and following the primarily siliciclastic deposits of the Bare Formation (Figure 2.2). However, these pre- and post-Bare Formation siliciclastics were likely mainly sequestered in nearshore environments whereas carbonate production and accumulation dominated on the shelf throughout these periods (Trealla and Delambre Formations, Figure 2.2). Furthermore, an early Miocene episode of relative sea-level fall and subaerial exposure of the paleoshelf resulted in karst development (Cathro and Austin, 2001) but not in the accumulation of prograding siliciclastics like is the case of the late-middle Miocene event discussed in this study. In contrast, new seismic data and interpretation herein suggest that the Bare Formation siliciclastic supply was sufficient to prograde across the entire shelf and to deliver siliciclastics into deep water continental slope areas during late-middle Miocene to Pliocene time.

2.7.2. Other Regions of Mid-Miocene Increase in Siliciclastic Sediment Supply

Upper-middle Miocene quartz sandstones occur as discrete units in the NCB, as represented by the Bare Formation offshore to the northeast, our study area, the Pilgramunna Formation and Vlaming Sandstone on the western flank of Cape Range, and

the Lamont Sandstone and Pindilya Formation farther south (Hocking et al., 1987; Hocking, 2000) in the Cape Range area (Figure 2.1A). Hocking (2000) proposed that the Pilgramunna Formation is a lateral equivalent of the Bare Formation. These siliciclastic units represent a major pulse of siliciclastic sediment flux out onto the preexisting middle Miocene carbonate shelf in the NCB.

Other continental margin studies have also revealed anomalous influx of siliciclastic sediments during the middle Miocene that do not correlate well with known episodes of tectonic uplift in their sediment source areas (Molnar, 2004). Well-constrained examples include the New Jersey shelf (Poag and Sevon, 1989; Pazzaglia and Brandon, 1996; Steckler et al., 1999), the Canterbury Basin (Lu et al., 2005), the Angola continental margin (Lavier et al., 2001) and the Maltese Islands (John et al., 2003). Age estimates of these influxes vary, but range from 12-15 Ma. The NCB case is particularly striking because the influx of siliciclastics occurred onto a carbonate margin; a similar lithologic transition occurred in the Maltese Islands (John et al., 2003). In the Canterbury Basin, although a mountain range lies nearby today, the mid-Miocene sediment influx is not linked to tectonism in the Southern Alps (Lu et al., 2005). Sedimentation rates actually decline following the middle Miocene influx before increasing gradually in parallel with a well-defined period of increasing convergence rates at the Alpine Fault (Lu et al., 2005).

2.7.3. Climatic Change and Increase of Siliciclastic Sediment Supply

Reconstructed vegetation patterns from onshore Australia indicate that, with the exception of the warm early Miocene, climate on the Australian continent has become

progressively more arid since the Oligocene (White, 1998). Such an increase in aridity in the hinterland adjacent to the NCB most likely contributed to the general decrease in siliciclastic input to the coastline and shelf since the Oligocene. However, the trend of decreasing terrigenous input to the NCB was interrupted in the late-middle Miocene when siliciclastics prograded across shelf.

The estimated age of sequence boundary SB-MMK at the base of the NCB siliciclastic progradational episode, 12.7 +/- 2.5 Ma (Table 2.1), correlates with the global middle Miocene increase in $\delta^{18}O$, believed to be the result of expansion of the West Antarctica ice-sheet, associated global cooling (Shackleton and Kennett,1975; Miller et al., 1991; Zachos et al., 2001), and a long-term global sea-level fall (Haq et al., 1987).

Increased global aridity and erosion rates are a possible cause for amplified sediment yield in the late-middle Miocene. The transition from Greenhouse to Icehouse conditions in general is accompanied by increasing seasonal and latitudinal temperature gradients, as well as a strong continent/ocean temperature contrast that implies more arid conditions (Serranne, 1999). Molnar (2001) proposes that globally increased erosion could be the result of more rare, large-magnitude floods per small, annual floods in arid settings. Another possible reason for globally enhanced erosion is the alternation between drier and wetter periods resulting under Icehouse conditions, as these fluctuations can negatively impact vegetation and decrease its stabilizing action on landscapes. An additional possible cause for increased erosion could be stronger seasonality producing a change to scrubbier vegetation that is easier to erode (Clift 2010).

SB-PL1 (Table 2.1) marks the end of NCB siliciclastic deposition. Correlation of this surface with foraminiferal zone analysis (Moss et al., 2004) indicates an age of ≤3 Ma, suggesting a possible correlation with the onset of major Northern Hemisphere glaciation at ~2.7 Ma (Shackleton and Kennett, 1975; Lisiecki and Raymo, 2005). Ice-

sheet growth in the Northern Hemisphere may also have induced drier global climate that in turn reduced river runoff and terrigenous clastic input delivered to the NCB. Alternatively, SB-PL1 could correlate with the mid-Pleistocene (~1.4 Ma) transition of dominant periodicity of glacial cycles from 41,000 to ~100,000 years (Lisiecki and Raymo, 2007). Perhaps this decrease in the frequency of cyclicity of climatic changes also induced a relative reduction in continental erosion and terrigenous sediment input to the NWS. As an alternative, increase in the Indonesian Throughflow at 1.6 Ma might also have modified climate in the hinterland, also influencing siliciclastic delivery to the adjacent shelf (Gallagher et al., 2009).

2.7.4. Impact of Falling Mid-Miocene Sea level

Relative sea-level fall during the middle Miocene is unlikely to have been the cause of the increased terrigenous sediment influx, but on the other hand it is likely to have been a major driver of enhanced delta progradation and siliciclastic shelf building across the preexisting heterozoan carbonate shelf of the NCB (see discussion of accommodation vs. supply as drivers of cross-shelf progradation of Porebski and Steel, 2006). Our correlation of the vertical position (degradation and aggradation) of the shelf-edge in the profile (Figure 2.5) with the long-term global sea level fall and subsequent rise during the late-middle to late Miocene (Figure 2.15) supports this hypothesis. Assuming this correlation with the sea-level curve to be correct, it is likely that each delta lobe was deposited and transgressed within ~100 ky periods (20 delta lobes deposited in a ~2.9 My interval between SB-MMK and SB-LM1, probably including some hiatuses, Table 2.1). Likewise, the cumulative progradation of delta lobes (Figures 2.7 and 2.13) to

the shelf-edge and the associated progradation of the shelf-edge during deposition of lobes 6 through 15 (Figure 2.6) may be linked to this long-term global sea-level fall during the late-middle Miocene (Haq et al., 1987). Similarly the long-term backstepping of lobes 16-20 may result from the subsequent sea-level rise that started in the late Miocene (Figures 2.14 and 2.15). The cumulative magnitude for shelf-edge aggradation/degradation (up to 280 m, Figure 2.15) is expected to be larger than the magnitudes of eustatic sea-level change because the former results from a combination of subsidence and global sea-level change.

On the modern arid Pilbara Coast and its adjacent shelf, tidal flat evaporites and deltas grade basinward into carbonate sands and gravels, with a transition zone of mixed terrigenous and carbonate gravels, sands, and mud (Semeniuk, 1996; James et al., 2004). Using this modern highstand coastal facies distribution as an analog, a basinward shift of coastal siliciclastic facies as a consequence of relative base-level fall, coupled with climatically enhanced erosion in the hinterland, could have driven the observed NCB siliciclastic progradation.

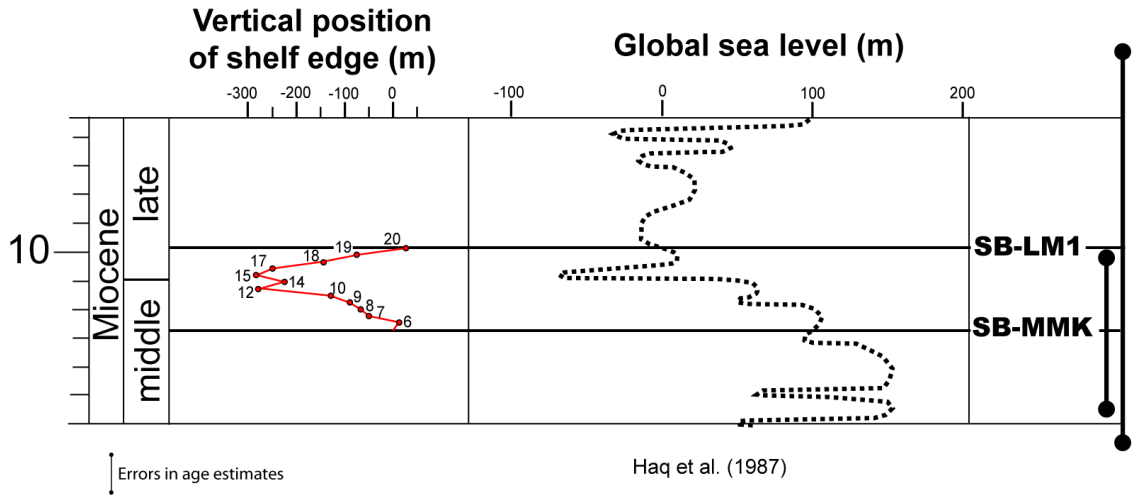

Figure 2.15. Comparison of shelf-edge aggradation/degradation (changes in vertical position of the shelf-edge) to one postulated eustatic curve (Haq et al., 1987). Notice interval between SB-MMK (base of siliciclastics) and SB-LM1, which encompasses deposition of lobes 1-20. This comparison shows a close match between shelf-edge aggradation/degradation and global sea level during deposition of lobes 1-20.

This scenario is somewhat analogous to the reciprocal sedimentation model of Meissner (1972), in which carbonates accumulate on the shelf during sea-level highstand, whereas siliciclastics bypass and accumulate in the deep-water basin during sea level lowstand, with one important difference. In the NCB, individual delta clinoforms reach up to 100 m in height, implying similar minimum water depths on the shelf. On this mixed carbonate-siliciclastic shelf, siliciclastics were able to accumulate widely on the shelf, instead of mostly bypassing to deep water, as occurred in the Permian Basin of West Texas (Meissner, 1972). This may have been a result of availability of accommodation space above the preexisting cool-water carbonate "distally steepened ramp" (Pomar, 2001; Cathro et al., 2003), which differs from the flat-topped, i.e., platform margin aggrading to sea level, carbonate shelf used by Meissner (1972) to postulate the reciprocal model. Indeed, Cathro et al. (2003) have documented paleo-water depths in the NCB of up to 100 m for this quartz-sand rich interval, suggesting abundant accommodation space for deposition of deltaic clastics.

The fluvial sources of the NCB Miocene-Pliocene deltaic systems may have been antecedents of the modern Fortescue and DeGrey rivers of the present Pilbara Coast (Figure 2.1A); these rivers may have been active since the Valanginian (Romine et al., 1997). Modern onshore elevation and shelf bathymetry data (Webster and Petkovic, 2005) both suggest that these rivers would incise and deliver terrigenous sediment northward, directly towards the NCB, during sea-level lowstands.

2.7.5. Role of Tectonism

Tectonic uplift and the creation of source-area relief is also a well known way to increase terrigenous clastic sediment yield. Ongoing collision between the Banda Arc and Australia during the late Miocene has occurred as a result of convergence between the Indo-Australian and Pacific plates (Veevers et al., 1991). Cathro and Karner (2006) concluded that this collision has caused pulses of localized uplift (up to 75 m) in response to inversion of Mesozoic structures in the NCB since ~17 Ma (Figures 2.1A and 2.12). The localized nature and limited amount of relief on inversion structures caused by this ongoing collision make such a tectonic event an unlikely cause for major middle-Miocene to Pliocene increase in siliciclastic sediment supply in the NCB.

2.8. CONCLUSIONS

Mapping of the toplap surfaces above the clinoform sets that correlate to the quartz-sands of the Bare Formation reveals strike-elongated to dip-elongated sedimentary planview morphologies interpreted as delta lobes. Twenty-seven lobes were mapped. Most lobes show evidence of some degree of wave reworking.

Delta lobes show greater migration distances along strike during relative sea level rise than during fall. These delta lobes show a long-term northeastward migration trend likely caused by steering of the fluvial source by uplift pulses of an inversion structure located landward (southeast) of the delta. The cumulative delta lobe progradation chart shows long-term progradation followed by long-term backstepping. This progradation-backstepping pattern can be correlated to the global sea level curve of Haq et al. (1987)

using our estimated age for the base of the siliciclastics and the vertical position of the shelf-edge corresponding to those delta lobes.

The late middle Miocene to Pliocene delta system in the NCB reached the paleo-shelf edge, and likely delivered quartz-sands to the adjacent slope and basin. The direct mechanism for increasing sediment supply rates on the NCB shelf is unclear; a combination of forcing mechanisms was likely involved. First, progradation was likely initiated by long-term relative sea-level fall, likely accompanying global cooling and aridification, starting in the late middle Miocene. Subsequent backstepping suggests late Miocene-Pliocene sea-level rise, in line with the global eustatic curve. Second, progradation distances of individual delta lobes, up to 16 km, and the larger areas covered by these lobes (when compared to modern deltas in the area), suggest that much higher volumes of siliciclastics were delivered to the shelf by one or more rivers during the late-middle Miocene to Pliocene relative to the Pleistocene-Present. During times of siliciclastic progradation in the NCB, increased continental erosion that allowed these delta lobes to prograde to the shelf-edge during long-term sea-level fall was a response to climatic conditions that do not prevail today. Either climate in Western Australia was more humid than at present, allowing greater river runoff, or it was simply changing to more arid conditions, impacting vegetation cover while retaining sufficient rainfall, possibly seasonal, to generate erosion. With less vegetation, erosion in the hinterland and terrigenous clastic sediment input to the shelf could have increased significantly.

Chapter 3: Miocene Shelf-Edge Deltas and their Impact on Deepwater Slope Progradation and Morphology, Northwest Shelf of Australia

3.1. INTRODUCTION

The Northern Carnarvon Basin (NCB) is located on the Northwest Shelf of Australia (NWS). A wealth of industry subsurface data has been collected from oil and gas exploration and production efforts in the four sub-basins of the NCB: Exmouth, Barrow, Dampier, and Beagle (Figure 3.1). The data used for this study cover the shelf to slope of successive middle to late Miocene margins that occur below the modern continental shelf and slope of the Dampier Sub-basin (Figure 3.1A). Clinoform sets interpreted as shelf and self-edge deltas were deposited on paleoshelves associated with these margins.

The goal of this study is to investigate the effects of shelf-edge deltas on margin progradation and on the characteristics of the adjacent slope, addressing the following questions:

- How sensitive are shelf-margin progradation rates, from areas along-strike where shelf-edge deltas were active to areas where these deltas were absent?
- Are the slope types developed in front of shelf-edge deltas different than the slopes developed away from the main deltaic fairway?
- How does the longer-term shelf-edge trajectory change along-strike, from areas where shelf-edge deltas dominate to where other coeval depositional systems operated?

- Do observed slope incisions serve as conduits for sediment gravity flows sourced from shelf-edge delta fronts?

Chapter 2 results documented a series of upper-middle Miocene to Pliocene delta lobes that prograded across the coeval NCB shelf. The delta interpretation is based on the correlation between Bare Formation sandstones and delta-scale clinoform sets, many of which are revealed by 3D seismic data to be lobate shaped and composed of 40-100 m-high foresets. These clinoform heights are within the normal range for shelf deltas (10s of m) to shelf-edge deltas (≤150 m; Steel et al., 2008). Similar sets of high-angle, prograding clinoforms near or at the shelf edge have been documented using seismic data from the Quaternary Gulf of Mexico (Suter and Berryhill, 1985) and the Tertiary succession offshore Norway (Bullimore et al., 2005).

Shelf-edge or shelf-margin deltas have been shown to be a major driver of shelf margin and slope progradation (Steel at al., 2000). Criteria used to recognize shelf-edge deltas include clinoform heights of up to 150 m and clinoform lengths up to tens of kilometers (Porebski and Steel, 2003). Most of the delta lobes mapped are >40 meters high (Chapter 2) and are located at or near the shelf break: the distance between their distal end and the shelf break ranges between 0 and 22 km. More importantly, our results show that a group of these deltas located ~10 km or closer to their coeval shelf edges contribute to significantly higher shelf margin progradation distances and rates.

The contribution that shelf-edge deltas, a primary source of sediment supply to deep-water settings, have made to shelf-margin growth in the NCB is assessed in this paper by evaluating the longer-term shelf-edge trajectory with respect to the progradation distances of delta lobes. In this study, the progradation fairway of these delta lobes defines the shoreline trajectory (Helland-Hansen and Hampson, 2009). In contrast to the shoreline trajectory, the shelf-edge trajectory corresponds to the pathway formed by

successive shelf breaks over time periods ranging between several hundred thousand years to several million years in response to the changing interaction between relative sea-level and sediment supply (Steel and Olsen, 2002; Helland-Hansen and Hampson, 2009). In this study, I have quantified shelf-edge progradation in three dip-oriented profiles over a time interval of ~3 My and compared to the location/trajectory of the mapped deltas to assess the contribution these deltas made to margin growth and to the along-strike variability of the shelf margin.

The processes that initiate slope incisions have long been a source of investigation (Reynolds and Gorsline, 1988; Piper et al., 1990; Fulthorpe et al., 2000; Pratson et al., 2007; Fedele et al., 2009). Gullies were a prominent feature of the NCB slope region in the early-middle Miocene (Cathro et al., 2003), before deltas reached the shelf-edge. The initiation of the gullies in the NCB is therefore not tied to these deltas. However, our results suggest that deltas arriving at the shelf edge modify the dimensions of the existing slope incisions while using them as conduits for sediment gravity flows sourced from the delta front.

This study provides a unique view of the along-strike variability of sediment supply on a prograding Neogene shelf-margin using a combination of large, high-quality 3D seismic data with a dense 2D seismic grid and well data. This study also contributes to current knowledge of the NCB with new insights for the prediction of deep-water deposits sourced from shelf-edge deltas during the middle to late Miocene. These results also help in the understanding of the impact of shelf-edge deltas on shelf-margin progradation rates, shelf-edge trajectory, and the adjacent gullied slope.

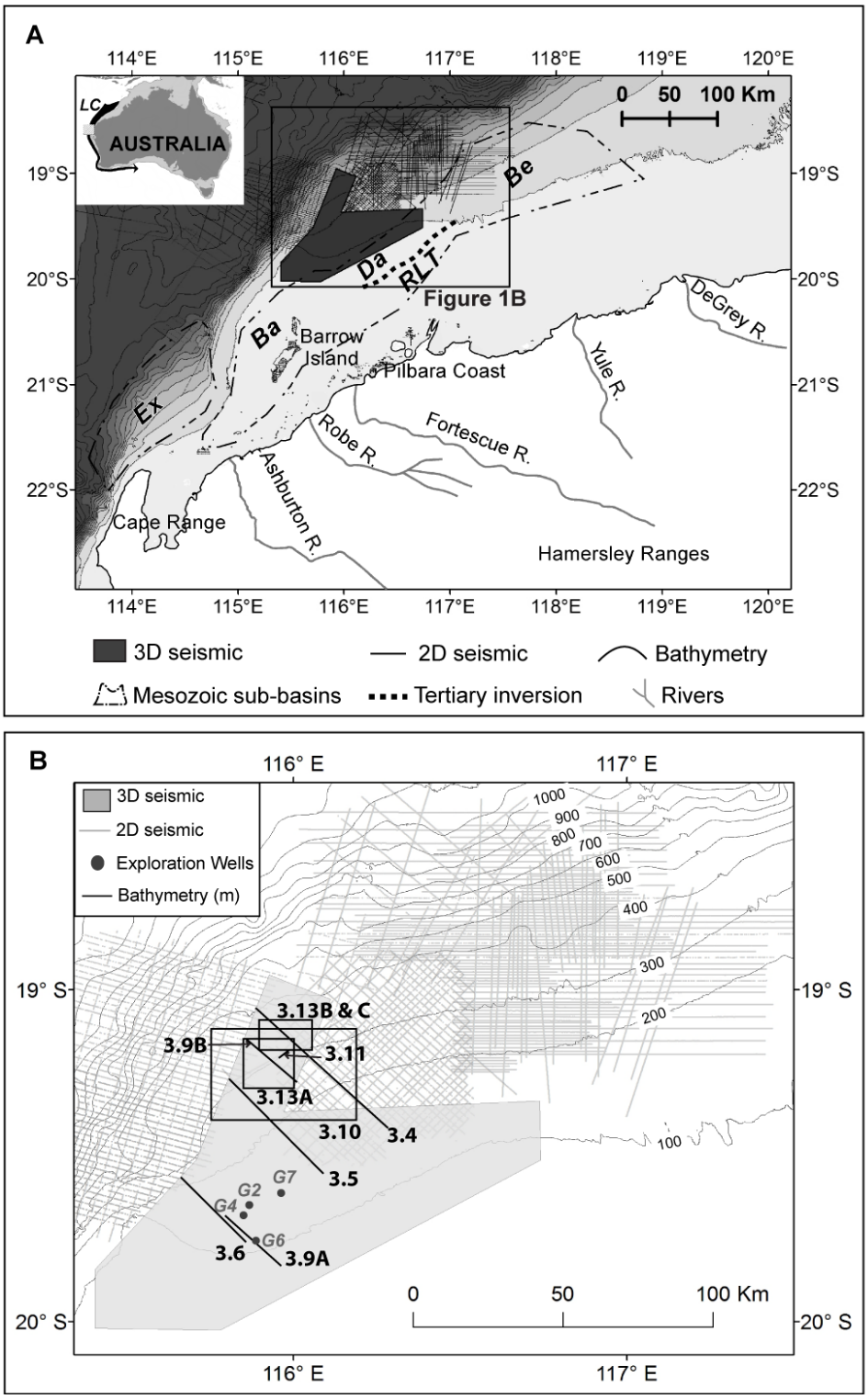

Figure 3.1: **(A)** Available seismic data, Mesozoic sub-basins offshore (*Ex*=Exmouth,

Ba=Barrow, *Da*=Dampier, *Be*=Beagle; Stagg and Colwell, 1994; Romine et al., 1997; Cathro et al., 2003), and modern rivers draining the Hamersley Ranges (Semeniuk, 1996). Bathymetric contours are at 100 m intervals. Inset map shows a box with the location of the study area with respect to the Australian continent and the Leeuwin Current (LC), which flows along the western Australia shelf edge (Tomczac and Godfrey, 1994). **(B)** Area covered by 3D and 2D seismic data used in this study. Exploration wells (G2=Goodwyn_2, G4=Goodwyn_4, G6=Goodwyn_6, and G7=Goodwyn_7) were used to obtain age estimates and for seismic facies correlation to lithostratigraphy (after Moss et al., 2004). Location of figures 3.4, 3.7, 3.8, 3.9, and 3.10 are also shown.

3.2. GEOLOGIC SETTING

Formation of the NCB began with Late Permian rifting (Baillie et al., 1994; Bradshaw et al., 1988). Triassic-Cretaceous rifting built and reactivated the four component sub-basins (Baillie et al., 1994; Bradshaw et al., 1988; Veevers et al., 1991; Figure 3.1A). Thermal subsidence has dominated since the Early Cretaceous (Veevers et al., 1991; Baillie et al., 1994; Driscoll and Karner, 1998; Cathro and Karner, 2006). Collision between the Banda Arc and Australia began in the late Miocene (Veevers et al., 1991; Baillie et al., 1994; Lee and Lawver, 1995; Driscoll and Karner, 1998; Hull and Griffiths, 2002; Pryer et al., 2002; Cathro and Karner, 2006) and has produced localized uplift events (reliefs up to 75 m) on the Rosemary-Legendre structural trend (Figure 3.1A; Cathro and Karner 2006).

Dominant sediment type in the NCB changed from siliciclastics to carbonates during the Cenozoic (Apthorpe, 1988) as the Australian Plate drifted northward from between 36° and 40° south to its present location within the tropical zone at 18° and 22° south (Veevers et al., 1991; Lawver et al., 1999). After carbonate sedimentation had been established, a substantial pulse of siliciclastic progradation occurred through the late-middle and late Miocene, probably as a result of long-term global sea-level fall and

climatic change (Figure 3.2). This siliciclastic unit, the focus of the present study, has been recognized in offshore industry wells as the Bare Formation (Figure 3.2). Chapter 2 results indicate that these siliciclastics record active delta systems and corresponding margin growth. The point-source nature of this delta complex produced significant three-dimensional variability in the resultant shelf and slope stratigraphy. That variability is the focus of this paper.

3.3. DATA AND METHODS

The data used for this study include large, high-quality 3D seismic volumes (area 7,500 km2) and dense 2D seismic data (55,700 line-km) with a vertical resolution of ~10-15 m in the study interval, as well as industry well reports and wireline logs. The data are ideal for addressing the questions raised above because they allow detailed mapping of stratigraphic surfaces over a large portion of the paleo-shelf and slope. The 3D data also reveal the variability in the character and dimensions of slope incisions. Well data provide estimated geologic ages. This large seismic dataset allows: 1) construction of several dip-oriented profiles for calculation of progradation rates and shelf-edge trajectories at different along-strike locations, 2) investigation of the along-strike variability of depositional systems and how this affects the shelf-edge trajectory.

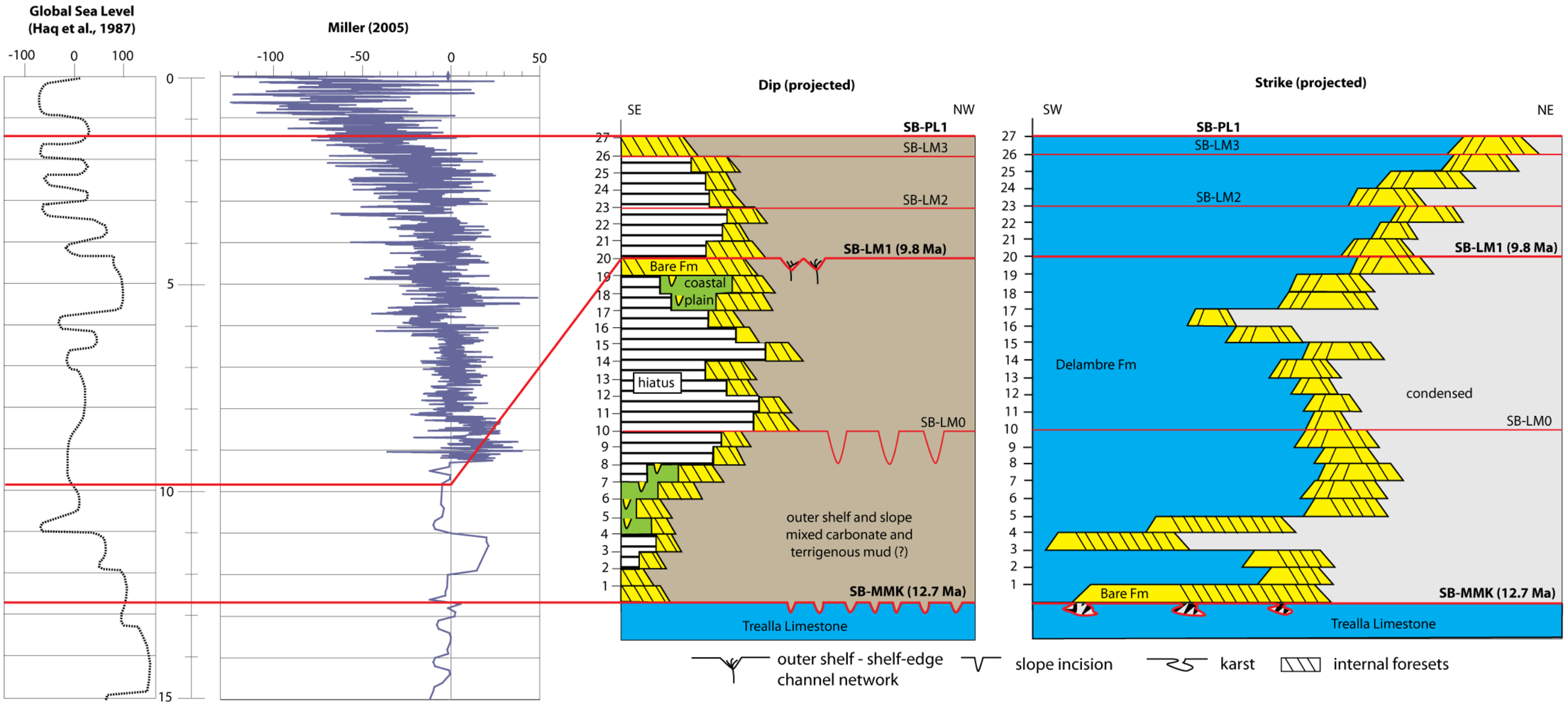

Figure 3.2: Stratigraphic chart reflecting dip- and strike-oriented deposition of the siliciclastics composing the Bare Formation in the NCB. Sequence boundaries derived from this study are calibrated to the Berggren et al. (1995) timescale. Sequence boundaries SB-MMK and SB-PL1 represent the base and top, respectively, of siliciclastic progradation in the NCB (Bare Formation). Potential errors in estimated ages are shown in Table 2.1.

3.3.1. Sequence Boundaries

Five sequence boundaries have been mapped in the 2D and 3D seismic data using Seisworks®. These key stratigraphic surfaces have been interpreted using identified seismic terminations (onlap, truncation, and toplap; Vail, 1987). Seismic to well ties have been obtained for wells Goodwyn_2, Goodwyn_4, Goodwyn_6, and Goodwyn_7 using synthetic seismograms created in Synthetics (Geoframe®) and Syntool (Landmark®) using density and acoustic velocity logs from wireline log data. These seismograms have been calibrated using checkshot surveys. Age estimates (average along with minimum and maximum, Table 3.1) for the interpreted sequence boundaries (Figure 3.2) are based on Cathro (2002) and Moss et al. (2004), who originally defined foraminiferal zones in these exploration wells within our study area. The error bars for these estimated ages are on the order of 10^6 years.

3.3.2. Delta lobe and shelf-edge trajectories

Three dip-oriented (with respect to shelf gradient) seismic profiles (spacing 25-37 km) are used to illustrate the along-strike changes in shelf-edge trajectory (Figure 3.4) and their relationship to the temporal and spatial distribution of deltas near or at the shelf edge. The southern and northern profiles were selected to represent end-member cases between areas where deltas did not reach the area adjacent to the shelf edge (≤ 10 km from the shelf break) to areas with repeated shelf-edge deltaic deposition, respectively. Shelf-edge locations were defined visually as the first point of major increase in shelf gradient coeval with the end of deposition of individual delta lobes or groups of lobes. These shelf-breaks have been plotted on contour maps of sequence boundaries to define

the shelf-edge for these surfaces in plan-view, whereas the shelf-edge positions recognized in the cross-sections defined the shelf-edge trajectory. Shelf-edge progradation during intervals of delta progradation has been measured on a dip-oriented profile that intersects many of the mapped delta lobes (North Profile, Figure 3.4). These progradation measurements correspond to the horizontal component of shelf-edge migration segments (Figure 3.4). The distances between the most basinward points of successive siliciclastic clinoform sets (lobes), along depositional dip, were measured using their map view extent (Figure 3.3), using the oldest lobe as the initial reference point.

Spectral decomposition volumes were used to help the identification of subtle geomorphologic features, e.g., shelf channels, that may not be evident in the regular multifrequency seismic volume (Partyka et al., 1999), but that helped interpretation of depositional systems in plan view. The frequency that showed the best images for depositional features was 50 HZ. Horizon slicing through this volume was used to obtain a geomorphic image of the paleo shelf-slope-basin seascape.

Three-dimensional oblique-views of seismic profiles intersecting deltas lobes and mapped stratigraphic surfaces were built using GeoProbe®. These views allow us to compare the dimensions of slope incisions coeval with outer-shelf deltas with those coeval with deltas that were near or at the shelf-edge. The distance from any delta lobe to its coeval shelf edge was measured as the horizontal distance between the basinward end of that lobe and the coeval shelf edge.

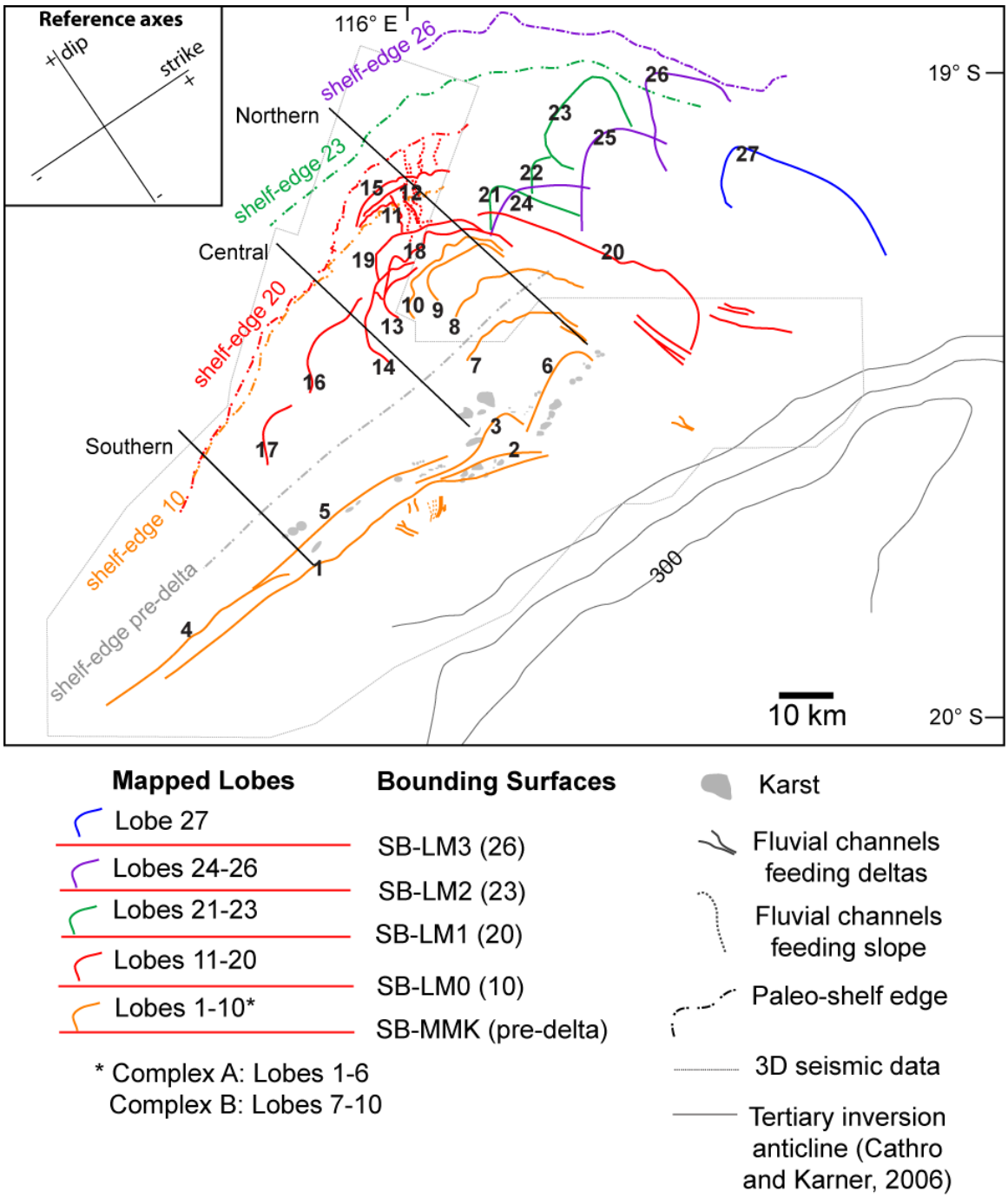

Figure 3.3. Mapped delta lobes and positions of paleoshelf edges at the ends of deltaic progradation pulses between SB-MMK and SB-LM3. The outline of each lobe corresponds to the rollover of the youngest clinoform, or top bounding unconformity, of the mapped clinoform set representing that lobe. The paleoshelf edges are numbered according to the last lobe deposited beneath

that paleo-shelf profile, and allow association of shelf-edge geometry with delta progradation. Note Tertiary inversion anticline in the southwest, contour interval 100 milliseconds (Cathro and Karner, 2006). Interpreted karst underlies lobes 1-6. Interpreted fluvial channels within the siliciclastic interval are shown in colors corresponding to the interval within which they occurred. Inset in the upper left corner shows reference axes for changes in position of delta lobes along strike and dip. Note positions of the three profiles shown in Figures 3.4, 3.5, and 3.6.

Sequence Boundary	Seismic terminations	Estimated age (Ma)
SB-PL1	Below: toplap, Above: onlap, downlap	1.5 +/- 1.5
SB-LM3	Below: truncation, toplap Above: onlap, downlap	6.1 +/- 4.2
SB-LM2	Below: toplap, Above: onlap, downlap	7.1 +/- 4.1
SB-LM1	Below: truncation, toplap Above: onlap, downlap	9.8 +/- 6.8
SB-LM0	Below: truncation Above: onlap, downlap	9.8 +/- 6.8
SB-MMK	Below: truncation, Above: onlap, downlap	12.7 +/- 2.5
SB-MM	Below: toplap Above: onlap, downlap	12.7 +/- 2.5

Table 3.1. Interpreted sequence boundaries, characteristic seismic terminations observed above and/or below these surfaces, and estimated ages (after Moss et al., 2004).

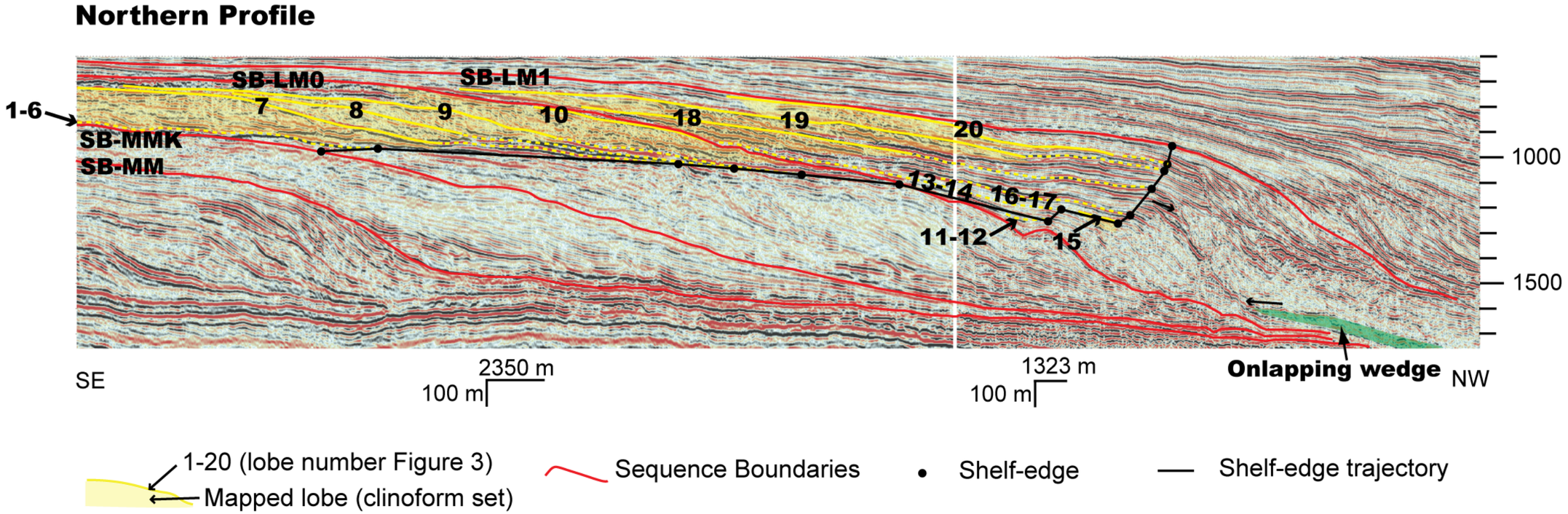

Figure 3.4. Northern dip-oriented seismic profile. Delta lobes (highlighted in yellow) or time lines corresponding to lobes located outside the plane of the profile (dashed yellow lines), shelf-edge positions at times of lobe deposition (small black circles), and shelf-edge trajectory (black line). Shelf-edge trajectory is summarized in Table 3.5. See Figures 3.1 and 3.3 for profile locations.

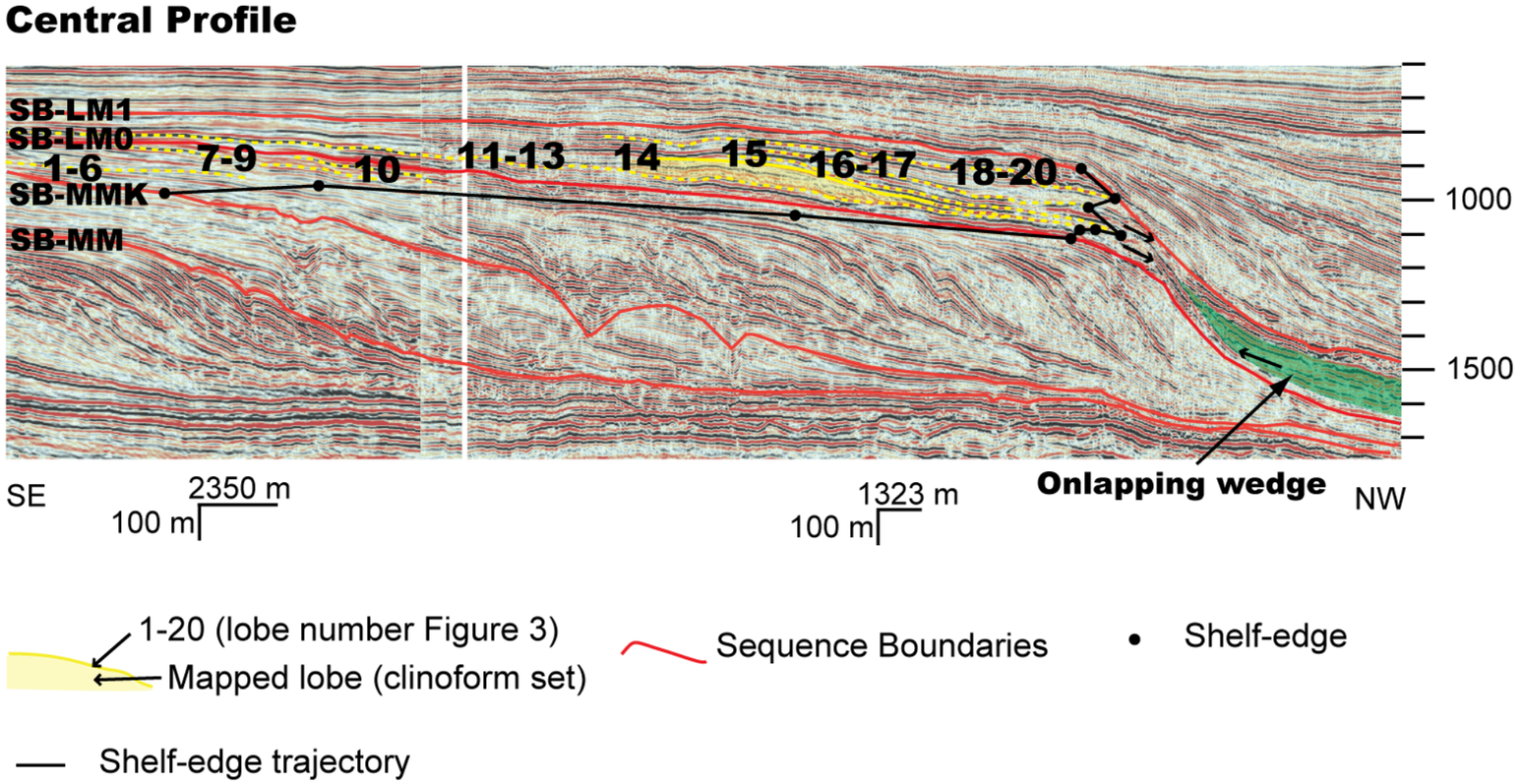

Figure 3.5. Central dip-oriented seismic profile showing delta lobes (highlighted in yellow) or time lines corresponding to lobes located outside the plane of the profile (dashed yellow lines), shelf-edge positions at times of lobe deposition (small black circles), and shelf-edge trajectory (black line). Shelf-edge trajectory is summarized in Table 3.4. See Figures 3.1 and 3.3 for profile location.

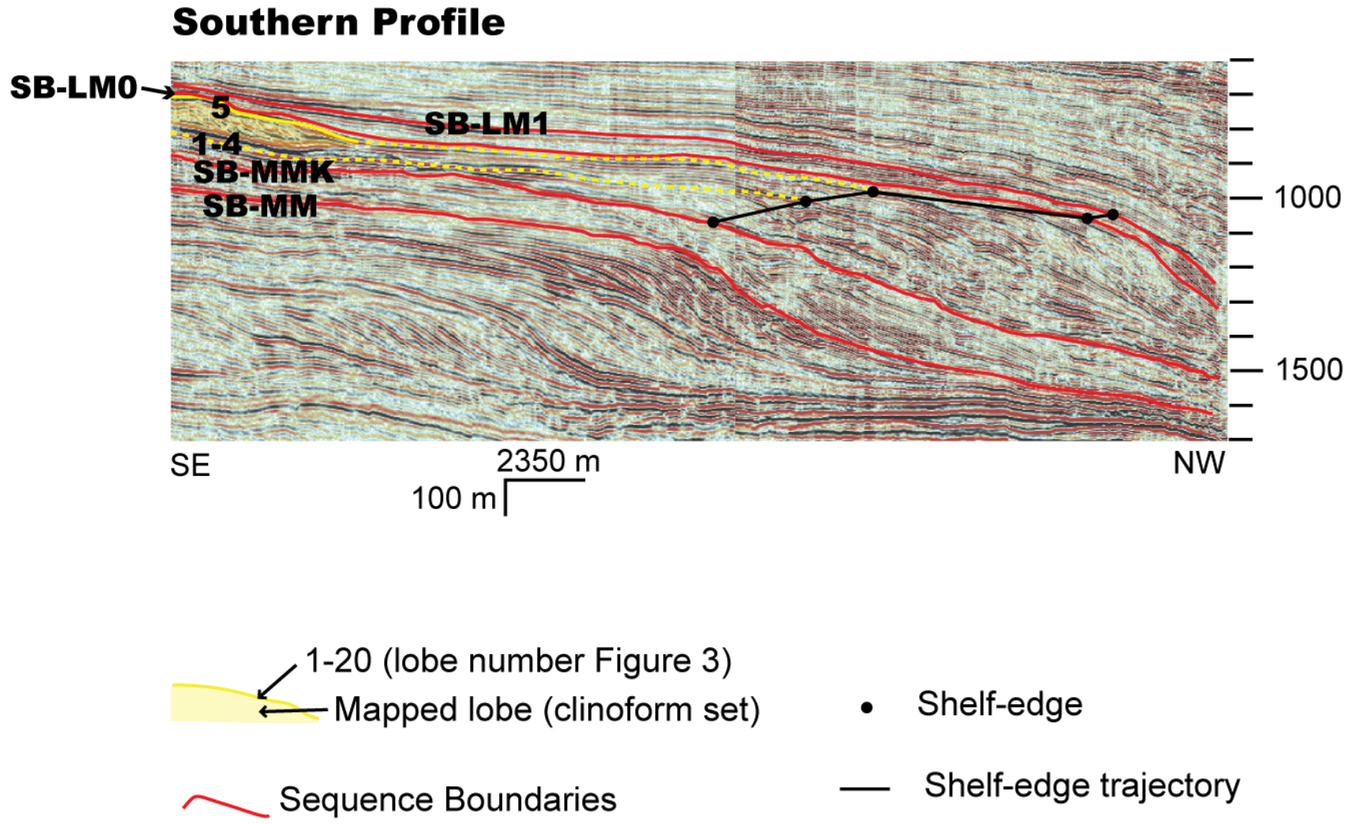

Figure 3.6. Southern dip-oriented seismic profile showing delta lobes (highlighted in yellow) or time lines corresponding to lobes located outside the plane of the profile (dashed yellow lines), shelf-edge positions at times of lobe deposition (small black circles), and shelf-edge trajectory (black line). Shelf-edge trajectory is summarized in Table 3.3. See Figures 3.1 and 3.3 for profile location.

3.4. Analysis and Results

3.4.1. Temporal and Spatial (along-strike) Variability of Shelf-edge Migration

Shelf-edge progradation increased significantly with the beginning of deltaic progradation across paleo-shelves between SB-MMK and SB-LM0 (Figure 3.7). This increase is well imaged on all three selected profiles (Figures 3.4, 3.5, and 3.6) although the increase is more dramatic in the "northern" (Figure 3.4) and "central" (Figure 3.5) profiles, where the shelf-edge prograded 23 and 27 km respectively, than on the "southern" (Figure 3.6) profile where shelf-edge progradation was only 11 km. Shelf-edge progradation distance then decreased to ~1 km between SB-LM0 and SB-LM1 in the southern and central profiles, whereas it decreased to 11 km in the northern profile for the same interval (Figures 3.4, 3.5, 3.6, and 3.7).

A plot of shelf-edge progradation (northern profile) versus delta lobe progradation shows that the former increased when delta lobes actively prograded on the shelf and decreased when delta lobes backstepped (Figure 3.8). Distances between these delta lobes (1 to 20) and the corresponding shelf-edges range from being 0 km (i.e., delta at the shelf edge) to 22 km landward of the shelf edge (Table 3.2). Total progradation between SB-MMK and SB-LM1 increases from south to north, i.e. 13 km in the southern (Figure 3.6), 27 km in the central (Figure 3.5), and 34 km in the northern profile (Figure 3.4). Progradation rates between SB-MMK and SB-LM1, including deposition of lobes 1-20, are 11.8 km/Ma in the northern profile, 9.2 km/Ma in the central profile, and 4.5 km/Ma in the southern profile.

3.4.2. Along-strike Variability of Slope Character

Shelf margin growth seen along the northern profile between SB-LM0 and SB-LM1 produced a basinward-thickening prograding wedge. Though there are a few surfaces that truncate underlying strata, there is also an onlapping wedge (up to 50 m thick, Figure 3.4). In contrast, the shelf margin and slope between SB-LM0 and SB-LM1 in the central profile, 27 km south of the northern profile, shows clear truncation of strata against SB-LM1 at the shelf-edge and a thick (up to 130 m) apron that onlapped the slope between SB-LM0 and SB-LM1 (Figure 3.5). The southern profile is not long enough to show the full extent of the slope between SB-LM0 and SB-LM1 (Figure 3.6).

3.4.3. Along-Strike Variability of the Shelf-edge Trajectory

3.4.3.1. Between SB-MMK and SB-LMO:

The shelf-edge trajectory between SB-MMK and SB-LM0 is similar on all three profiles (Figures 3.4, 3.5, and 3.6). The shelf-edge trajectory rose during the time interval covering deposition of lobes 1 to 6, but fell slightly during deposition of lobes 7-10.

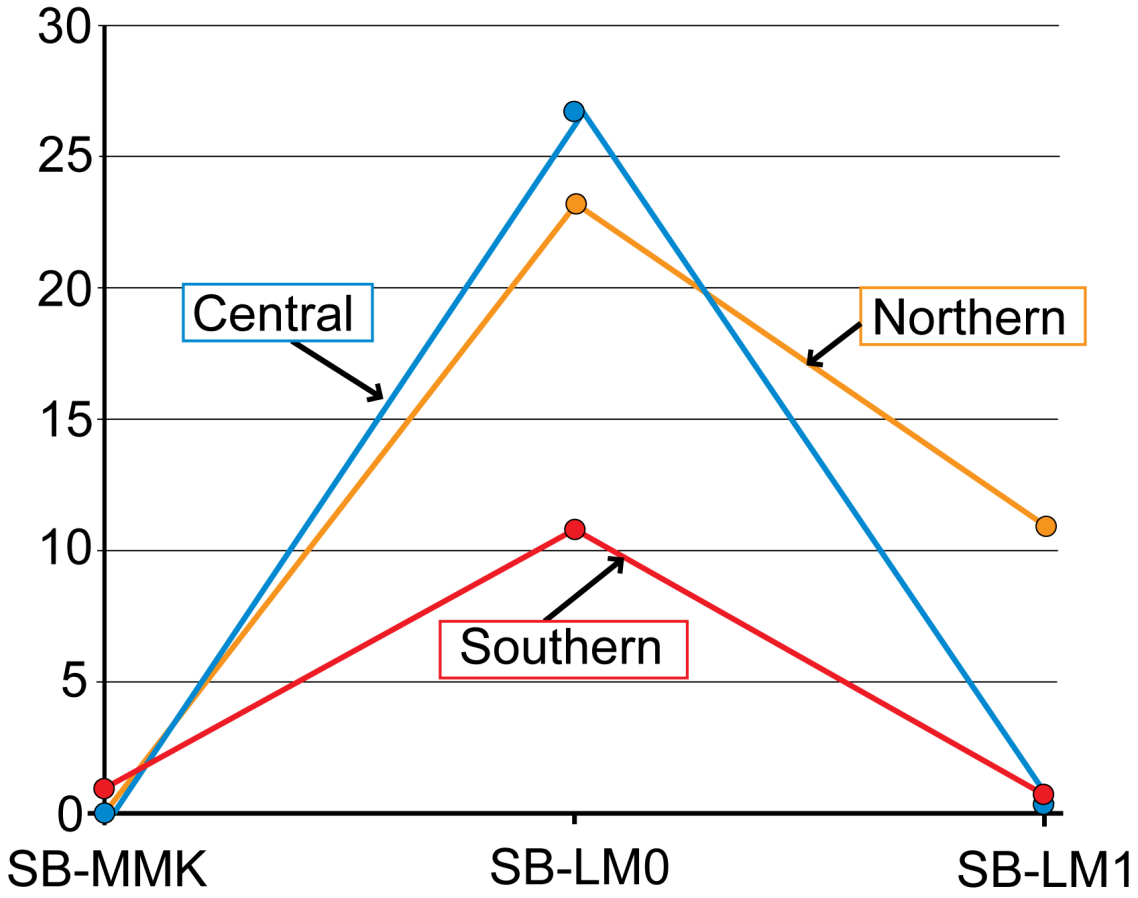

Figure 3.7. Plots of shelf-edge progradation distances. Observe that the location of maximum progradation switches from the Central Profile at SB-LM0 time to the North Profile at SB-LM1 time.

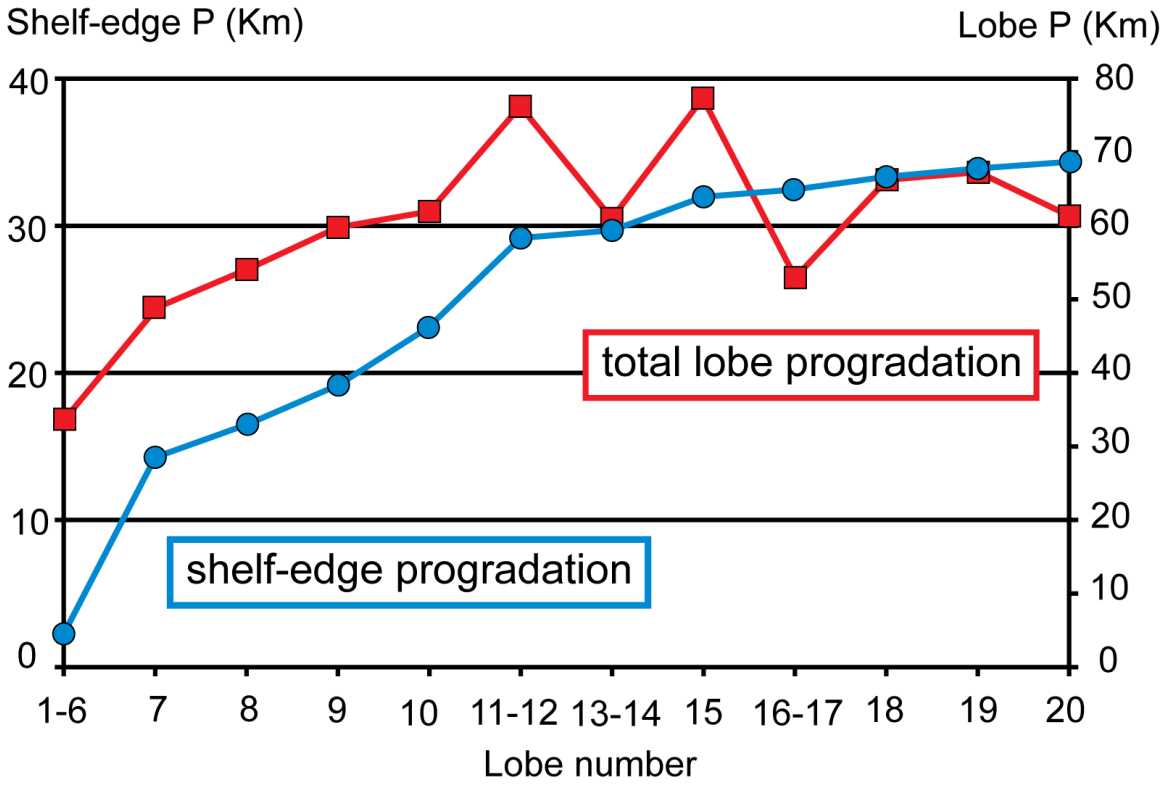

Figure 3.8. Delta lobes and shelf-edge progradation. The red line corresponds to cumulative progradation/backstepping of delta lobes in Figure 3.3. The blue line shows shelf-edge progradation during deposition of specific lobes or groups of lobes (see horizontal axis). Rate of shelf-edge progradation is higher when delta lobes prograded larger distances, this rate decreases when delta lobes backstep.

Delta Lobe	Distance to Shelf Edge (Km)
1	18.3
2	22.4
3	17.4
4	19.5
5	14.8
6	14.8
7	10.7
8	8.6
9	6.5
10	5.2
11	0.0
12	0.0
13	8.0
14	4.3
15	0.0
16	4.0
17	3.2
18	10.0
19	6.2
20	1.6

Table 3.2: Measured distance from distal end of delta lobe to the coeval shelf edge.

South Profile			
Shelf Break Point (lobe)	**Progradation (km)**	**Aggradation (m)**	**Trajectory**
1-4	1	87	rising
5-6	4	8	rising
7-10	6	-71	falling
11-SB-LM1	1	9	rising

Table 3.3: Summary of shelf-edge trajectory in South Profile (Figure 3.6)

Central Profile			
Shelf Break Point (lobe)	**Progradation (km)**	**Aggradation (m)**	**Trajectory**
1-6	5	22	rising
7-9	14	-87	falling
10	8	-68	falling
11-13	0	26	rising
14	0	4	rising
15	0	-16	falling
16-17	-1	69	retrogradational
18-20	1	26	rising
SB-LM1	-1	88	retrogradational

Table 3.4: Summary of shelf-edge trajectory in Central Profile (Figure 3.5)

North Profile			
Shelf Break Point (lobe)	**Progradation (km)**	**Aggradation (m)**	**SE Trajectory**
1-6	2.3	11	rising
7	12.0	-61	falling
8	2.2	-18	falling
9	2.7	-24	falling
10	3.9	-38	falling
11-12	6.0	-143	falling
13-14	0.5	48	rising
15	2.3	-56	falling
16-17	0.5	32	rising
18	0.9	105	rising
19	0.6	72	rising
20	0.2	20	aggradational
SB-LM1	0.1	80	aggradational

Table 3.5: Summary of shelf-edge trajectory in North Profile (Figure 3.4)

3.4.3.2. Between SB-LM0 and SB-LM1:

The shelf-edge trajectory between SB-LM0 and SB-LM1 varies between the northern, central, and southern profiles (Figures 3.4, 3.5, and 3.6). The southern profile, which does not intersect delta lobes 11-20, exhibits a simple rising trajectory between SB-LM0 and SB-LM1 (Table 3.3, Figure 3.6). The central profile displays a rising trajectory between times of deposition of lobes 11 through 14, then a slight fall when lobe 15 was deposited. The trajectory was retrogradational (rising landwards) during times of lobes 16 and 17, rising for 18 and 19 and retrogradational while lobe 20 was deposited and until formation of SB-LM1 (Table 3.4, Figure 3.5). The northern profile shows a falling trajectory for the shelf-edge coeval with delta lobes 11 to 12, a rising trajectory during deposition of lobes 13 and 14, falling again during lobe 15, then rising for lobes 16 to 19, and aggradational (or near vertical) for lobe 20 and until the development of SB-LM1 (Table 3.5, Figure 3.4).

3.4.4. Impact of Shelf-edge Deltas on Slope Incisions

The dimensions and infill character of slope incisions vary both spatially and temporally. Slope incisions coeval with lobes 1-6 are ~ 400 m wide and 20 m deep in all three regions. These dimensions increase between the time of deposition of delta lobes 10 and 11, when deltas has reached the shelf edge, particularly in the northern region. Slope incisions at this time reached 700 m wide and 25 m deep in the central area that had a few deltas near the shelf edge (e.g. lobes 14 and 16; Figures 3.3, 3.5, and 3.9B) and >1 km wide and 100 m deep in the north (SB-LM0, Figures 3.10 and 3.9B).

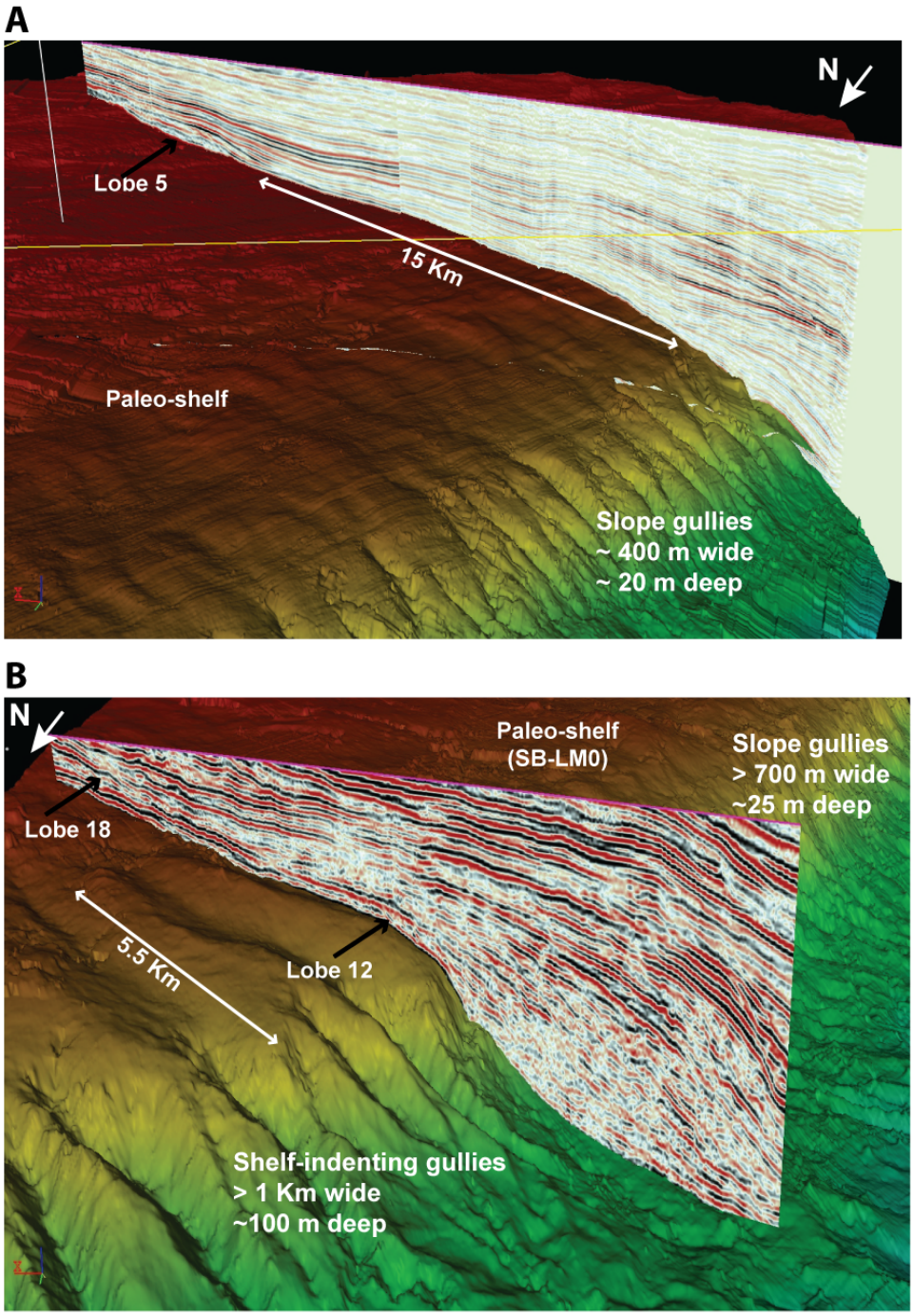

Figure 3.9. Oblique 3D views, looking from the northwest, of seismic profiles and stratigraphic surfaces that extend from paleo-shelf downslope to the basin. Warm colors represent shallower water and cool colors deeper water. A) Slope incisions during deposition of lobes 1-6 were smaller than in B). B)

Slope incisions during deposition of lobes 11-15. Note differences in dimensions of slope incisions along strike from northern area (where shelf-edge deltas where deposited, e.g. lobe 12) compared to southern area represented in A). See location of vertical profiles in Figure 3.1B.

3.4.5. Complex Geologic History of Slope Incisions: Mixed Deposition and Erosion

Seismic reflections within the infill of these V-shaped slope incisions are commonly aggradational and parallel to gully flanks converging towards the edges of these incisions (Figure 3.11). However, there can also be truncations within the fill. In such cases, the lowermost reflections are truncated by an overlying surface that creates a new channel with parallel, overlying reflections. Ultimately, the topmost fill reflections are truncated by a surface coeval with the top of a delta lobe. Estimated total aggradation between SB-LM0 and the top boundary of lobe 12 as shown in Figure 3.11 is approximately 153 m. Estimated total thickness truncated between the same surfaces in Figure 3.11 is 129 m.

3.5. DISCUSSION

3.5.1. Effect Of Shelf-Edge Deltas On Shelf-Edge Migration

3.5.1.1. Shelf-edge Deltas and their Impact on Temporal Along-strike Variability of Shelf-edge Progradation

Progradation rates of margin clinoforms are commonly linked to sediment supply (Carvajal et al., 2009); sediment supply, in turn, depends on the size of the sediment

drainage area as well as relief and climate. In the current results I show that margin progradation rates vary significantly along strike as a function of location of active delta lobes.

Higher shelf-edge progradation rates are observed in the area where shelf-edge deltas accumulated (northern area, Figures 3.3 and 3.4). Shelf-edge progradation rates increased significantly from 4.5 km/Ma in the southern profile (Figure 3.6), where deltas where deposited >14 km landward of the shelf-edge, to 11.8 km/Ma in the northern profile which intersects many deltas deposited near or at the shelf-edge (10 km or less from the shelf break). The greatest shelf-edge progradation rate is therefore reached in the area where sediment supply is highest; i.e. where shelf-edge deltas delivered sediment directly to the margin. The observed relationship between shelf-edge and delta lobe progradation (Figure 3.8) further supports the hypothesis that sediment sourced from these shelf-edge deltas reached the shelf margin and contributed to its accretion.

Progradation rates in the NCB increased along-strike by a factor of almost three towards the locus of shelf-edge delta accumulation (northern profile area, Figure 3.3). As a consequence, the plan-view morphology of the Miocene shelf-margin changed from being linear before the deltaic progradation pulse overlying SB-MMK (pre-delta shelf-edge, Figure 3.3) to convex outward after delta lobes prograded to the outer-shelf and shelf-edge. The mapview width of this deltaic depocenter, ~126 km, is also the fairway width of high sediment supply. It is also suggested that it is outboard of this ~126 km fairway that there will be the highest probability of locating deep-water sands. The map relationship between the protruding area in the mid-late Miocene shelf-edges (shelf-edge 10 and shelf-edge 20, Figure 3.3) and higher sediment supply fairway (shelf-edge delta deposition in the NCB northern area Figure 3.3), as well as the width of the high-

sediment supply area marked by this shelf protrusion, agrees with the results of Olariu and Steel (2009) for modern high-supply shelves.

A wider continental shelf in front of high sediment supply fairways (e.g. large rivers) has been documented using modern bathymetry of several shelves and margins (Olariu and Steel, 2009) and also based on results from forward stratigraphic modeling (Burgess and Steel, 2008). The results in this study support their conclusions because the higher progradation related to deltas reaching the shelf edge built a wider shelf along this main sediment fairway.

The area of highest sediment supply shifted along strike through time as delta depocenters migrated northeastwards (Figure 3.3). The locus of maximum total shelf-edge progradation switched through time from the location of the southern profile at SB-MMK, to central profile at SB-LM0, and to northern profile at SB-LM1 (Figures 3.3 and 3.5) as a response to the northeastward shift of the fluvial feeder (Chapter 2). The fluvial feeder system was likely steered to the northeast by a growing inversion anticline in the Rosemary-Legendre Trend (Figures 3.1 and 3.3; Cathro and Karner, 2006).

3.5.1.2. Along-strike Change from Erosional to Depositional slope – A Function of the Supply Distribution, Shelf-edge Deltas Support a Constructional Slope

The slope character between SB-LM0 and SB-LM1 changes along-strike. From being dominated by bypass and/or mass wasting in the central profile (Figure 3.5), which shows substantial truncation of strata at the shelf edge, virtually no progradation of the shelf edge (<1 km), and a thick (> 100 m) deep-water apron that onlaps the slope, to dominantly depositional in the northern profile where the slope shows prominent accretion (>10 km), few truncation surfaces, and only one thin (<50 m) deep-water apron

(Figure 3.4). This spatial variation in slope character can be interpreted in terms of the along-strike change in sediment supply to the shelf margin. The area of the central profile was somewhat starved of sediment towards the corresponding shelf edge. This likely resulted in shelf aggradation, as well as increased slope height and gradient (~5-6°). On the other hand, at least three deltas intersected by the north profile were deposited at the shelf-edge (lobes 11, 12, and 15; Figure 3.3) and the others (lobes 18, 19, and 20; Figure 3.3) were deposited nearby (<10 km) and consequently provided enough sediment to the slope for it to maintain a lower gradient (~3°) and to prograde significantly (Figure 3.4). The slope between SB-LM0 and SB-LM1 on the southern profile is even less constructional than that on the central profile, because the deltas to the south are even farther from this margin area during that time interval (Figures 3.3 and 3.6).

The thickness of the onlapping wedge observed in the central profile (Figure 3.5) is similar to the thickness of 5th order cycles that compose the sandstone-rich Permian Brushy Canyon Formation from west Texas, which onlaps a steep bypass margin (Hadler-Jacobsen et al., 2007).

Bypass slopes have been proposed to be developed in three main ways (Ross et al., 1994): 1) tectonic uplift along the basin margin; such is the case of the Paleogene Porcupine Basin in western Ireland (Ryan et al., 2009); 2) alternating carbonate and siliciclastic depositional regimes; this is the case of the Permian Brushy Canyon Formation (Gardner et al., 2000; Hadler-Jacobsen et al., 2007) and could also play a role in central area in this study as just a few deltas seem to have reached this central margin and as a result carbonate-siliciclastic sedimentation might have alternated; and 3) rising relative sea-level that overwhelms sediment supply; this is a possible scenario for the bypass slope of the central area because the locus of sediment supply to the margin essentially shifted to the northeast toward the northern profile area during that time

interval, causing sediment starvation and later an oversteepened slope when shoreline or shelf-edge systems returned to the shelf-edge.

Because the main factor influencing the erosional or accretionary character of the slope in the mid-late Miocene NCB margin is sediment supply and this is variable along strike, the change of slope character here changes in space within a given stratigraphic interval (SB-LM0 to SB-LM1). Significant changes in the architecture of deep-water deposits in erosional versus depositional slopes has been proposed by Hadler-Jacobsen et al. (2007) and Ryan et al. (2009). Then, the along-strike variations in the type of margin within the same interval documented here likely have a strong influence in deep-water depositional patterns encountered along a margin.

3.5.1.3. Impact of the Along-Strike Distribution of Depositional Systems on the Shelf-edge Trajectory

Comparison of shelf-edge trajectories in the three profiles (Figures 3.4, 3.5, and 3.6) shows how along-strike variability of depositional systems affects trajectory style along a margin within a given stratigraphic interval. These spatial changes occur because the shelf-edge trajectory is a record of the interaction between relative sea level and sediment supply and this supply varies in time and space. Henriksen et al. (2009) also noted this limitation of the trajectory analysis concept and the results presented here confirm the significance of the 3D variability of depositional systems. In addition to showing the relationship between increased shelf-margin accretion related to relatively higher sediment supply (Burgess and Steel, 2008; Olariu and Steel, 2009), this study documents the along-strike migration of the primary sediment source through time and

how this migration affects margin progradation and the shelf-edge trajectories formed in different locations along-strike.

Shelf-edges are commonly non-linear in plan view (Henriksen et al., 2009; Olariu and Steel, 2009); this is the case for middle to upper Miocene shelf edges in the NCB (SB-LM0, SB-LM1; Figure 3.3). Protuberances in the planview morphology of the shelf-edge can represent a problem when selecting true depositional dip cross-sections. However, this is not a concern in our study because of the availability of 3D seismic data.

The shelf-edge trajectory between SB-LM0 and SB-LM1 changes significantly along strike (Figures 3.4, 3.5, and 3.6) as the result of the variability of sediment supply. The trajectory rises between these surfaces in the southern profile (Figures 3.3 and 3.6, Table 3.3), which has an incomplete record of the interplay between accommodation and sediment supply because most of the sediment was being routed towards the northern profile area during that time. The shelf-edge trajectory in the central profile within the same interval is more complex as it alternates between rising, falling, and backstepping (Figure 3.5, Table 3.4). This trajectory difference is likely caused by the impact of varying sediment supply on relative sea-level fall and rise in this area where some deltas were deposited near the shelf-edge (Figure 3.3). The trajectory in the north, where the profile intersects the most delta lobes and where shelf-edge deltas occur most frequently (Figure 3.3), varies between rising, falling, and aggradational (Figure 3.4). This profile has the most complete stratigraphic record of the three selected cross-sections because it received more sediment during the studied time interval due to the concentration of delta lobes in this northern area.

The observed rising progradational trajectory portions are a product of relatively high sediment supply (localized according to the location of delta lobes) combined with rising relative sea level (Henriksen et al., 2009). Particular depositional systems have

been proposed to develop in relation to specific styles of shelf-edge trajectory (i.e. steep-positive, flat-negative, steep-negative, and low-angle positive; Ryan et al., 2009). The results here show that the variability of depositional systems affect the preserved shelf-edge trajectory and therefore agree with the statement that the trajectory and operating depositional systems are likely related but go a step further by showing that significant complexity related to the development of different but coeval depositional systems can be a modifying agent in the preserved trajectory.

The retrogradational shelf-edge trajectory on the central profile between lobe 20 and SB-LM1 (Figure 3.5) resulted from degradation of the shelf margin by erosion caused by the development of dendritic outer-shelf channel networks (Figure 3.13A). These dendritic networks were active after deposition of lobe 20 and lasted until the development of SB-LM1 (Figure 3.13, A and B). In contrast, the trajectory for the same time interval in the northern area (Figure 3.4), dominated by deltaic and fluvial (Figure 3.13C) deposition from times of lobe 19 until SB-LM1, with a shorter lived, shallower, outer-shelf erosional channel network (Figure 3.13B), is aggradational (Figure 3.4). In the absence of substantial erosion caused by outer-shelf channels, the central profile would probably also have an aggradational trajectory between the shelf edge coeval to lobe 19 and SB-LM1 similar to the northern profile. The reduced sediment supply to the southern area (Figure 3.6) after deposition of lobe 6 (Figure 3.3) prevents recording parts of the shelf-edge trajectory that are observed in the central and northern profiles (Figures 3.4 and 3.5).

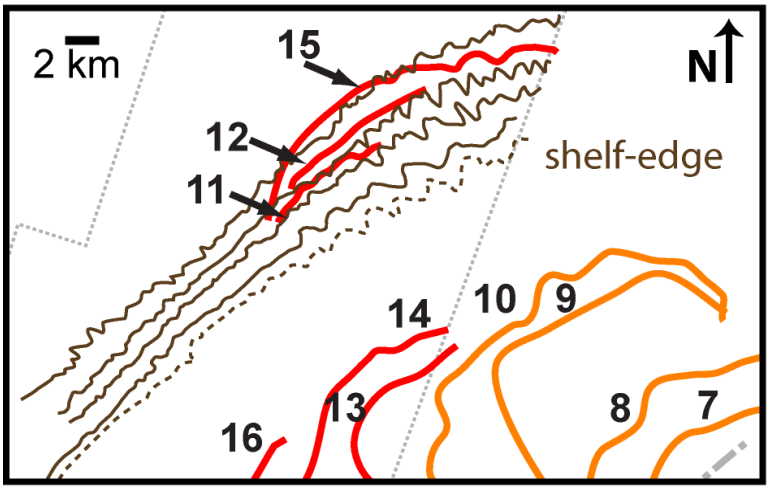

Figure 3.10. Mapped delta lobes 7-15 (red) and contours from shelf-edge to slope for SB-LM0 (brown). Note that larger slope incisions occur to the northeast where shelf-edge deltas were deposited. See also Figure 3.9.

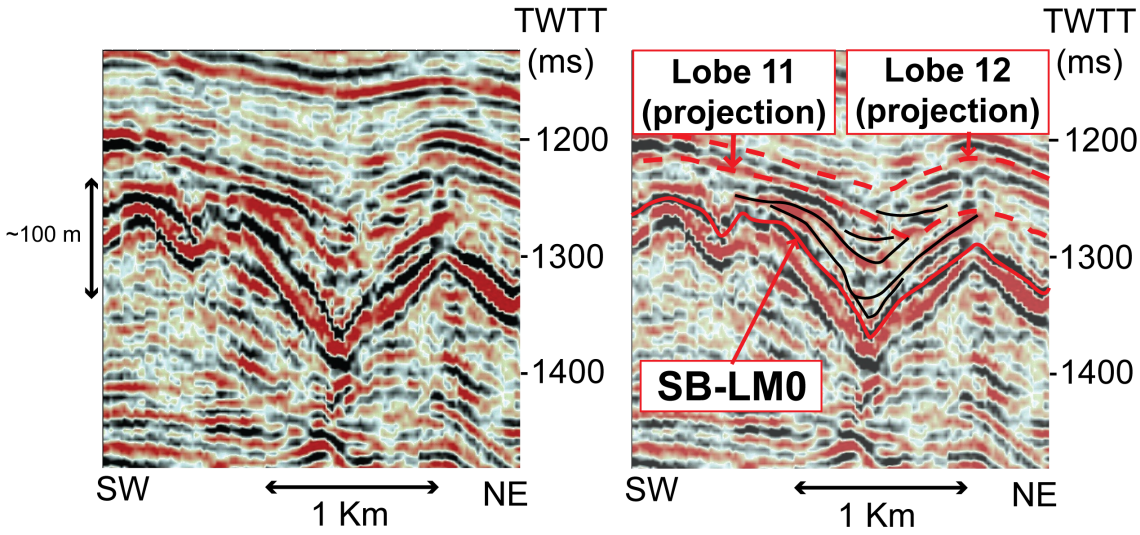

Figure 3.11: Uninterpreted (A) and interpreted (B) strike-oriented seismic profile that illustrates the character of the fill of slope incisions between deposition of lobes 10 and 12. Observe evidence of repeated deposition and erosion (cut-and-fill) within these incisions.

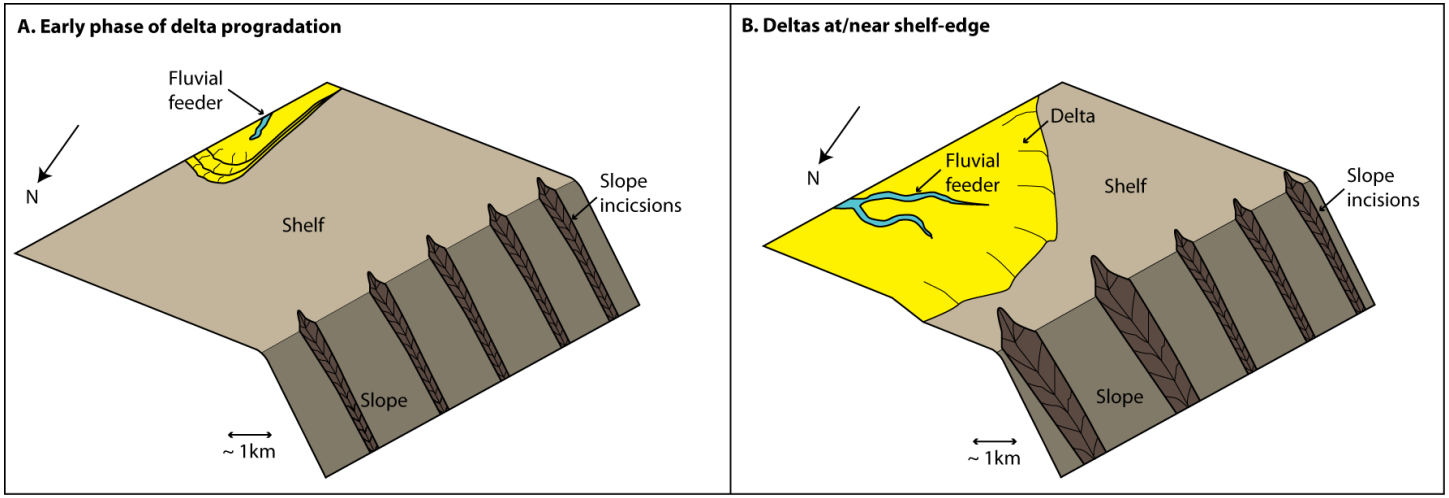

Figure 3.12.Diagrams illustrating: (A) Smaller slope incisions (Figure 3.9A) existing during early delta progradation, before delta lobes reached to the shelf-edge. (B) Enlarged slope incisions (Figures 3.9B and 3.10) developed once deltas reached the shelf-edge area.

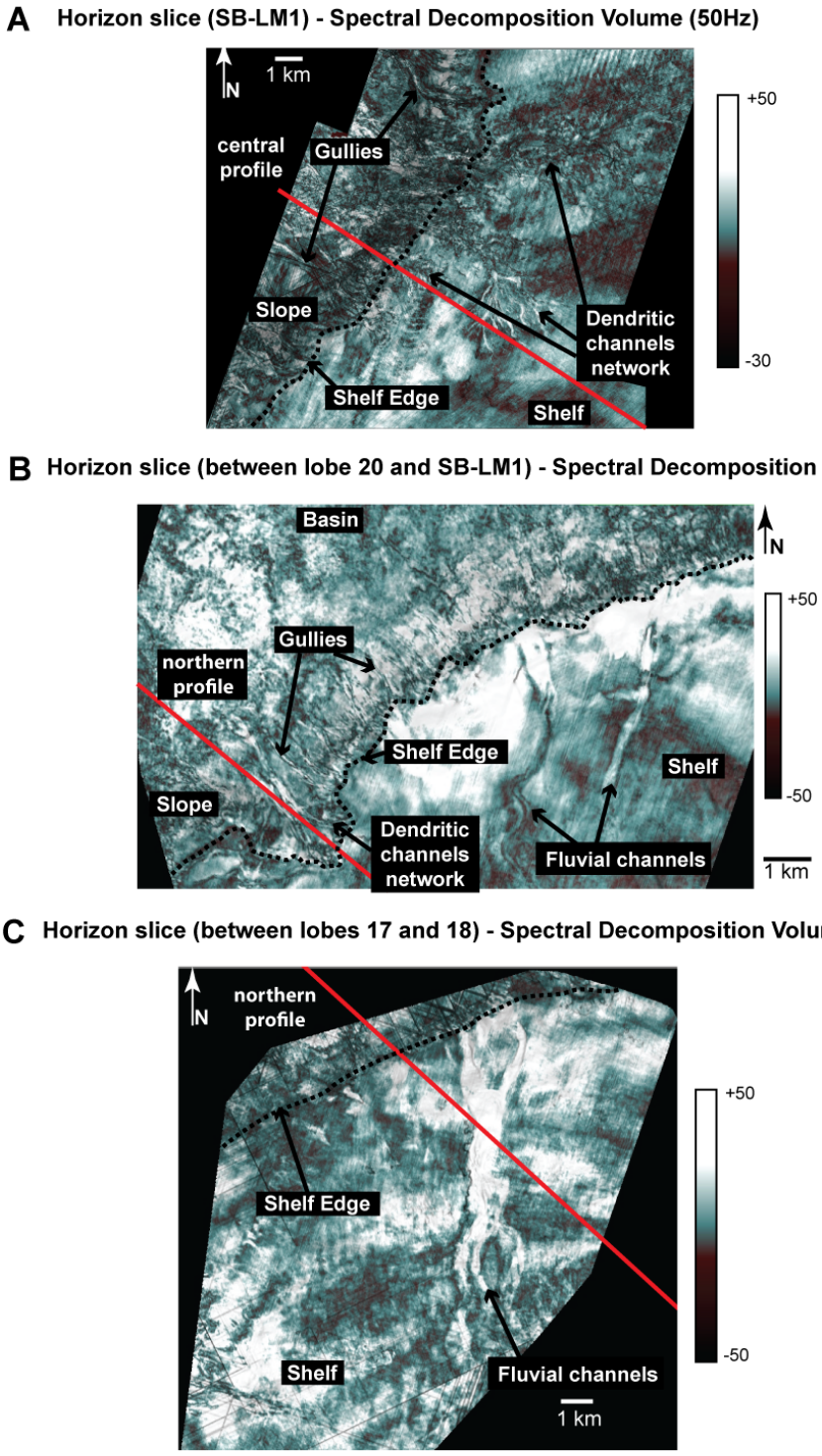

Figure 3.13: Horizon slices though spectral decomposition volumes (40 and 50 Hz). A) Dendritic channels network, common towards then end of this sequence

between SB-LM0 and SB-LM1; these erosional channels modified the shelf-edge trajectory in the central profile between lobe 20 and SB-LM1 (Figure 3.5). B) Channelized features developed between lobe 20 and SB-LM1. Interpreted fluvial channels feeding directly to the shelf edge, dendritic channel networks developed ≤10 km to the south, also at the shelf-edge. C) Fluvial channels feeding the margin between deposition of lobes 17 and 18. Note intersecting profiles: central in A) and northern in B) and C).

3.5.2. Effect of Shelf-Edge Deltas on Slope Incisions

3.5.2.1. Shelf-edge Deltas and Enlarged Slope Gullies: Slope Incisions as Conduits for Delta Front Sourced Sediment Gravity Flows

Slope gullies were ubiquitous features in the NCB before deltas mapped between SB-MMK and SB-LM1 (Figure 3.3) reached the outer shelf and shelf edge. Cathro et al. (2003) documented slope incisions that were initiated during the mid-Miocene climatic optimum and proposed upper slope oversteepening to gradients of 6-8° as the driving mechanism behind these incisions. That study also suggested that once these incisions have been formed they are maintained and likely enlarged due to their role as downslope conduits for erosive sediment flows. It's been proposed that slope gullies could be initiated by unconfined turbidity currents flowing over an increase in surface gradient like is the case of the continental shelf break (Fedele et al., 2009), this could have been the case of the early slope incisions documented in Cathro et al. (2003). It is unlikely that these earlier gullies, which developed before the delta progradation discussed in this study, were initiated by retrogressive slope failure (Farre et al., 1983), because all of the imaged incisions affect the upper slope and most of them breach the shelf edge (Figure 3.9A).

Although slope gullies were common features on the NCB shelf-margin even before any deltas reached the shelf-edge (Figures 3.3 and 3.9A), these slope incisions became wider and deeper as the deltas approached the shelf-edge (e.g., deltas 10 and 11, Figure 3.10). This strongly suggests that there was increased slope erosion as a response to sediment gravity flows released from the deltas when they reached the shelf-edge. Dimensions of these incisions increase greatly from the time when the deltas (lobes 1-6) were restricted to the shelf (incisions were 400 m wide and 20 m deep, Figure 3.9A) to when deltas (lobes 7-20) were very near or at the shelf edge (incisions were 0.7-1.2 km wide, 25-100 m deep, Figure 3.9B). The maximum increase in incision dimensions occurred in the northern area where deltas were at the shelf-edge (lobes 11 and 12 in the north, Table 3.2, Figure 3.10).

These observations indicate that progradation of deltas to the shelf edge, during long-term relative sea level fall, was not the driving mechanism for slope gully initiation. Gullies existed on the slope prior to siliciclastic deposition. Instead, this study shows that existing gullies immediately basinward of shelf-edge deltas were enlarged to small canyons, as these incisions became active conduits for sediment gravity flows sourced from the deltas. Another example of shelf-edge deltas linked to the deep-water basin through slope incisions has been documented from the Pleistocene in offshore Indonesia (Saller et al., 2004).

3.5.2.2. Mixed Erosional/Depositional Slope Incision Infill

The character of the larger slope gullies located basinward of shelf-edge deltas 11 and 12 can be interpreted as mixed erosional/depositional based on stratal relationships

(Figure 3.11). This type of gully fill is likely the result of significant deposition interspersed with episodes of erosion once deltas arrive at the shelf-edge. Surfaces of major erosion correlate with the upper surfaces of deltas and likely formed during their maximum progradation or peak regression (Figure 3.11), suggesting slope bypass of high-concentration sediment gravity flows.

Infill of these slope gullies/canyons suggests that a considerable portion of the sediments presumably sourced from shelf-edge deltas was deposited within these incisions in addition to the fraction of sediment that accumulated on the slope area surrounding these incisions and to that which bypassed to the toe of slope and basin. This slope deposition caused increased margin progradation rates immediately basinward of the shelf-edge deltas (northern area, Figures 3.3 and 3.4). It has been proposed that slope incisions can begin as erosional features and later switch to depositional while relative sea level rises and sediment sources become more distal (Pratson et al., 1994; Spinelli and Field, 2001). This could explain the mixed erosional/depositional infill of slope incisions observed between successive delta lobes (Figure 3.11). Once a delta lobe reached its final, most basinward position during maximum regression, it probably was flooded during a subsequent relative sea level rise or lobe avulsion, causing the main sediment source to move landwards and a switch from erosion to deposition in the slope interrupted again during the next maximum regression.

Downslope transport of shelf sediments via submarine canyons can occur even when rivers or deltas are not at the shelf edge if slope incisions breach the shelf edge connecting the shelf to the deep-water slope. Our results show that gullies incised landward up to 5.5 km into the shelf when located adjacent (basinward) of the shelf-edge deltas (Figure 3.9B). These shelf-indenting incisions can favor a link between coastal sediments and the deep-water margin as suggested by Posamentier and Allen (1999).

3.6. CONCLUSIONS

Progradation rates of a shelf margin can more than double in areas dominated by deposition of shelf-edge deltas, relative to areas along-strike where deltas do not reach the shelf edge. Shelf-edge deltas favor the development of a depositional or progradational slope, because the delta systems provided sufficient sediment to the adjacent slope to maintain accretion and reduce slope inclination.

Shelf-edge trajectory for a given stratigraphic interval also changes significantly along strike as a result of the three-dimensional variation of sediment supply. Where shelf-edge deltas occur, they provide sufficient sediment for the shelf-edge trajectory to record relative sea-level fluctuations. Trajectories in areas away from these deltaic depocenters, with lower sedimentation rates, may not fully record these sea-level changes. The along-strike variation from primary deposition in the northern area (with deposition of shelf-edge deltas and fluvial systems), to erosion in the central area (where all delta lobes accumulated several kilometers away from the shelf-edge and shelf-edge dendritic channel networks occur) results in dramatic north-to-south changes in the character of the shelf-edge trajectory, e.g., from aggradational to retrogradational. Therefore, careful examination of facies to determine the type of depositional system is essential in order to use shelf-edge trajectory to estimate changes in relative sea level and/or sediment supply rates.

Significant along-strike variation of slope incisions dimensions can result when these serve as conduits for sediment gravity flows to the deep water. Progradation of deltas to the shelf-edge in the late-middle Miocene caused a substantial increase of the general dimensions of, already common, slope gullies that were located immediately basinwards as well as how far landward these gullies/canyons incised the shelf. The infill

of these enlarged incisions suggests that noticeable erosion occurred at times of maximum regression of deltas, whereas aggradation within the gullies/canyons prevailed between times of deltas retreat and progradation, until the next maximum delta regression.

Chapter 4: Plio-Pleistocene Tropical Carbonate Platforms in the Northern Carnarvon Basin, Northwest Shelf Of Australia: Controls on Initiation, Demise, and Configuration

4.1. INTRODUCTION

The Northern Carnarvon Basin (NCB) is today an area of widespread shelfal carbonate sedimentation. Modern tropical carbonate systems consists of narrow fringing and patch coral reefs, concentrated mainly around the Barrow and Monte Bello Islands and the Dampier Archipelago (Figure 4.1A; James et al., 2004). However, the early history of photozoan carbonate development on this margin is poorly constrained. Small (~1 km diameter), isolated, mounded buildups have been identified on middle Miocene paleoshelves using 2D and 3D seismic data (Romine et al., 1997; Cathro, 2002; Liu et al., submitted), but extensive, tropical carbonate platforms (≥10 km wide) have not previously been identified in the subsurface. The large areal extent and resolution of the seismic surveys available for this study make them ideally suited for interpretation and three-dimensional mapping of such large carbonate platforms.

I propose that extensive tropical carbonate platforms developed in the NCB during the Plio-Pleistocene. These platforms differ from the middle Miocene carbonate buildups previously documented by Cathro (2002), both in size and seismic character. The platforms documented in this study are characterized by high-amplitude reflections and flat platform tops with asymmetrical slopes and internal, bidirectional clinoform foresets. In contrast, Cathro (2002) observed one relatively small (< 1 km wide) mound with low-amplitude seismic reflections, internal reflections parallel to the mound top.

Judging by their size and distribution, the Plio-Pleistocene tropical platforms discussed here likely represent the first significant occurrence of photozoan carbonate production in the NCB.

Furthermore, our interpretations suggest that underlying, upper Miocene to Pliocene, shelf-edge delta lobes (Chapters 2 and 3) created subtle topographic highs that influenced the spatial distribution of the overlying, tropical, flat-topped carbonate platforms (Read, 1985; Pomar 2001). These platforms likely developed as paleoenvironmental conditions for carbonate production improved due to waning siliciclastic sediment input to the outer shelf, continued northward movement of Australia during the Neogene (Veevers et al., 1991), and the possible influx of warm water from the Western Pacific and initiation of the Leeuwin Current (Kendrick et al., 1991; Gallagher et al., 2009). These platforms developed on the outer paleoshelf; therefore the Leeuwin Current may also have influenced their growth and internal architecture by controlling nutrient flow and affecting downcurrent patterns of offbank deposition.

In this paper, we: 1) document the spatial relationship between the distribution of Plio-Pleistocene flat-topped carbonate platforms and underlying mid-Miocene to Pliocene delta lobes, 2) interpret paleocurrent directions based on platform asymmetry, and 3) discuss possible conditions favoring initial development of these tropical carbonate systems and what changes could have resulted in their termination.

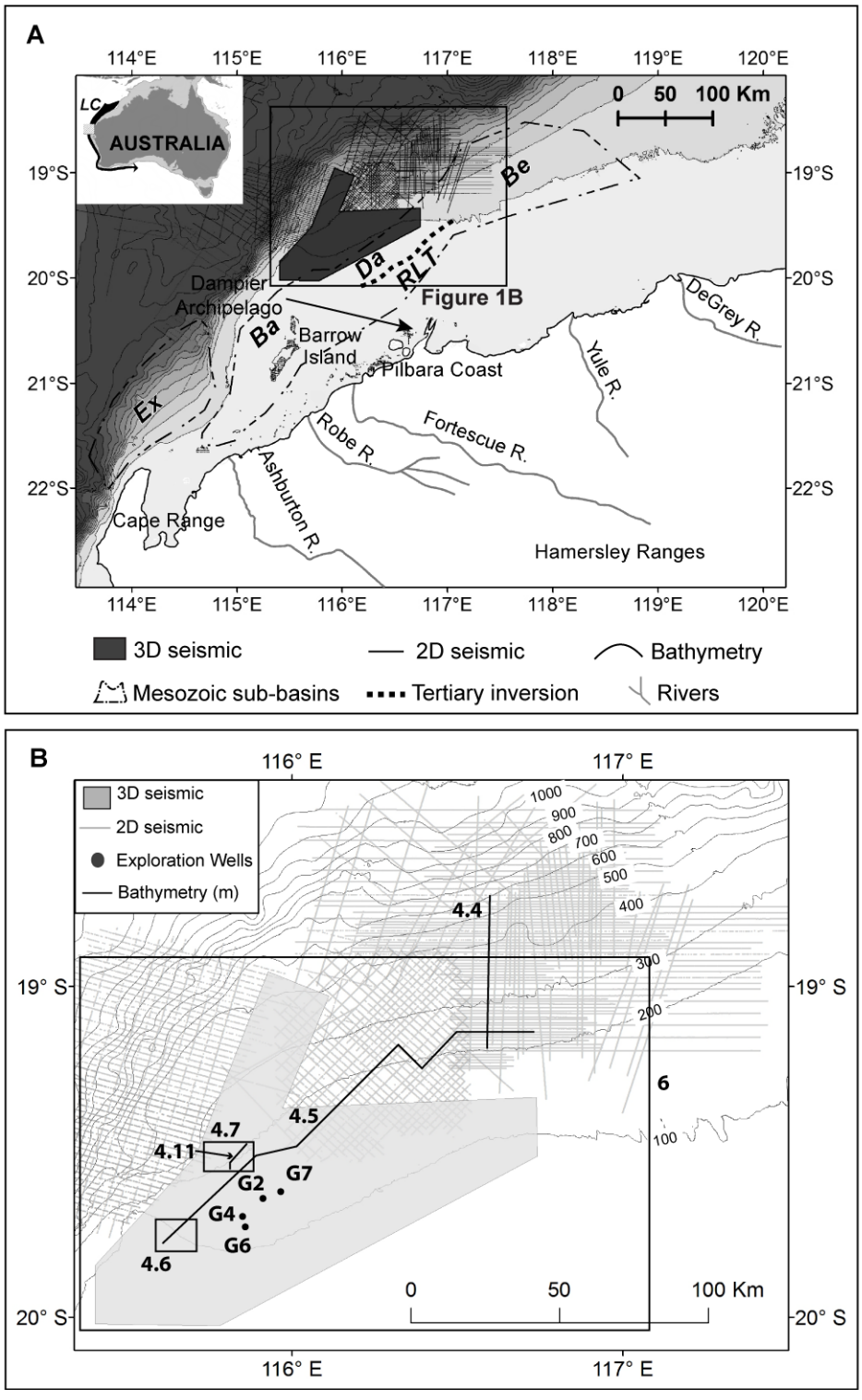

Figure 4.1: (A) Location of study area showing available multichannel seismic data (dark

grey polygon represents 3D volume; lines represent 2D profiles), Mesozoic sub-basins offshore (outlined by black dashed lines; Ex=Exmouth, Ba=Barrow, Da=Dampier, Be=Beagle; Stagg and Colwell, 1994; Romine et al., 1997; Cathro et al., 2003), and modern rivers draining the Hamersley Ranges (solid gray lines onshore; Semeniuk, 1996). Bathymetric contours (solid black) are at 100 m intervals (Webster and Petkovic, 2005). Thick, short black dashed line shows the location of localized Miocene inversion along the Rosemary-Legendre Trend (RLT) caused by collision of Australia with the Indonesian arc (Cathro and Karner, 2006). Inset map shows he location of the study area (box), the Australian continent, and the Leeuwin Current (LC), represented by a black arrow along the Western Australian shelf edge (Tomczac and Godfrey, 1994). (B) 3D and 2D seismic data used in this study, provided by Woodside Petroleum Ltd. Modern bathymetry contour interval is 100 m (Webster and Petkovic, 2005). Exploration wells referenced are also shown: G2 = Goodwyn-2; G4 = Goodwyn-4; G6 = Goodwyn-6; G7 = Goodwyn-7. Area covered by 3D seismic volume is 7,500 km2; the total area covered by 2D and 3D seismic data is ~31,000 km2. Note locations of Figures 4.4, 4.5, 4.6, 4.7, and 4.11.

4.2. GEOLOGIC SETTING

4.2.1. Tectonic overview

Three main phases of rifting affected the NWS during the Phanerozoic: Late Permian, Late Triassic - Early Jurassic, and Late Jurassic (Bradshaw et al., 1988; Veevers et al., 1991; Baillie et al., 1994; Driscoll and Karner, 1998). These rifting episodes controlled the configuration of NE-SW oriented sub-basins beneath the NCB (Cathro et al., 2003). From southwest to northeast these are the Exmouth, Barrow, Dampier and Beagle sub-basins (Figure 4.1A). Thermal-cooling subsidence of the NCB has been dominant since the Early Cretaceous (Veevers et al., 1991; Baillie et al., 1994; Driscoll and Karner, 1998; Kaiko and Tait, 2001; Cathro and Karner, 2006); this subsidence

pattern has been shown using subsidence plots from exploration wells in the NCB (Kaiko and Tait, 2001). Beginning in the late Miocene, collision between the Banda Arc and Australia (Figure 4.1A; Veevers et al., 1991; Baillie et al., 1994; Lee and Lawver, 1995; Driscoll and Karner, 1998) has resulted in localized uplift at the northwest end of the Rosemary-Legendre Structural Trend (Figure 4.1A; Cathro and Karner, 2006).

4.2.2. Stratigraphy

Cenozoic strata have been deposited in the NCB under the influence of northward drift of the Australian continent since the Mesozoic (Baillie et al., 1994; Bradshaw et al., 1988). During this drift, as the Australian Plate has moved towards the equator, predominant sediment type on the NCB has changed from siliciclastics in the Mesozoic to largely carbonate sediments in the Cenozoic (Apthorpe, 1988; Romine et al., 1997). As a result, the NCB has been a region of widespread carbonate sedimentation since the late Paleogene (Romine et al., 1997; Cathro et al., 2003). The Oligocene to Miocene shelf of the NCB was dominated by heterozoan carbonate sedimentation with a northwestward progradation direction (Cathro, 2002; Cathro et al., 2003). However, dominant carbonate sedimentation was interrupted in the middle Miocene when a complex series of siliciclastic progradation pulses deposited the Bare Formation (see Chapters 2 and 3; Figure 4.2). Shelfal carbonate sedimentation (Delambre Formation, Figure 4.2) resumed between the late Miocene and the Pliocene under continued northward movement of the NCB and waning siliciclastic sedimentation (Delambre Formation, Figure 4.2).

Modern sedimentation in the NCB is influenced by the arid climate of northwest Australia, resulting in low terrigenous input to the shelf (Semeniuk, 1996). On the

modern Pilbara coast (Figure 4.1A), siliciclastics are deposited mainly along barrier islands, whereas carbonates and evaporites occur in tidal flats and as foreshore skeletal calcarenite sheets (Semeniuk, 1996). Farther offshore, modern shelf sedimentation is dominated by heterozoan carbonate growth, typical of cooler water eastern sides of oceans or temperate to polar latitudes (James, 1997; James et al., 2004).

4.2.3. Oceanographic setting

The modern, poleward-flowing Leeuwin Current (LC), composed of warm (>24°C), low-salinity water (34‰; Cresswell, 1991; Martinez et al., 1999), has been observed near the shelf edge in the study area (Figure 4.1A, inset; Holloway and Nye, 1985; Tomczak and Godfrey, 1994; Holloway, 1995). The LC is 250 km wide and 440 m deep along the NWS and flows at speeds of up to 20 cm/s, with greatest strength from February to July, although that can vary significantly from year to year (Holloway, 1995).

There is active debate about the timing of initiation of the LC. The existence of a proto-LC since the Eocene has been postulated based on nannoplankton evidence (Shafik, 1990) and biogeographic analysis (McGowran et al., 1997). An active Miocene proto-LC has also been proposed (Feary and James, 1998). Gallagher et al. (2009) suggest that the modern LC commenced 1.6 Ma based on foraminiferal analysis. In contrast, Gingele et al. (2001) suggest that the modern LC initiated only 12 ka, during the last deglaciation, based on analysis of clays from cores.

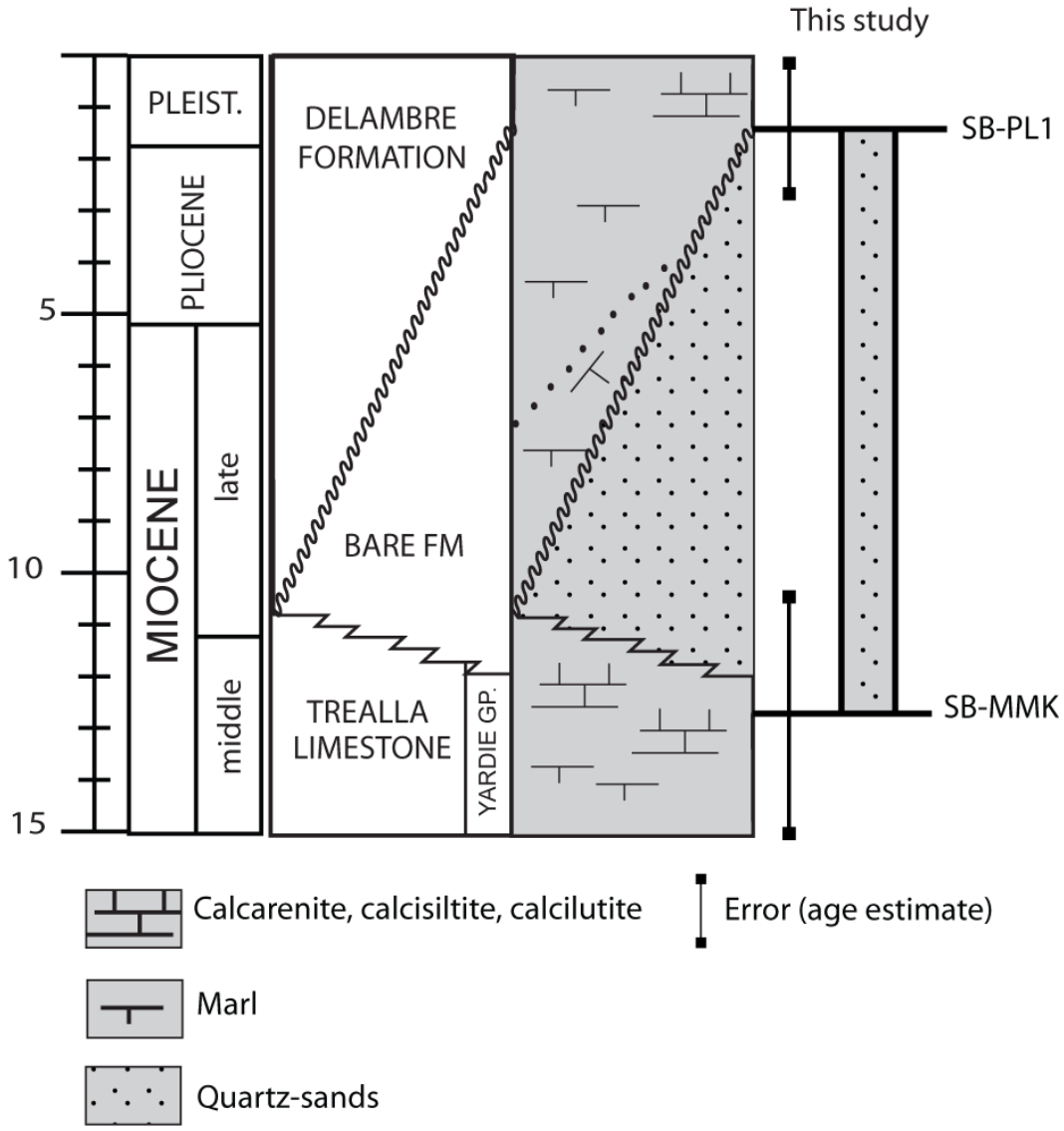

Figure 4.2: Generalized Miocene-Pleistocene stratigraphy of the NCB. Sequence boundaries derived from this study are calibrated to the Berggren et al. (1995) timescale. SB-PL1 represents the base of the interval containing the carbonate platforms. Vertical bars represent errors in estimated ages. Modified from Cathro (2002).

4.3. DATA

This study makes use of high-resolution industry-acquired 3D and 2D multichannel seismic data (Figure 4.1B) that were donated to the University of Texas Institute for Geophysics (UTIG) by Woodside Petroleum, Ltd. and Geoscience Australia (Figure 4.1B). Well completion reports, wireline logs, and checkshot surveys from 4 wells on the modern outer shelf and upper slope, provided by OCCAM Technology, were also included in this study to estimate the age of the studied interval.

The 3D seismic volume covers 7,500 km^2; the total area covered by 2D and 3D seismic data combined is ~31,000 km^2 (Figure 4.1B). The central frequency for the seismic interval under investigation is ~55 Hz, which results in a theoretical vertical resolution of ~18m, assuming an average velocity of 4,000 m/s for carbonate lithology (Schlager, 2005). The available wireline logs do not cover this shallow interval of study, which made necessary to assume that average acoustic velocity for carbonate lithology.

4.4. METHODS

The seismic unconformities bounding the features of interest were defined using characteristic seismic terminations (toplap and/or truncation below, onlap and/or downlap above; Figure 4.3) and mapped through the 2D and 3D seismic surveys. Key seismic facies, parallel and progradational, were also identified within the packages under study. The order of occurrence of the mapped stratigraphic packages was determined by following seismic reflection "time" horizons.

Foraminiferal zones, defined by Moss et al. (2004), allowed calculation of an estimated age interval for the development of the tropical carbonate accumulations. Industry wells were tied to the seismic data using traveltime-to-depth curves derived using synthetic seismograms. These synthetic seismograms were generated from sonic and density wireline logs and calibrated with checkshot surveys, when available, using GeoFrame® Synthetics software.

The inclinations of foresets within each carbonate platform were calculated using the same assumed seismic velocity for carbonates (4,000 m/s) used to estimate vertical resolution. These inclinations were used to interpret paleocurrent directions. The supposition is that asymmetry of carbonate platforms is a result of contrasts between higher energy and lower energy environments, corresponding to either windward versus leeward, or upcurrent versus downcurrent margins. Prograding platform foresets facing high-energy wind-driven waves and/or currents should exhibit steeper gradients, whereas foresets dipping in the opposite direction on the lower energy side of the platform should display more gentle gradients (Eberli and Ginsburg, 1987; Isern et al., 2004).

4.5. RESULTS

The study interval is defined by two bounding seismic unconformities, SB-PL2 above and SB-PL1 below. These unconformities are associated with toplap/truncation terminations below and onlap/downlap terminations above the surfaces and can therefore be interpreted as seismic sequence boundaries (Figure 4.3). SB-PL1 and SB-PL2 are the youngest sequence boundaries interpreted within the NCB Tertiary succession. Their ages are poorly constrained, because samples are not available from the uppermost

interval penetrated by the exploration wells that provide age control. Both surfaces correlate with an interval defined as foraminiferal zone N21 or younger (Cathro 2002; Moss et al. 2004), yielding estimates of 3 Ma or younger, the Plio-Pleistocene, for both surfaces (Berggren et al., 1985; Figure 4.2).

The interval between sequence boundaries SB-PL1 and SB-PL2 displays three key seismic facies: high-amplitude parallel, high-amplitude progradational, and low-amplitude parallel, all of these three are composed of continuous reflections (Figure 4.3). Six seismic packages, composed of high-amplitude progradational reflections (foresets) and high-amplitude parallel reflections, are interpreted within this interval (Figures 4.4 and 4.5). These packages display asymmetric bidirectional progradation on strike-oriented (northeast-southwest) profiles and cause subtle velocity pull-up of underlying reflections (Figure 4.3). Progradation distances within these packages are greater to the southwest (20-25 km) than to the northeast (9-15 km). The asymmetric foresets dip southwestward at ~7˚ and northeastward at ~30˚. Foreset height is ~140-150 m (Figures 4.3, 4.4, and 4.5). Trajectories followed by clinoform rollovers within these packages are ascending to flat to descending (Figure 4.5). A comparison between the final clinoform rollover for each unit in planview to the delta lobes of the Bare Formation suggest a spatial relationship between the underlying siliciclastic depocenters and the development of these units (Figure 4.6). Successive packages downlap against the seismic surface overlying the previous package but the packages are not stacked vertically (Figure 4.5). The upper surface of each package is a toplap/truncation surface formed by terminations of prograding foresets against a sub-horizontal, high-amplitude reflection. The high-amplitude facies packages are surrounded by lower-amplitude parallel facies (Figure 4.5).

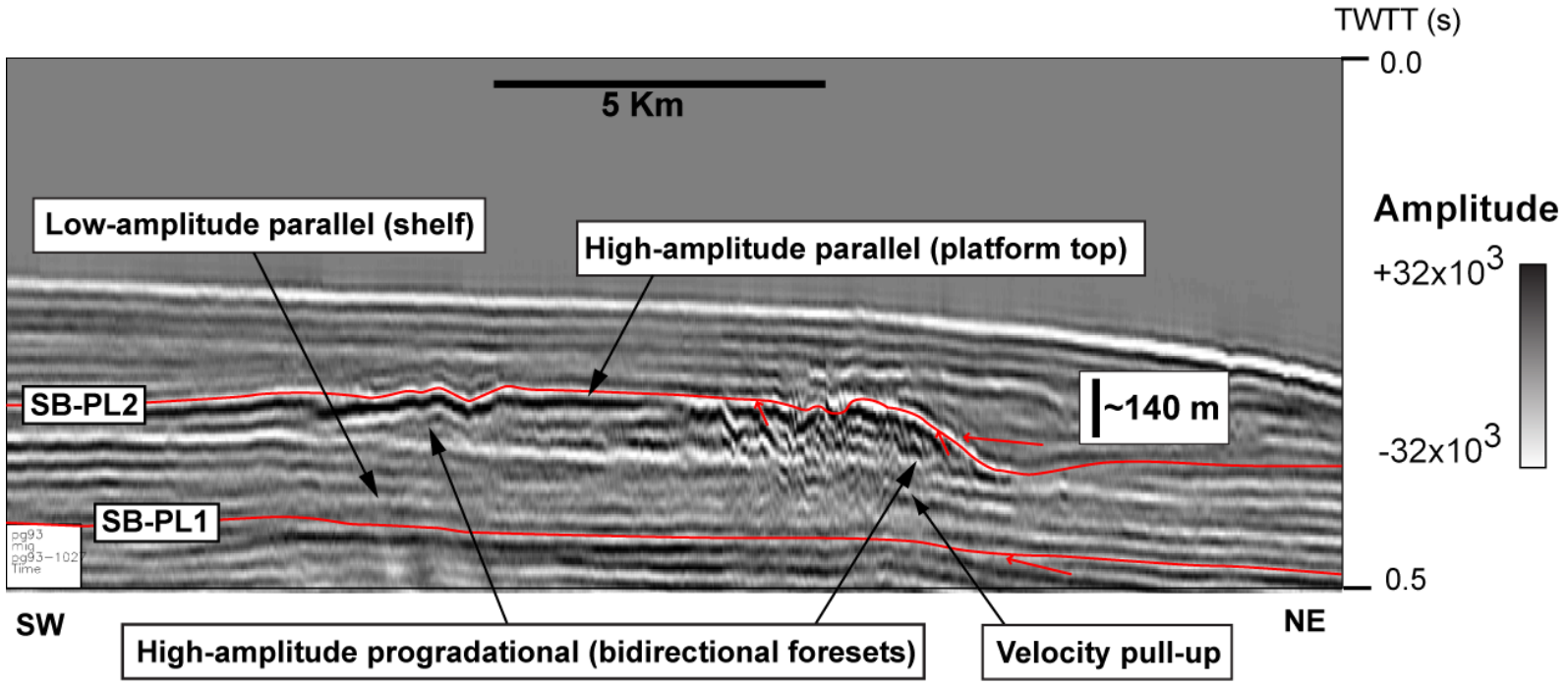

Figure 4.3: Strike-oriented (northeast-southwest) seismic profile showing seismic facies associated with flat-topped carbonate platforms and surrounding shelf (the "basin" for these platforms). Note bidirectional foresets of the platform progradational margins, horizontal reflections of the platform top, and subtle velocity pull-up of underlying reflections. Red arrows denote seismic terminations and highlight toplap surfaces interpreted as sequence boundaries. Same profile shown in inset of Figure 4.5.

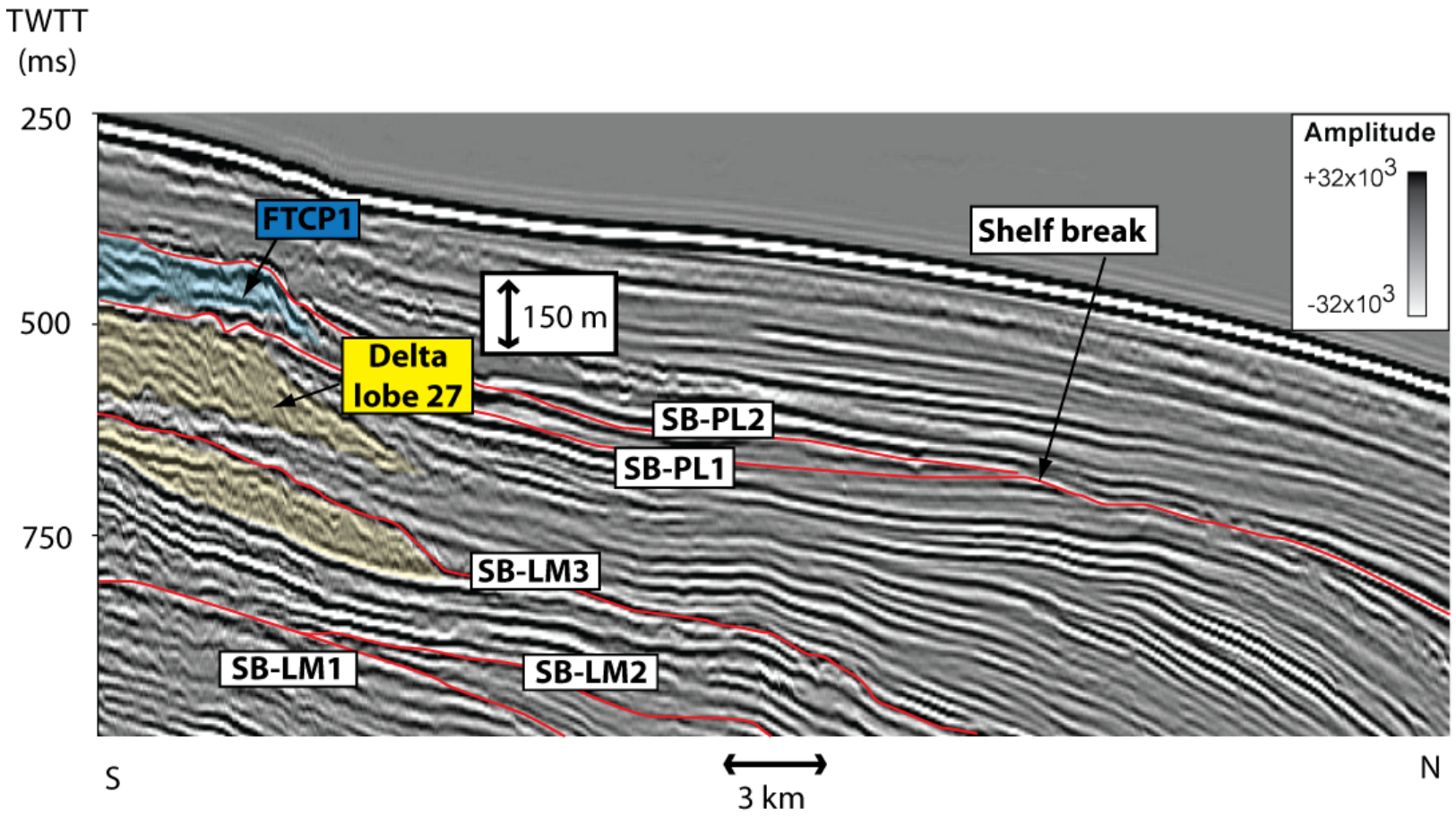

Figure 4.4: Dip-oriented (northwest-southeast) seismic profile showing the oldest interpreted tropical carbonate platform (FTCP1), overlying the youngest deltaic lobe (27) that is part of the mid-Miocene – Pliocene siliciclastic interval (Chapters 2 and 3). The distance from the platform margin to the shelf edge is ~ 21 km. See Figure 4.1B for location.

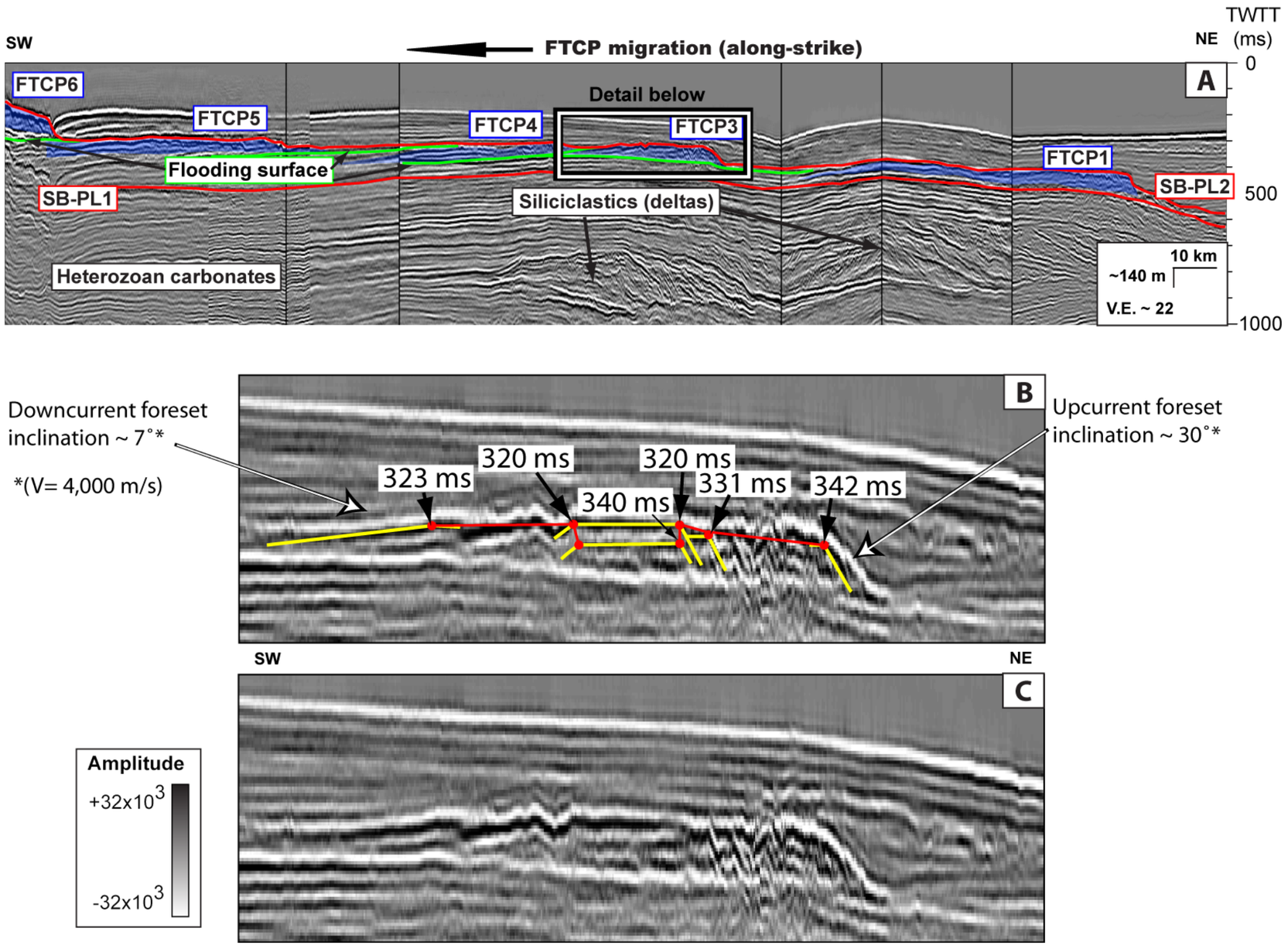

Figure 4.5: Strike-oriented (northeast-southwest) seismic profile showing five of the six mapped carbonate platforms along strike (1, 3, 4, 5, and 6). Flooding surfaces (green) separate these platforms. Inset shows interpreted upcurrent (northeast) and downcurrent (southwest) sides of FTCP3, based on the observed variation of foreset inclinations. Clinoform rollovers are highlighted with red circles and their trajectory with a red solid line. See Figure 4.1B for location.

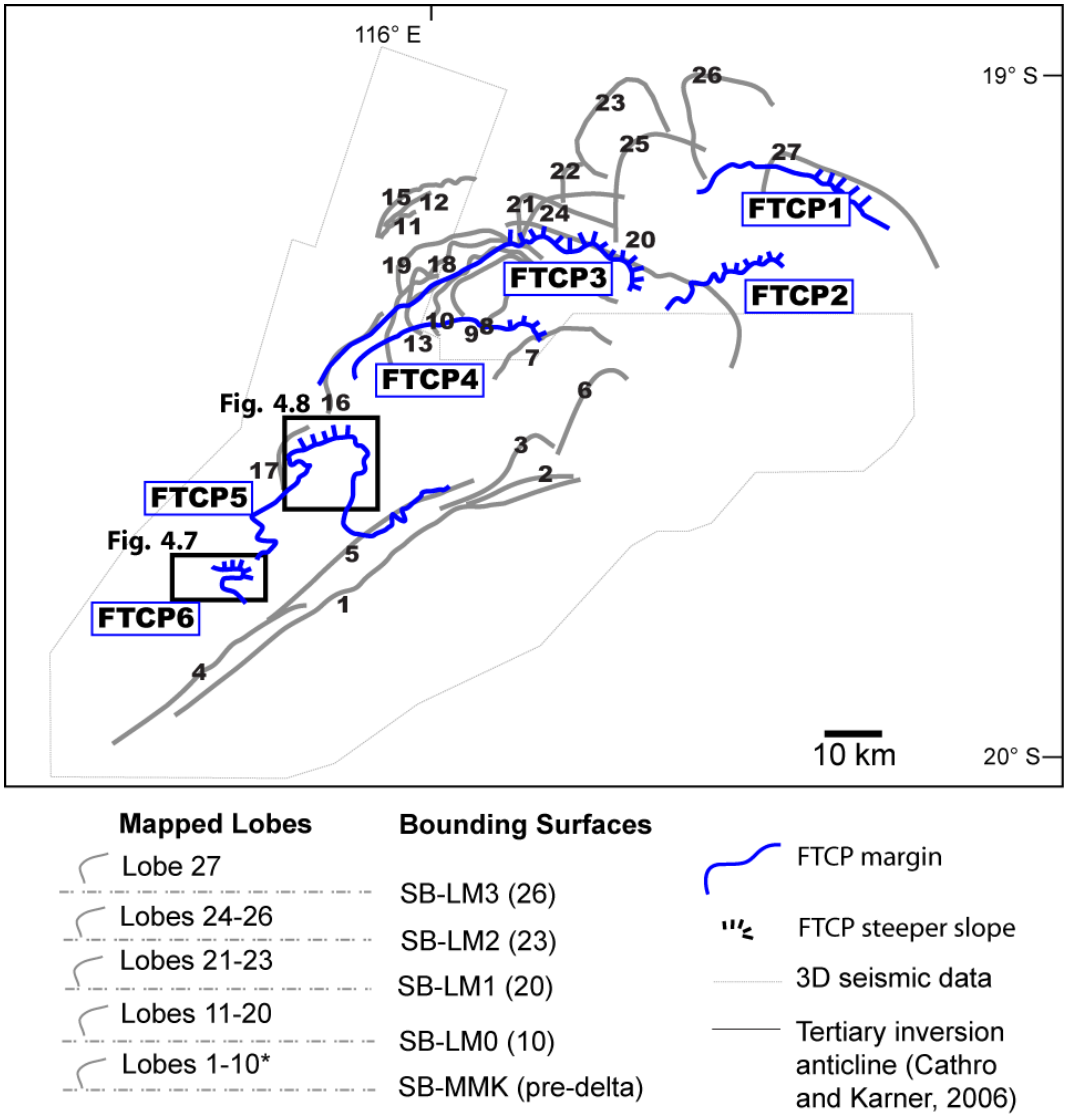

Figure 4.6: Flat-topped carbonate platform margins (FTCP1-6; thick, black solid lines) superimposed on interpreted delta lobe complexes (grey lines, numbered 1-27). FTCP1 is the oldest platform (see Figure 4.5) and lobe 1 is the oldest delta lobe (see Chapters 2 and 3). Note that the first carbonate platform (FTCP1) is located above the youngest deltaic lobe and subsequent FTCPs overlie progressively older deltaic depocenters.

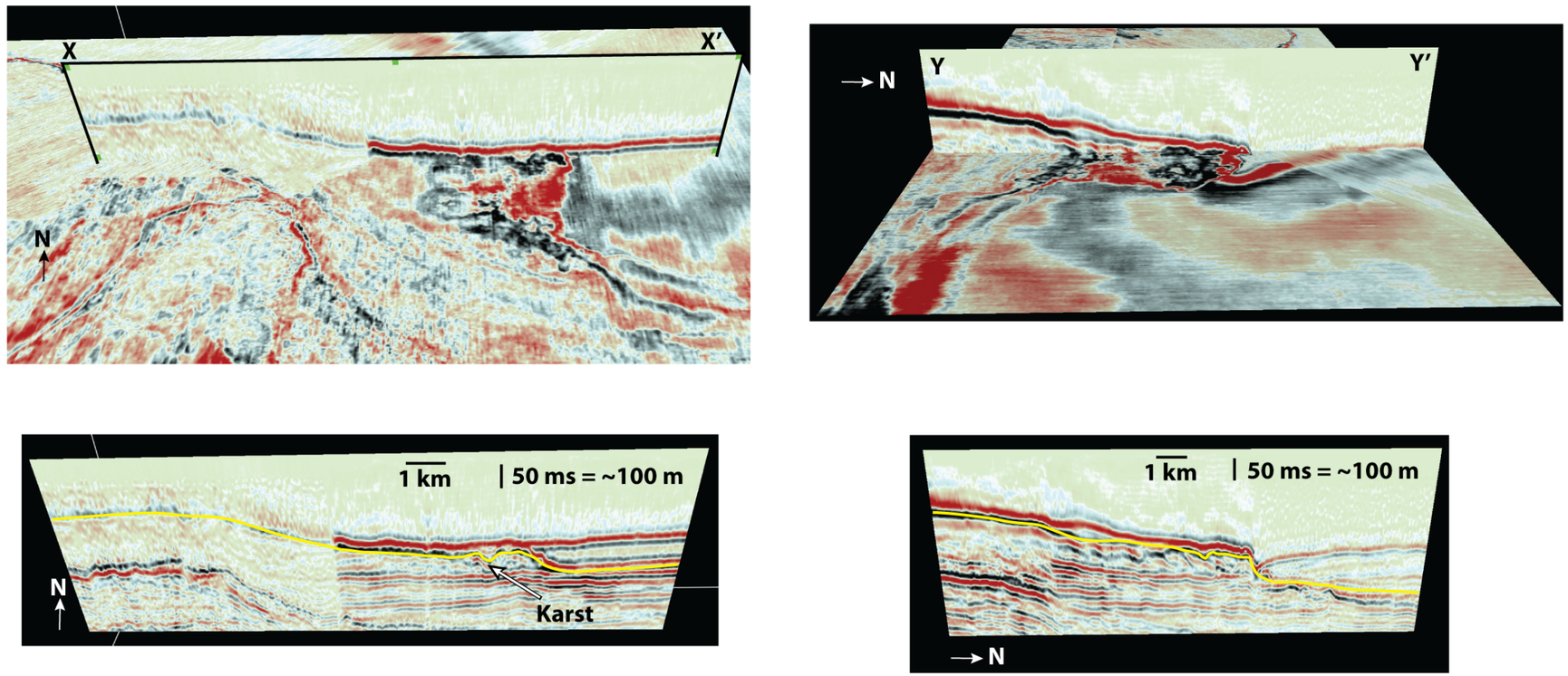

Time slice (216 ms)

Figure 4.7. Time slice and vertical profiles intersecting FTCP6. Top: Time slice showing reflection associated to the platform margin and circular feature that corresponds to a depression shown in the vertical profiles shown in the bottom images. This feature is interpreted as related to karstification of the platform top. The middle images show where the profiles intersect the time slice.

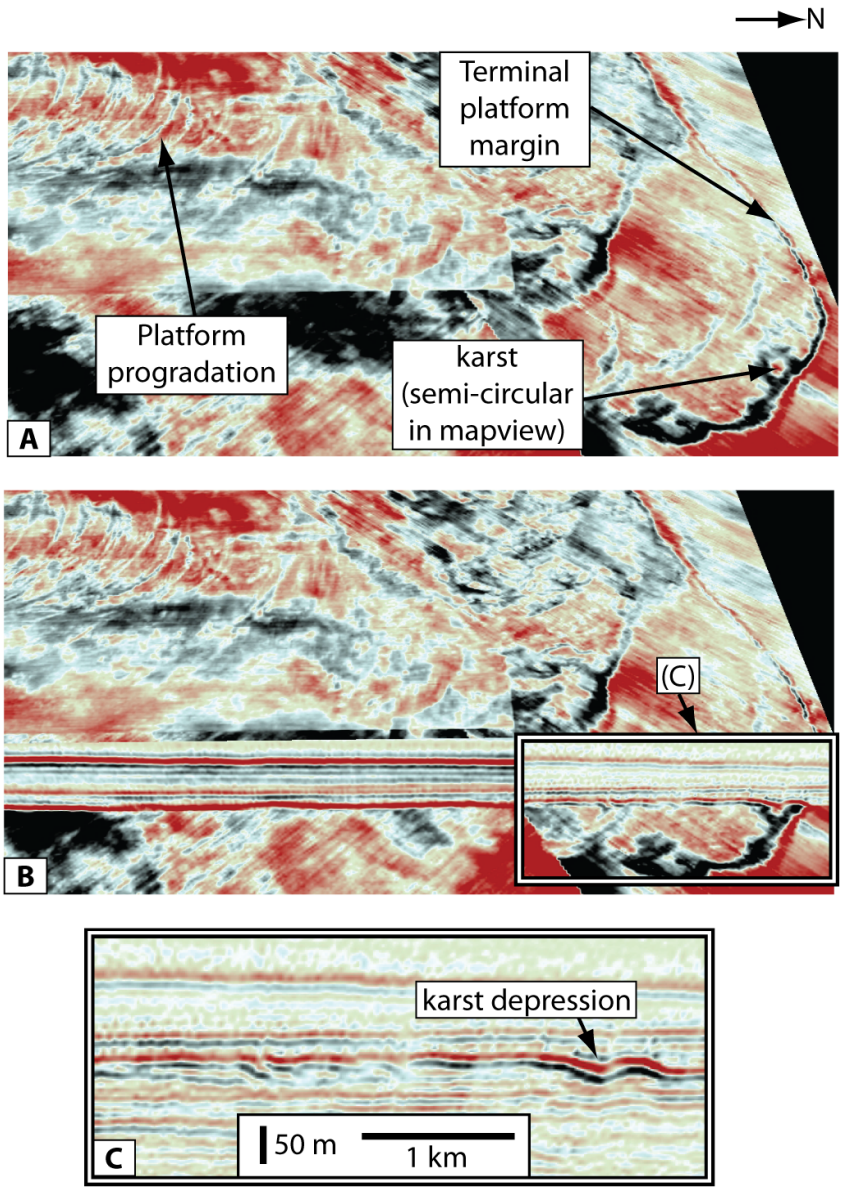

Figure 4.8. Top: time slice. Center: time slice with intersecting vertical profile. Bottom: vertical profile showing interpreted karst depression corresponding to semi-circular feature in the time slice (top).

4.6. DISCUSSION

4.6.1. Processes Controlling Tropical Carbonate Platform Initiation and Termination

I interpret the high-amplitude packages as flat-topped carbonate platforms (FTCP). The geometries of the high-amplitude packages are similar to those of rimmed carbonate "shelves" with flat tops, which are observed in other places (e.g. Great Barrier Reef in Australia, South Florida Shelf, and Belize Shelf; Read 1985).

These carbonate platforms overlie delta lobes of the Bare Formation (Figures 4.2, and 4.4), which had retreated in the Pliocene and whose topsets were at or near sea level (Chapters 2 and 3). Therefore, these platforms initiated while the area was likely close to sea level, in the photic zone, which is a necessary condition for photozoan carbonate growth (Bosscher and Schlager, 1992).

The observed flat tops and reflection toplap could be caused by growth to sea level, which is a primary characteristic of a tropical carbonate platform (Schlager, 2003). Another possibility is erosion in shallow water of a feature originally more mounded (formed in deeper water). However, the relatively flat tops show some depressions (Figures 4.3), perhaps caused by karstification of the platform top (Figures 4.7 and 4.8), which would not be expected if mounded features had been flattened by erosion during a relative sea level fall.

Heterozoan mounds differ from these platforms both in size and seismic character; these buildups are only ~1 km wide (Feary and James, 1998; Cathro, 2002). In contrast, the broad FTCPs are 10s of kilometers wide (Figure 4.5). Feary and James

(1998) listed low to moderate amplitude for both 1) the surface outlining the buildup (caused by low-moderate impedance contrast between the buildup and the surrounding sediments) and 2) the internal reflections that mimic the mound's external geometry, as the key seismic characteristics of biogenic (cooler water) mounds. In addition, minor velocity pull-up and low-amplitude, discontinuous reflections are common underneath coralgal accumulations (Feary and James, 1998).

The five high-amplitude, flat-topped seismic packages between SB-PL1 and SB-PL2 are interpreted here as land-attached, tropical, carbonate platforms (FTCP) built by photozoan organisms (Figures 4.4 and 4.5; Read, 1985; Pomar, 2001; Schlager, 2003). The lower-amplitude parallel facies likely represent background shelf sedimentation around the carbonate platforms and therefore could be composed of mixed, fine-grained carbonate and siliciclastic sediments.

Australia's ongoing northward drift has caused the NCB to migrate into progressively warmer tropical latitudes. Plate tectonic reconstructions indicate that the NCB was at 24-28˚S in the late Miocene (~10 Ma) and at 22-26˚S in the Pliocene (~5 Ma) (Veevers et al., 1991; Lawver et al., 1999), so the NCB has long been within the latitude range for tropical photozoan carbonate production. However, the location of this eastern ocean boundary margin within the tropical zone is not sufficient for tropical carbonate growth; in fact, the modern NCB shelf lacks extensive photozoan production. Modern reef growth is limited to Barrow and Monte Bello Island and the Dampier Archipelago (Figure 4.1A; James et al., 2004). Therefore, in order for the FTCPs to be comprised of photozoan carbonates, a different environmental setting, more favorable to tropical carbonates production and deposition, must have existed when they formed.

Regional changes in ocean circulation may have been the key leading to formation of tropical FTCPs in the NCB during the Plio-Pleistocene. Upwelling of cold,

nutrient rich water, common on the east sides of major ocean basins, inhibits growth of photozoan faunal assemblages with high calcification rates, while simultaneously encouraging high rates of bioerosion by heterozoans (Mutti and Hallock, 2003). The net effect of upwelling deepwater currents is a diminished tropical carbonate factory. The modern warm, low salinity LC seasonally suppresses such upwelling that would otherwise constantly affect the NCB (Smith, 1992; James et al., 2004). Today, the seasonality of the modern LC periodically allows upwelling of cold and nutrient-rich water, likely minimizing modern photozoan carbonate production in the NCB.

The Leeuwin Current transports larvae of Pacific and Asian species to the NWS that contribute with reef development along the NWS (e.g. Ningaloo Reef, Scott Reef, and the Rowley Shoals; Collins, 2002). The Ningaloo Reef is fringing (land-attached) the Northwest Cape anticline. In contrast, the isolated Scott Reef platform is located on the distal portion of a carbonate ramp, rising from water depths in excess of 400 m. The Rowley Shoals, other isolated platforms, are located in the modern outer shelf to upper slope area with surrounding water depths of more than 200 m (Collins, 2002). These isolated platforms, which exhibit abundant coral reef growth, have been possibly influenced by increased subsidence rates since the collision between Australia and the Banda Arc started in the late Miocene. However, they have been able to keep up growing in the distal ramp area. This was not the case with the mapped FTCPs in the NCB, all of which terminated by SB-PL2 time (Figure 4.5).

An episode of weaker or absent LC during the latest Plio-Pleistocene has been interpreted as the main possible cause for a reduction in reef dimensions in the Cape Range area (Kendrick et al., 1991). It is possible that a relatively stronger LC favored growth of these tropical platforms in the NCB during the Pliocene-middle Pleistocene. As the current weakened in the mid-Pleistocene (Kendrick et al., 1991) these broad platforms

became extinct, although the seasonal LC supports minor photozoan carbonate growth to the Present.

4.6.2. Controls on Distribution of Post-siliciclastic Carbonate Platforms

4.6.2.1. Distribution of underlying siliciclastic lobes

Reconstructed vegetation patterns from onshore Australia indicate that, with the exception of the warm early Miocene, climate on the Australian continent has become progressively more arid since the Oligocene (White, 1998). Such an increase in aridity in the hinterland adjacent to the NCB was a probable cause of the general decrease in siliciclastic input to the middle-to-outer shelf since the Oligocene. Despite this long-term decrease, a spike of siliciclastic supply occurred during the middle to late Miocene. This resulted in progradation of deltas to the shelf-edge (Figure 4.6; Chapters 2 and 3). These deltas retreated during the Pliocene, possibly in response to decreased siliciclastic supply, allowing carbonate sedimentation to resume in the NCB shelf with development of the FTCPs (Figure 4.2).

The outlines of the platform margins for the four oldest platforms, FTCP1-FTCP4, appear to be spatially related to the distribution of underlying, mid- to late-Miocene delta lobes (Figure 4.6). This spatial relationship suggests that delta lobes produced subtle topographic highs that controlled the positions of the tropical carbonate systems (Figure 4.9). This relationship provides further evidence for the shallow–water origins of the platforms, since the delta topsets must have been deposited near sea level.

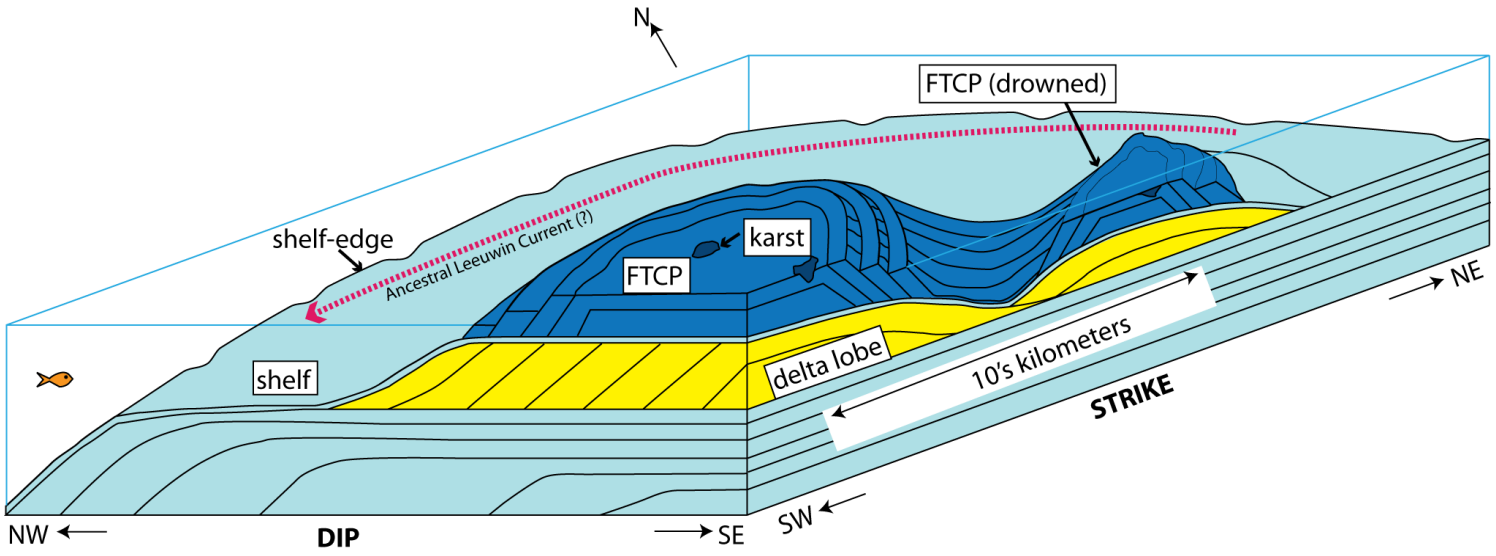

Figure 4.9. Diagram illustrating the development of subsequent FTCPs from NE to SW (along strike). These platforms initiated on top of bathymetric highs resulting from the underlying deltaic depocenters.

The interpreted FTCPs were not contemporaneous. The oldest platform, FTCP1, is located to the northeast, above the youngest siliciclastic lobe (lobe 27, in Figures 4.4, 4.5, and 4.6). Younger carbonate platforms migrated along strike to the southwest (Figures 4.5 and 4.6). I believe that these platforms initiated on remnant topographic highs created by underlying deltaic complexes, although a direct relationship is not always clear, e.g. FTCP 5 (Figure 4.6). Deltaic siliciclastics at the paleo-shelf edge have also served as the substrate for photozoan carbonate sedimentation offshore Belize (Choi and Ginsburg, 1990; Ferro et al. 1999) and on the southeast Florida platform (Cunningham et al., 2003).

4.6.2.2. Differential subsidence and along-strike migration of carbonate platforms

The observed along-strike migration of these platforms could be the result of differential subsidence induced by: 1) variations in the degree of compaction of underlying delta packages, or 2) spatial variations in tectonic subsidence that caused the northeastern portions of the NCB to subside faster than those to the southwest. Differential compaction can have several origins: 1) occurrence of different lithologies juxtaposed against one another; 2) variable underlying topography, created in this case by migrating deltaic lobe complexes (Figure 4.6); and/or 3) differential sediment loading (Collier, 1989; Schmoker and Gautier, 1989). The first occurrence of shallow-water, photozoan carbonate sedimentation is on top of the youngest delta lobe (27 in Figure 4.8), which was likely the least compacted lobe at this time and the highest bathymetrically. Initiation of carbonate platform development at the northeastern edge of the siliciclastic depocenter (Figures 4.5 and 4.6) was probably also favored by high-energy conditions

associated with onset of the southwestward-flowing LC. As this first platform (FTCP1) aggraded and prograded, the increasing sediment load on the substrate contributed to further compaction of underlying deltaic sediments (Figure 4.10A). After inferred exposure of the platform top during the interpreted forced regression, the ensuing transgression could have favored a switch to the next adjacent topographic high to the southwest (next older deltaic depocenter) for initiation of a new tropical carbonate platform (Figure 4.5).

Another possible cause for the southwestward migration of discrete carbonate platforms is differential subsidence induced by the collision between the Banda Arc and Australia (Figure 4.10B). The observed migration pattern would be possible if the northeast portion of the NCB was subsiding at a faster rate than the southwest area. This mechanism has been proposed to be responsible for differences in the degree of lagoon infill of the Rowley Shoals (also located on the NWS between 16-18° S; Collins, 2002). Cathro and Karner (2006) proposed that the ongoing compression has caused only localized uplift at the northwest end of the Rosemary-Legendre Structural Trend (Figure 4.1A); however, their results were obtained using one dip-oriented seismic transect and they did not model subsidence along strike. Incorporating another dip-oriented transect in the modeling could reveal along-strike differences in tectonic subsidence across the NCB related to the collision.

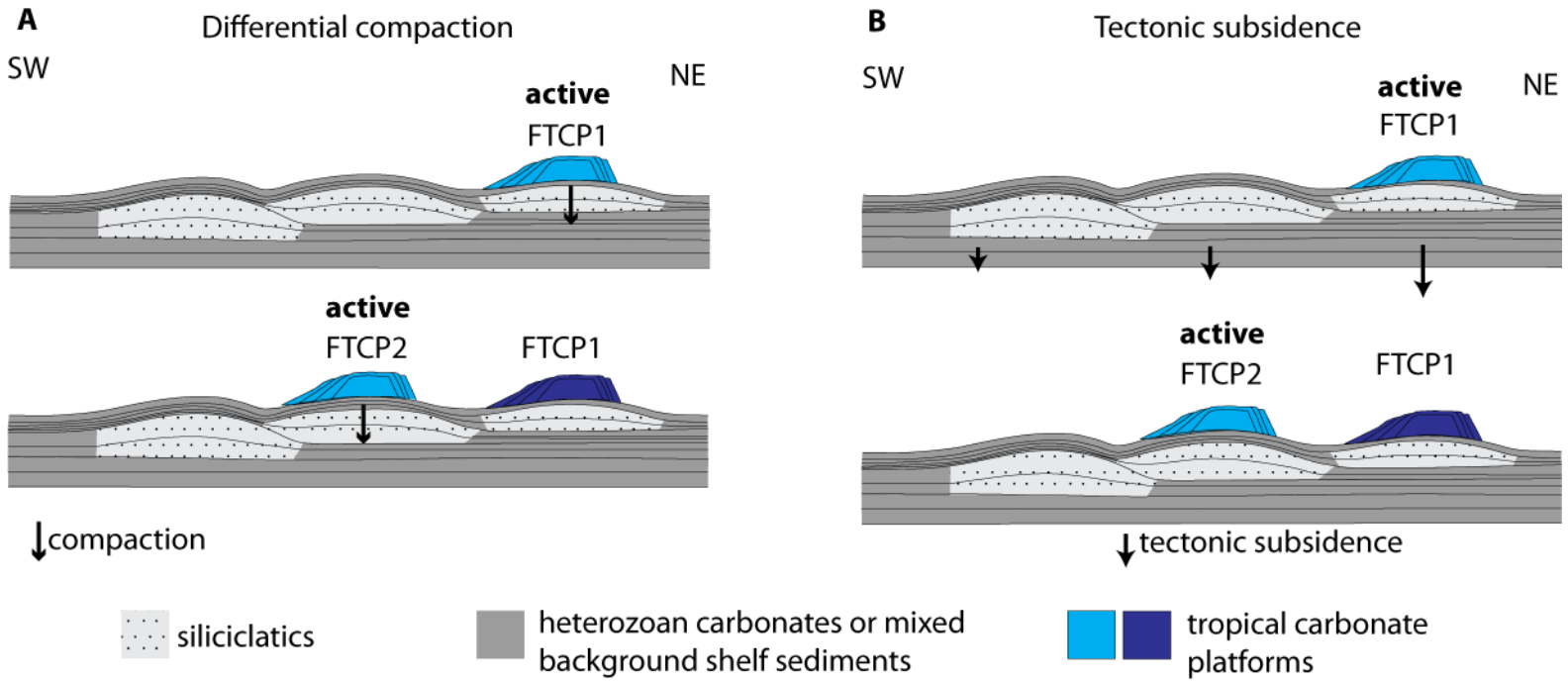

Figure 4.10: Diagram showing alternative hypotheses for along-strike migration of carbonate platforms: A) Differential subsidence along-strike induced by compaction of underlying siliciclastic lobes as a result of load by carbonate platforms; B) Differential subsidence along-strike caused by tectonic collision of Australia and the Banda Arc, similar to the Rowley Shoals area (Collins, 2002).

4.6.3. Processes Controlling Platform Architecture

4.6.3.1. Relative Sea Level

I propose that relative sea level fluctuations are at least in part responsible for the observed stratal patterns internal to these carbonate platforms. The pattern of ascending to descending rollover trajectories within platforms (Figure 4.5) suggests a transition from rising relative sea level to forced regression. For instance, FTCP3 exhibits ~40 m of aggradation and later a falling trajectory with a vertical component of ~44 m (Figure 4.5). Each FTCP seems to be formed by aggradation during relative sea level rise, followed by progradation during forced regression in the subsequent fall. The platforms may have been exposed during the fall that caused the forced regression pattern (falling platform margin trajectory, Figure 4.11), terminating platform growth. Each platform displays downlap terminations against a surface that overlies the previous FTCP, but platforms are not stacked vertically (Figure 4.5). I interpret these downlap surfaces as flooding surfaces. Each platform was initiated after a flooding event, although platform geometries record primarily progradation.

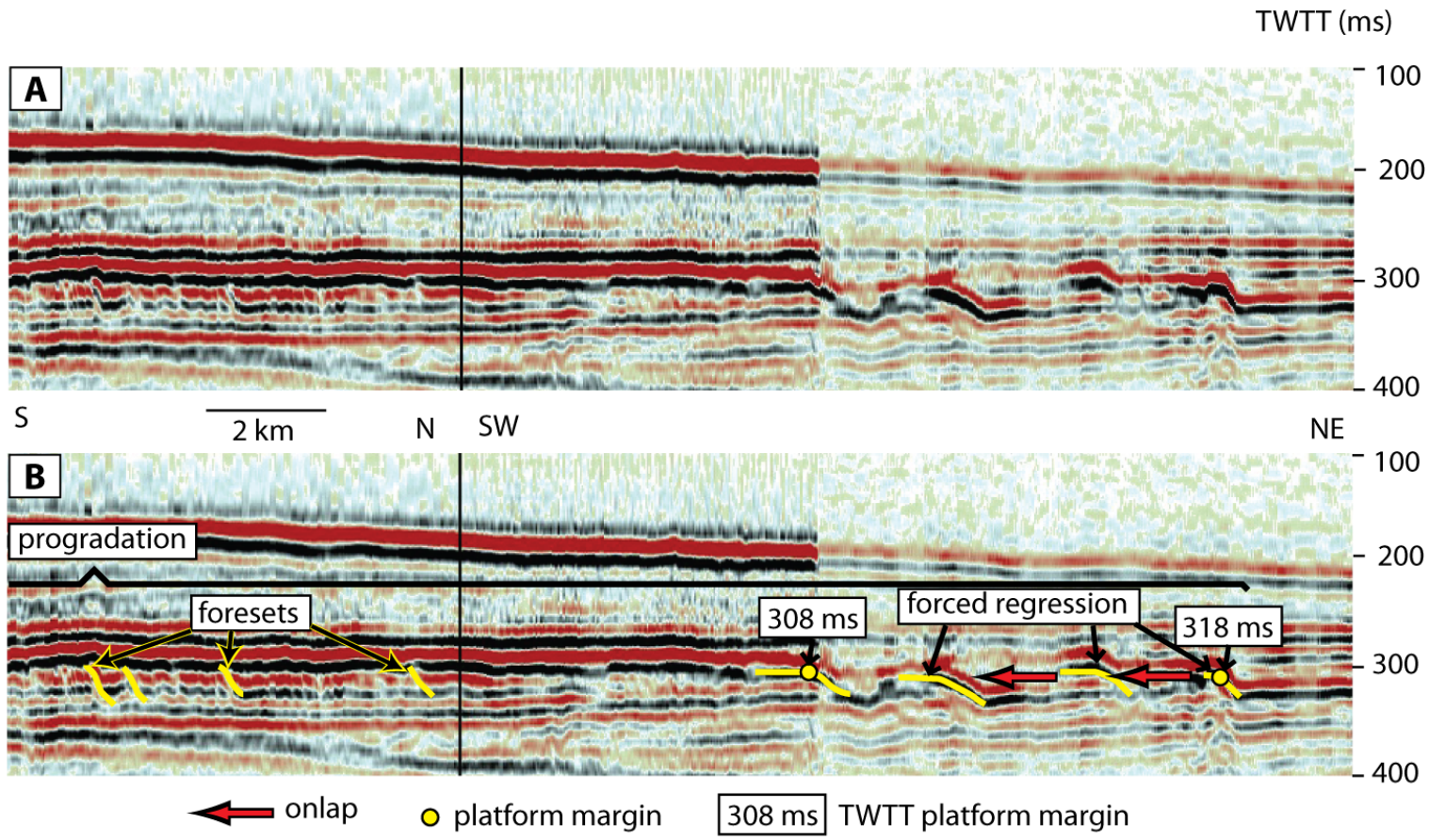

Figure 4.11. (A) Uninterpreted and (B) interpreted, seismic profile showing progradation of FTCP5 (Figure 4.6). Notice falling platform margin trajectory and onlap of subsequent platform tops onto previous slope.

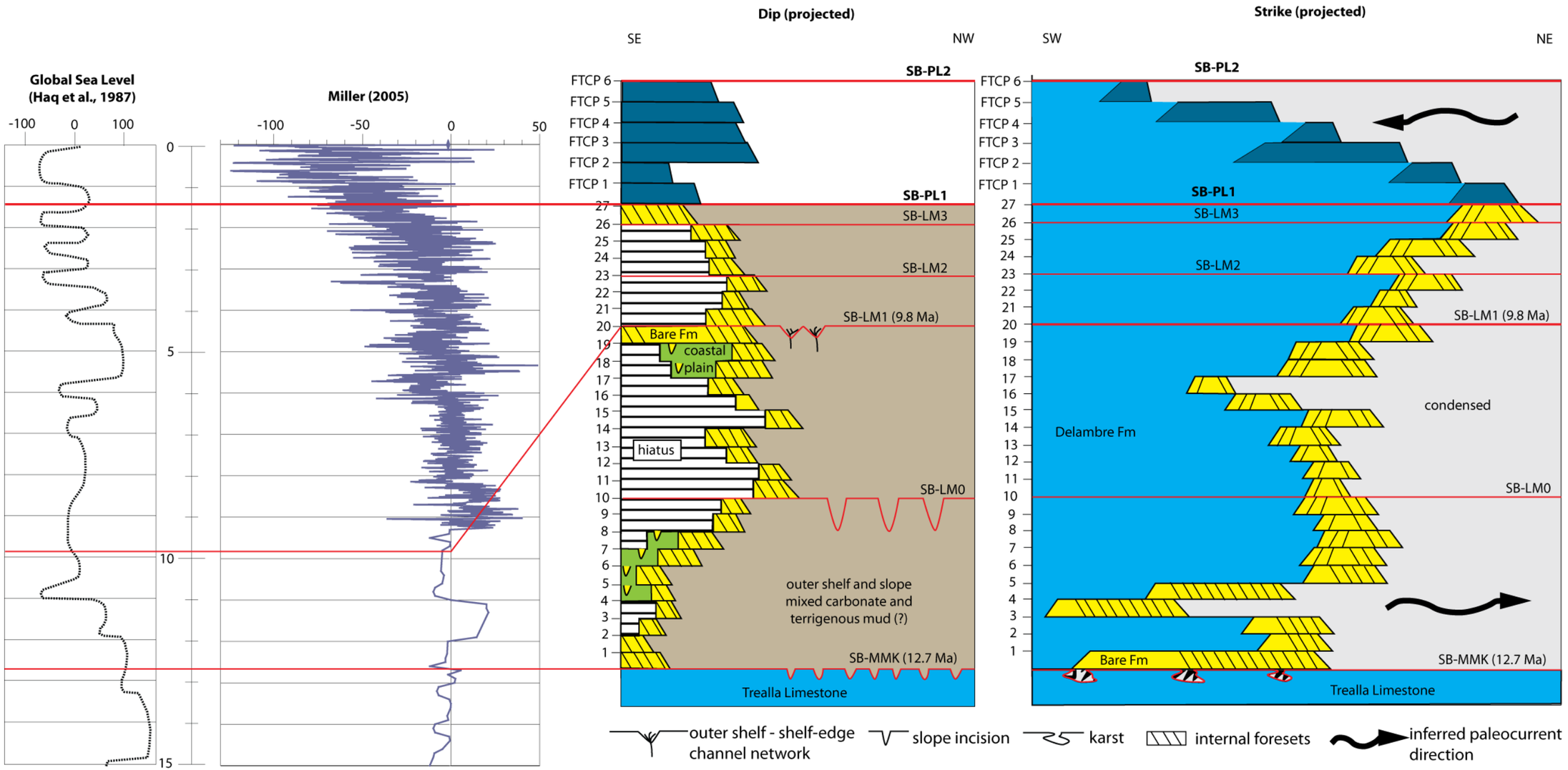

Figure 4.12. Miocene-Pleistocene stratigraphic chart for the NCB. Sequence boundaries SB-PL1 and SB-PL2 represent the base and top of the FTCPs. Age of these surfaces is ~3 Ma or younger. Potential errors in estimated ages are shown in Table 2.1. Notice the reversal of ocean currents from the time of deposition of the Bare Fm to the time carbonate platform development.

4.6.3.2. Current Direction and Clinoform Inclination

Generally, slope inclination on carbonate platform flanks is a result of differences in sediment fabric (Kenter, 1990). End members are grain-dominated, non-cohesive sediment, which result in maximum declivities of 40°, and muddy cohesive sediment, which produces slopes with maximum declivities of 5°. This suggests that the northeast-facing margins of the FTCPs in the NCB, with inclinations of ~30°, are comprised of carbonates with a greater proportion of coarse-grained components than those on the southwest-facing margins, where inclinations are ~7° (Figure 4.5, inset). The inferred lower mud content on the slopes facing northeast implies that they were deposited in a higher energy environment which winnowed mud and favored reef growth (Hine et al., 1981; Kenter, 1990). A strong LC coming flowing southwest could explain such winnowing during FTCP formation.

The asymmetry of clinoform inclinations between the northeastern and southwestern sides of the FTCPs (Figure 4.5, inset) may be a consequence of different energy regimes on the upcurrent versus downcurrent platform margins. If so, this asymmetry can be used to interpret paleocurrent direction during platform development. For example, Isern et al. (2004) have observed steeper inclinations on the upcurrent sides and more gentle slopes on the downcurrent sides of shallow-water carbonate platforms composing the Marion Plateau off northeastern Australia. In the NCB, therefore, the northeast-facing margins with higher-angle foresets (Figure 4.5, inset) probably represent the upcurrent sides and the southwest margins with lower-angle foresets the downcurrent sides. The distances prograded by the northeastern platform margins are also typically smaller than those prograded by the southwestern margins (Figures 4.3 and 4.5). I suggest

that this results from current reworking and redistribution of sediments from northeast to southwest.

The inference of higher energy on the northeastern platform margins, coupled with enhanced progradation toward the southwest (Figure 4.5), suggests dominant southwestard current flow when these platforms were developing (Figure 4.12). This implies a reversal in flow direction relative to that inferred to have acted during early progradation of the underlying siliciclastics (Chapter 2). The onset of such a southwest-flowing current in the late Pliocene-early Pleistocene could represent the start of one of the active episodes of the LC during the late Cenozoic proposed by McGowran et al. (1997), or as postulated by Gallagher et al. (2009), the inception of the modern Leeuwin Current at 1.6 Ma.

4.7. CONCLUSIONS

Five Pliocene, flat-topped, asymmetrically progradational deposits in the NCB are interpreted as flat-topped tropical carbonate platforms, based on seismic facies and because they developed on top of shelf-edge deltas that must have been deposited near ambient sea level. The main controls on the initiation of these platforms were most likely: 1) increasingly arid climate that led to a reduction of siliciclastic supply to the outer paleo-shelf during the Pliocene and 2) development of a southwestward-flowing, warm-water Leeuwin Current.

The carbonate platforms display smaller progradation distances and steeper foreset slopes to the northeast, and greater progradation coupled with more gentle slopes to the southwest. This asymmetry was likely caused by the ancestral LC, which created

higher-angle, upcurrent platform margins facing northeast, into the current, and lower-angle clinoforms on the downcurrent sides to the southwest.

Subtle topographic highs originally formed by deposition of deltaic lobes, gradually modified by differential compaction, served as the substrate for the carbonate platforms. The marked along-strike (northeast to southwest) long-term migration trend of the platforms could be the result of differential subsidence along strike of the NCB, with higher rates to northeast than to the southwest. This differential subsidence could be caused either by the ongoing collision of Australia and the Banda Arc or by differential compaction of underlying deltaic packages. Future work will be necessary to test these possible hypotheses, such work would include 1) along-strike subsidence modeling, either in 2D using transects or in 1D using exploration wells aligned along strike, and 2) modeling compaction of the substrate for the carbonate platforms and integrating its effect with subsidence.

Therefore, dynamic paleobathymetry, in conjunction with a strong LC, a carrier of tropical faunal assemblages and suppressor of oceanic upwelling, were the key factors contributing to FTCP development. These platforms constitute the evidence for widespread accumulation of photozoan carbonates in the NCB. Although age control is poor, I speculate that they formed during a Pliocene-mid Pleistocene period of strong LC flow. They became extinct after the mid-Pleistocene when the LC weakened or became more seasonal.

Chapter 5: Conclusions

The results presented in this dissertation illustrate the importance of variations in sediment supply and other regional factors, such as paleo-oceanography in controlling the preserved stratigraphy on a continental margin. These effects need to be considered when stratigraphic analysis is performed to understand the processes related to margin sedimentation and the spatial and temporal distribution of the sedimentary deposits. Specific conclusions have been presented in each chapter; in addition some general conclusions are summarized in this section.

The Northern Carnarvon Basin (NCB), dominated by carbonate shelf sedimentation in the Early Miocene, received a significant influx of siliciclastics in the late-middle Miocene during a time a long-term relative sea-level fall. A similar influx of siliciclastic sediment between 12-13 Ma has been documented in other margins (e.g. New Jersey Shelf, Maltese Islands, and the Canterbury Basin). Previous Miocene lowstands of relative sea level exposed the NCB carbonate shelf causing karstification, but did not result in accumulation of siliciclastics on the outer shelf and shelf margin. Therefore, an additional control, likely related to ongoing global climatic change during the middle Miocene played a key role in delivering siliciclastics to this area. Mapping of clinoform sets, which correlate with these mid-Miocene to Pliocene sandstones, reveals a deltaic system that prograded across the NCB shelf and reached its margin.

Rising shelf-edge trajectory (indicating increased shelf accommodation) encourages delta avulsion. On the other hand, flat-falling trajectory results in a much narrower belt of delta lobes as the system progrades towards the shelf margin. The point-source nature of delta systems results in significant spatial variations in sediment supply,

which affect along-strike margin progradation rates. In the NCB, margin progradation rate increases almost three times from where shelf-edge deltas were absent to where these deltas were concentrated. Shelf-edge trajectory, an alternative approach to classical sequence stratigraphic analysis, can also be significantly affected by spatial variations in sediment supply and the coexistence of different depositional systems along the vicinity of the shelf margin.

Slope gullies in the NCB served as conduits for sediment derived from shelf-edge deltas. This is reflected in temporal and spatial variations of the dimensions of these incisions. Mixed erosion-deposition within the infill in these incisions suggests that these gullies/canyons can also store a portion of the sediment delivered by the shelf-edge deltas.

Plio-Pleistocene, flat-topped, carbonate platforms may be the first occurrence of broad photozoan carbonate accumulation in the NCB. These tropical platforms developed after deltas retreated and likely initiated in response to the onset of a strong, ancestral (?), southwestward-flowing Leeuwin Current (LC) and while sea level was relatively low after deposition of the underlying deltas. The spatial distribution of these platforms seems to be strongly related to the underlying deltaic depocenters. In addition, these platforms show significant asymmetry in the along-strike direction suggesting possible current influence, also likely related to the activity of the LC.

References

Abreu, V.S., and Anderson, J.B., 1998, Glacial eustasy during the Cenozoic; sequence stratigraphic implications AAPG Bulletin, v. 82, p. 1385-1400.

Apthorpe, M., 1988, Cainozoic Depositional History of the North West Shelf in Purcell, P.G., and Purcell, R.R., eds., The North West Shelf Australia: Proceedings of Petroleum Exploration Society: Perth, p. 55-84.

Baillie, P.W., Powell, C.M., Li, Z.-X., and Ryall, A.M., 1994, The tectonic framework of Western Australia's Neoproterozoic to Recent sedimentary basins, Sedimentary Basins of Western Australia: Proceedings of Petroleum Exploration Society of Australia Symposium, Volume 1: Australia, Petroleum Exploration Society of Australia : Perth, West. Aust., Australia, p. 45-62.

Bartek, L.R., Vail, P.R., Anderson, J.B., Emmet, P.A., and Wu, S., 1991, Effect of Cenozoic ice sheet fluctuations in Antarctica on the stratigraphic signature of the Neogene: Journal of Geophysical Research, v. 96, p. 6753-6778.

Berggren, W.A., 1985, Cenozoic geochronology: Geological Society of America Bulletin, v. 96, p. 1407-1418.

Bhattacharya, J.P., 2006, Deltas, in Walker, H.W.P.a.R.G., ed., Facies models revisited, Volume 84: Special Publication: Tulsa, Oklahoma, SEPM, p. 237-292.

Bhattacharya, J.P., and Walker, R.G., 1992, Deltas, in Walker, R.G., and James, N.P., eds., Facies Models: Response to Sea Level Change, Geological Association of Canada, p. 157-177.

Blow, W.H., 1969, Late Middle Eocene to Recent planktonic foraminiferal biostratigraphy, in Brönnimann, P., and Renz, H.H., eds., First International Conference on Planktonic Microfossils: Proceedings, p. 199-421.

Bosscher, H., and Schlager, W., 1992, Computer simulation of reef growth: Sedimentology, v. 39, p. 503-512.

Bradshaw, M.T., Yeates, A.N., Beynon, R.M., Brakel, A.T., Langford, R.P., Totterdell, J.M., and Yeung, M., 1988, Paleogeographic Evolution of the North West Shelf Region, in Purcell, P.G., and Purcell, R.R., eds., The North West Shelf Australia: Proceedings North West Shelf Symposium Perth, p. 29-54.

Bullimore, S., Henriksen, S., Liestøl, F.M., and Helland-Hansen, W., 2005, Clinoform stacking patterns, shelf-edge trajectories and facies associations in Tertiary coastal deltas, offshore Norway: Implications for the prediction of lithology in prograding systems: Norwegian Journal of Geology, v. 85, p. 169-187.

Burgess, P.M., Steel, R.J., and Granjeon, D., 2008, Stratigraphic forward modeling of basin-margin clinoform systems; implications for controls on topset and shelf

width and timing of formation of shelf-edge deltas, in Hampson, G.J., Steel, R.J., Burgess, P.M., and Dalrymple, R.W., ed., Recent Advances in Models of Siliciclastic Shallow-Marine Stratigraphy, Volume 90: Special Publication, SEPM, p. 35-45.

Carvajal, C., 2009, Shelf-edge architecture and bypass of sand to deep water; influence of shelf-edge processes, sea level, and sediment supply, in Steel, R., ed., Journal of Sedimentary Research, Volume 79: United States, Society for Sedimentary Geology : Tulsa, OK, United States, p. 652-672.

Cathro, D.L., 2002, Three Dimensional Stratal Development of a Carbonate-Siliciclastic Sedimentary Regime, Northern Carnarvon Basin, Northwest Australia [Dissertation thesis]: Austin, Texas, The University of Texas at Austin.

Cathro, D.L., and Austin, J.A., Jr., 2001, An early mid-Miocene, strike parallel shelfal trough and possible karstification in the Northern Carnarvon Basin, northwest Australia: Marine Geology, v. 178, p. 157-169.

Cathro, D.L., Austin, J.A., Jr., and Moss, G.D., 2003, Progradation along a deeply submerged Oligocene-Miocene heterozoan carbonate shelf; how sensitive are clinoforms to sea level variations?: AAPG Bulletin, v. 87, p. 1547-1574.

Cathro, D.L., and Karner, G., 2006, Cretaceous–Tertiary inversion history of the Dampier Sub-basin, northwest Australia: Insights from quantitative basin modelling: Marine and Petroleum Geology, v. 23, p. 503–526.

Choi, D.R., and Ginsburg, R.N., 1990, Siliciclastic foundations of Quaternary reefs in the southernmost Belize Lagoon, British Honduras: Geological Society of America Bulletin, v. 93, p. 116-126.

Church, K.D., and Gawthorpe, R.L., 1997, Sediment supply as a control on the variability of sequences: an example from the late Namurian of northern England: Journal of the Geological Society, v. 154, p. 55-60.

Clift, P.D., 2010, Enhanced global continental erosion and exhumation driven by Oligo-Miocene climate change: Geophysical Research Letters, v. 37, p. L09402.

Coleman, J.M., and Gagliano, S.M., 1964, Cyclic sedimentation in the Mississippi River deltaic plain: Transactions - Gulf Coast Association of Geological Societies, v. 14, p. 67-80.

Coleman, J.M., and Roberts, H.H., 1991, The Mississippi River Depositional System: a model for the Gulf Coast Tertiary, in Goldthwaite, D., ed., An introduction to central Gulf Coast geology: New Orleans, New Orleans Geological Society, p. 99-121.

Collier, R.E.L., 1989, Modelling the role of differential compaction and tectonics upon Westphalian facies architecture in the Northumberland Basin: Occasional Publication Yorkshire Geological Society, v. 6, p. 189-199.

Collins, L.B., 2002, Tertiary foundations and Quaternary evolution of coral reef systems of Australia's North West Shelf, in Keep, M., and Moss, S.J., eds., The sedimentary basins of Western Australia 3: Perth, Western Australia, Proceedings of West Australian Basins Symposium, p. 129-152.

Cresswell, G.R., 1991, The Leeuwin Current - observations and recent models: Journal of the Royal Society of Western Australia, v. 74, p. 1-14.

Cunningham, K.J., Locker, S.D., Hine, A.C., Bukry, D., Barron, J.A., and Guertin, L.A., 2003, Interplay of Late Cenozoic siliciclastic supply and carbonate response on the southeast Florida Platform: Journal of Sedimentary Research, v. 73, p. 31-46.

Dix, G.R., James, N.P., Kyser, T.K., Bone, Y., and Collins, L.B., 2005, Genesis and Dispersal of Carbonate Mud Relative to Late Quaternary Sea-Level Change Along a Distally-Steepened Carbonate Ramp (Northwestern Shelf, Western Australia): Journal of Sedimentary Research, v. 75, p. 665-678.

Driscoll, N.W., and Karner, G.D., 1998, Lower crustal extension across the Northern Carnarvon basin, Australia: Evidence for an eastward dipping detachment: Journal of Geophysical Research, v. 103, p. 4975-4992.

Eberli, G.P., and Ginsburg, R.N., 1987, Segmentation and coalescence of Cenozoic carbonate platforms, northwestern Great Bahama Bank: Geology, v. 15, p. 75-79.

Farre, J.A., McGregor, B.A., Ryan, W.B.F., and Robb, J.M., 1983, Breaching the shelf break; passage from youthful to mature phase in submarine canyon evolution, in Stanley, D.J., and Moore, G.T., eds., The shelfbreak; critical interface on continental margins, Volume 33: Special Publication: Tulsa, Oklahoma, SEPM, p. 25-39.

Feary, D.A., and James, N.P., 1998, Seismic stratigraphy and geological evolution of the Cenozoic, cool-water Eucla Platform, Great Australian Bight: AAPG Bulletin, v. 82, p. 792-816.

Fedele, J.J., and Garcia, M.H., 2009, Laboratory experiments on the formation of subaqueous depositional gullies by turbidity currents: Marine Geology, v. 258, p. 48-59.

Ferro, C.E., 1999, Late Quaternary shift of mixed siliciclastic-carbonate environments induced by glacial eustatic sea-level fluctuations in Belize, in Droxler, A.W., Anderson, J.B., and Mucciarone, D., eds., Special Publication - Society for Sedimentary Geology, Volume 63: United States, Society for Sedimentary Geology (SEPM) : Tulsa, OK, United States, p. 385-411.

Fulthorpe, C.S., Austin, J.A., Jr., and Mountain, G.S., 2000, Morphology and distribution of Miocene slope incisions off New Jersey: Are they diagnostic of sequence boundaries?: Geological Society of America Bulletin, v. 112, p. 817-828.

Fulthorpe, C.S., and J.A. Austin, J., 2008, Assessing the significance of along-strike variations ofmiddle to lateMiocene prograding clinoformal sequence geometries beneath the New Jersey continental shelf: Basin Research, v. 20, p. 269-283.

Gallagher, S.J., Wallace, M.W., Li, C.L., Kinna, B., Bye, J.T., Akimoto, K., and Torii, M., 2009, Neogene history of the West Pacific Warm Pool, Kuroshio and Leeuwin currents: Paleoceanography, v. 24, p. PA1206.

Gardner, M.H., and Borer, J.M., 2000, Submarine channel architecture along a slope to basin profile, Brushy Canyon Formation, West Texas: AAPG Memoir, v. 72, p. 195-213.

Gingele, F.X., De Deckker, P., and Hillenbrand, C.-D., 2001, Clay mineral distribution in surface sediments between Indonesia and NW Australia; source and transport by ocean currents: Marine Geology, v. 179, p. 135-146.

Godfrey, J.S., and Golding, T.J., 1981, The Sverdrup Relation in the Indian Ocean, and the Effect of Pacific-Indian Ocean Throughflow on Indian Ocean Circulation and on the East Australian Current: Journal of Physical Oceanography, v. 11, p. 771-779.

Hadler-Jacobsen, F., Gardner, M.H., and Borer, J.M., 2007, Seismic stratigraphic and geomorphic analysis of deep-marine deposition along the West African continental margin: Geological Society Special Publications, v. 277, p. 47-84.

Hamilton, L.J., 1997, Methods to obtain representative surface wave spectra, illustrated for two ports of north-western Australia: Marine Freshwater Research, v. 48, p. 43-57.

Haq, B.U., Hardenbol, J., and Vail, P.R., 1987, Chronology of fluctuating sea levels since the Triassic: Science, v. 235, p. 1156-1167.

Heath, R.S., and Apthorpe, M.C., 1984, New formation names for the Late Cretaceous and Tertiary sequence of the southern North West Shelf, West. Australia Geol. Survey Record 1984/7.

Helland-Hansen, W., and Gjelberg, J.G., 1994, Conceptual basis and variability in sequence stratigraphy; a different perspective: Sedimentary Geology, v. 92, p. 31-52.

Helland-Hansen, W., Hampson, G.J., and Anonymous, 2009, Trajectory analysis; concepts and applications: Basin Research, v. 21, p. 454-483.

Helland-Hansen, W., and Martinsen, O.J., 1996, Shoreline trajectories and sequences; description of variable depositional-dip scenarios: Journal of Sedimentary Research, v. 66, p. 670-688.

Henriksen, S., Hampson, G.J., Helland-Hansen, W., Johannessen, E.P., and Steel, R.J., 2009, Shelf edge and shoreline trajectories, a dynamic approach to stratigraphic analysis: Basin Research, v. 21, p. 445-453.

Hine, A.C., Wilber, R.J., and Neumann, A.C., 1981, Carbonate sand bodies along contrasting shallow bank margins facing open seaways in northern Bahamas: AAPG Bulletin, v. 65, p. 261-290.

Hocking, R.M., Moors, H.T., and Van de Graaff, W.J.E., 1987, Geology of the Carnarvon Basin, Western Australia, 288 p.

Holloway, P.E., 1995, Leeuwin Current observations on the Australian North West Shelf, May-June 1993: Deep-Sea Research I, v. 42, p. 285-305.

Holloway, P.E., and Nye, H.C., 1985, Leeuwin Current and Wind Distributions on the Southern Part of the Australian North West Shelf between January 1982 and July 1983: Australian Journal of Marine and Freshwater Research, v. 36, p. 123-137.

Hull, J.N.F., and Griffiths, C.M., 2002, Sequence stratigraphic evolution of the Albian to Recent section of the Dampier Sub-basin, North West Shelf, Australia, in Keep, M., and Moss, S.J., eds., Sedimentary Basins of Western Australia 3: Proceedings of Petroleum Exploration Society of Austrialia Symposium, Volume 3: Perth, Australia, Petroleum Exploration Society of Australia p. 617-639.

Isern, A.R., Anselmetti, F.S., and Blum, P., 2004, A neogene carbonate platform, slope, and shelf edifice shaped by sea level and ocean currents, Marion Plateau (Northeast Australia), in Eberli, G.P., Masaferro, J.L., and Sarg, J.F., eds., Seismic imaging of carbonate reservoirs and systems: AAPG Memoir 81, p. 291-307.

James, N.P., 1997, The cool-water carbonate depositional realm: Special Publication - Society for Sedimentary Geology, v. 56, p. 1-20.

James, N.P., Bone, Y., Borch, C.C.V.D., and Gostini, V.A., 1992, Modern Carbonate and Terrigenous Clastic Sediments on a Cool Water, high energy, mid-latitude Shelf: Lacepede, southern Australia.: Sedimentology, v. 39, p. 877-903.

James, N.P., Bone, Y., Kyser, T.K., Dix, G.R., and Collins, L.B., 2004, The importance of changing oceanography in controlling late Quaternary carbonate sedimentation on a high-energy, tropical, oceanic ramp; north-western Australia: Sedimentology, v. 51, p. 1179-1205.

Johannessen, E.P., and Steel, R.J., 2005, Shelf-margin clinoforms and prediction of deepwater sands: Basin Research, v. 17, p. 521-550.

Kaiko, A.R., and Tait, A.M., 2001, Post-rift tectonic subsidence and palaeo-water depths in the northern Carnarvon Basin, Western Australia: APPEA Journal, v. 41, p. 367-379.

Kendall, C.G.S.C., and Schlager, W., 1981, Carbonates and relative changes in sea level: Marine Geology, v. 44, p. 181-212.

Kendrick, G.W., Wyrwoll, K.-H., and Szabo, B.J., 1991, Pliocene-Pleistocene coastal events and history along the western margin of Australia: Quaternary Science Reviews, v. 10, p. 419-439.

Kenter, J.A.M., 1990, Carbonate platform flanks; slope angle and sediment fabric: Sedimentology, v. 37, p. 777-794.

Lawver, L.A., Coffin, M.F., Dalziel, I.W.D., Gahagan, L.M., and Schmitz, R.M., 1999, The Plates 1999 atlas of paleogeographic reconstructions (Plates Progress Report No. 235), University of Texas Institute for Geophysics Technical Report No. 187, p. 84.

Leckie, D.A., 2001, Climatic controls on non-marine sedimentation – maximum aggradation during lowstand, incision during transgression and highstand, AAPG Annual Meeting 2001: Denver, USA, p. 114.

Lee, T.-Y., and Lawver, L.A., 1995, Cenozoic plate reconstruction of Southeast Asia: Tectonophysics, v. 251, p. 85-138.

Lisiecki, L.E., and Raymo, M.E., 2005, A Pliocene-Pleistocene stack of 57 globally distributed benthic δ18O records: Paleoceanography, v. 20, p. PA1003.

—, 2007, Plio-Pleistocene climate evolution; trends and transitions in glacial cycle dynamics: Quaternary Science Reviews, v. 26, p. 56-69.

Lu, H., and Fulthorpe, C.S., 2004, Controls on sequence stratigraphy of a middle-Miocene to Recent, current-swept, passive margin: offshore Canterbury Basin, New Zealand: Geological Society of America Bulletin, v. 116, p. 1345-1366.

Martinez, J.I., De Deckker, P., and Barrows, T.T., 1999, Palaeoceanography of the last glacial maximum in the eastern Indian Ocean; planktonic foraminiferal evidence: Palaeogeography, Palaeoclimatology, Palaeoecology, v. 147, p. 73-99.

Martinsen, O.J., and Helland-Hansen, W., 1995, Strike variability of clastic depositional systems: Does it matter for sequence-stratigraphic analysis?: Geology, v. 23, p. 439-442.

McGowran, B., Li, Q., Cann, J., Padley, D., McKirdy, D.M., and Shafik, S., 1997, Biogeographic impact of the Leeuwin Current in southern Australia since the late middle Eocene: Palaeogeography, Palaeoclimatology, Palaeoecology, v. 136, p. 19-40.

McMurray, L.S., and Gawthorpe, R.L., 2000, Along-strike variability of forced regressive deposits; late Quaternary, northern Peloponnesos, Greece: Geological Society Special Publications, v. 172, p. 363-377.

Meissner, F.F., 1972, Cyclic Sedimentation in Middle Permian Strata of the Permian Basin, West Texas and New Mexico, in Soc., W.T.G., ed., Cyclic sedimentation in the Permian Basin, ed. 2: Midland, United States, West Texas Geological Society, p. 203-232.

Miller, K.G., Wright, J.D., and Fairbanks, R.G., 1991, Unlocking the ice house; Oligocene-Miocene oxygen isotopes, eustasy, and margin erosion: Journal of Geophysical Research, v. 96, p. 6829-6848.

Molnar, P., 2001, Climate change, flooding in arid environments, and erosion rates: Geology, v. 29, p. 1071-1074.

—, 2004, Late Cenozoic increase in accumulation rates of terrestrial sediment; how might climate change have affected erosion rates?: Annual Review of Earth and Planetary Sciences, v. 32, p. 67-89.

Monteverde, D.H., Mountainn, G.S., and Miller, K.G., 2008, Early Miocene sequence development across the New Jerseymargin: Basin Research, v. 20, p. 249-267.

Moss, G.D., Cathro, D.L., and Austin, J.A., Jr., 2004, Sequence biostratigraphy of prograding clinoforms, Northern Carnarvon Basin, Western Australia: A proxy for variations in Oligocene to Pliocene global sea level?: Palaios, v. 19, p. 206-226.

Mutti, M., and Hallock, P., 2003, Carbonate systems along nutrient and temperature gradients; some sedimentological and geochemical constraints: Geologische Rundschau = International Journal of Earth Sciences (1999), v. 92, p. 465-475.

Olariu, C., and Bhattacharya, J.P., 2006, Terminal Distributary Channels and Delta Front Architecture of River-Dominated Delta Systems: Journal of Sedimentary Research, v. 76, p. 212-233.

Olariu, C., and Steel, R.J., 2009, Influence of point-source sediment-supply on modern shelf-slope morphology; implications for interpretation of ancient shelf margins: Basin Research, v. 21, p. 484-501.

Partyka, G., 1999, Interpretational applications of spectral decomposition in reservoir characterization, in Gridley, J., and Lopez, J., eds., Leading Edge [Tulsa, OK], Volume 18: United States, Society of Exploration Geophysicists : Tulsa, OK, United States, p. 353.

Pinous, O.V., Levchuk, M.A., and Sahagian, D.L., 2001, Regional Synthesis of the Productive Neocomian Complex of West Siberia: Sequence Stratigraphic Framework: AAPG Bulletin, v. 85, p. 1713-1730.

Piper, D.J.W., and Kontopoulos, N.A., C.; Chronis, G.; Panagos, A. G. , 1990, Modern fan deltas in the western Gulf of Corinth, Greece Geo-Marine Letters v. 10, p. 5-12.

Pomar, L., 2001, Types of carbonate platforms: a genetic approach: Basin Research, v. 13, p. 313-334.

Porebski, S.J., and Steel, R.J., 2003, Shelf-margin deltas; their stratigraphic significance and relation to deepwater sands: Earth-Science Reviews, v. 62, p. 283-326.

Pratson, L.F., Nittrouer, C.A., Wiberg, P.L., Steckler, M.S., Swenson, J.B., Cacchione, D.A., Karson, J.A., Murray, A.B., Wolinsky, M.A., Gerber, T.P., Mullenbach, B.L., Spinelli, G.A., Fulthorpe, C.S., O'Grady, D.B., Parker, G., Driscoll, N.W., Burger, R.L., Paola, C., Orange, D.L., Field, M.E., Friedrichs, C.T., and Fedele, J.J., 2007, Seascape evolution on clastic continental shelves and slopes: Special Publication of the International Association of Sedimentologists, v. 37, p. 339-380.

Pratson, L.F., Ryan, W.B.F., Mountain, G.S., and Twichell, D.C., 1994, Submarine canyon initiation by downslope-eroding sediment flows: Evidence in late Cenozoic strata on the New Jersey continental slope: Geological Society of America Bulletin, v. 106, p. 395-412.

Pryer, L.L., Romine, K.K., Loutit, T.S., and Barnes, R.G., 2002, Carnarvon Basin architecture and structure defined by the integration of mineral and petroleum exploration tools and techniques, APPEA Journal 42, Volume 42: Australia, Australian Petroleum Production and Exploration Association : Canberra, Australia, p. 287-309.

Read, J.F., 1985, Carbonate Platform Facies Models: The American Association of Petroleum Geologists Bulletin, v. 69, p. 1-21.

Reynolds, S., and Gorsline, D.S., 1988, Some enigmatic depressions of the Arguello Slope, California Geo-Marine Letters v. 8, p. 167-172.

Rich, J.L., 1951, THREE CRITICAL ENVIRONMENTS OF DEPOSITION, AND CRITERIA FOR RECOGNITION OF ROCKS DEPOSITED IN EACH OF THEM: Geological Society of America Bulletin, v. 62, p. 1-20.

Romine, K.K., Durrant, J.M., Cathro, D.L., and Bernardel, G., 1997, Petroleum Play Element Prediction for the Cretaceous-Tertiary Basin Phase, Norhtern Carnarvon Basin: Australian Petroleum Production and Exploration Association Limited (APPEA) Journal, v. 37, p. 315-339.

Ryan, M.C., Helland-Hansen, W., Johannessen, E.P., and Steel, R.J., 2009, Erosional vs. accretionary shelf margins; the influence of margin type on deepwater sedimentation; an example from the Porcupine Basin, offshore western Ireland: Basin Research, v. 21, p. 676-703.

Saller, A.H., Noah, J.T., Ruzuar, A.P., and Schneider, R., 2004, Linked lowstand delta to basin-floor fan deposition, offshore Indonesia: An analog for deep-water reservoir systems: AAPG Bulletin, v. 88, p. 21-46.

Schlager, W., 1991, Depositional Bias and Environmental-Change Important Factors in Sequence Stratigraphy: Sedimentary Geology, v. 70, p. 109-130.

—, 2003, Benthic carbonate factories of the Phanerozoic: Geologische Rundschau = International Journal of Earth Sciences (1999), v. 92, p. 445-464.

—, 2005, Carbonate Sedimentology and Sequence Stratigraphy, 200 p.

Schmoker, J.W., and Gautier, D.L., 1989, Compaction of basin sediments; modeling based on time-temperature history: Journal of Geophysical Research, v. 94, p. 7379-7386.

Semeniuk, V., 1996, Coastal forms and Quaternary processes along the arid Pilbara coast of northwestern Australia: Palaeogeography, Palaeoclimatology, Palaeoecology, v. 123, p. 49-84.

Seranne, M., 1999, Early Oligocene stratigraphic turnover on the West Africa continental margin: a signature of the Tertiary greenhouse-to-icehouse conditions: Terra Nova, v. 11, p. 135-140.

Sestini, G., 1989, Nile Delta; a review of depositional environments and geological history: Geological Society Special Publications, v. 41, p. 99-127.

Shackleton, N.J., and Kennett, J.P., 1975, Paleotemperature history of the Cenozoic and the initiation of Antarctic glaciation; oxygen and carbon isotope analyses in DSDP sites 277, 279, and 281: Initial Reports of the Deep Sea Drilling Project, v. 29, p. 743-755.

Shafik, S., 1990, The Maastrichtian and early Tertiary record of the Great Australian Bight basin and its onshore equivalents on the Australian southern margin; a nannofossil study: BMR Journal of Australian Geology and Geophysics, v. 11, p. 473-497.

Sheriff, R.E., 1985, Aspects of Seismic Resolution: Chapter 1, in Berg, O.R., and Woolverton, D.G., eds., M 39: Seismic Stratigraphy II: An Integrated Approach to Hydrocarbon Exploration, AAPG.

Smith, R.L., Huyer, A., Godfrey, J.S., and Church, J.A., 1991, The Leeuwin Current off Western Australia, 1986-1987: American Meteorological Society, p. 323-345.

Southard, J.B., and Stanley, D.J., 1976, Shelf-break processes and sedimentation: New York, N.Y., John Wiley & Sons, 351-377 p.

Spinelli, G.A., and Field, M.E., 2001, Evolution of Continental Slope Gullies on the Northern California Margin: Journal of Sedimentary Research, v. 71, p. 237-245.

Stagg, H.M.J., and Colwell, J.B., 1994, The Structural Foundations of the Northern Carnarvon Basin, in Purcell, P.G., and Purcell, R.R., eds., The sedimentary basins of Western Australia: Proceedings of Petroleum Exploration Society of Australia Symposium: Perth, p. 349-365.

Steel, R.J., Carvajal, C., Petter, A., and Uroza, C., 2008, Shelf and shelf-margin growth in scenarios of rising and falling sea level in Hampson, G.J., Steel, R.J., Burgess, P.M., and Dalrymple, R.W., eds., Recent advances in models of siliciclastic shallow-marine stratigraphy: SEPM Special Publication 90, p. 47-72.

Steel, R.J., Crabaugh, J., Schellpeper, M., Mellere, D., Plink-Bjorklund, P., Deibert, J., and Loeseth, T., 2000, Deltas vs. rivers on the shelf edge; their relative contributions to the growth of shelf-margins and basin-floor fans (Barremian and Eocene, Spitsbergen): Program and Abstracts - Society of Economic Paleontologists. Gulf Coast Section. Research Conference, v. 20, p. 981-1009.

Steel, R.J., and Olsen, T., 2002, Clinoforms, Clinoform Trajectories and Deepwater Sands, in Armentrout, J.M., and Rosen, N.C., eds., Sequence stratigraphic models for exploration and production: Evolving methodology, emerging models and application histories (CD-ROM): 22nd Annual Gulf Coast Section SEPM Foundation Bob Perkins Research Conference, p. 367-380.

Suter, J.R., and Berryhill, H.L., 1985, Late Quaternary shelf-margin deltas, Northwest Gulf of Mexico: AAPG Bulletin, v. 69, p. 77-91.

Sydow, J., Roberts, H.H., Bouma, A.H., and Winn, R., 1992, Constructional subcomponents of a shelf-edge delta, Northeast Gulf of Mexico: Transactions - Gulf Coast Association of Geological Societies, v. 42, p. 717-726.

Tomczak, M., and Godfrey, T.S., 1994, Regional oceanography; an introduction: United Kingdom, Pergamon, United Kingdom.

Vail, P.R., 1987, Seismic stratigraphy interpretation using sequence stratigraphy, part 1: seismic stratigraphy interpretation procedure, in Bally, A.W., ed., Atlas of Seismic Stratigraphy, Volume 1: American Association of Petroleum Geologists Studies in Geology No. 27, p. 1-10.

Vail, P.R., Audemard, F., Bowman, S.A., Eisner, P.N., and Perez-Cruz, C, 1991, The Stratigraphic Signatures of Tectonics, Eustasy and Sedimentology - an Overview, in Einsele, G., Ricken, W., and Seilacher, A., ed., Cycles and Events in Stratigraphy, p. 617-659.

Vail, P.R., Mitchum, R.M., and Thompson, S., 1977, Seismic Stratigraphy and Global Changes of Sea Level, Part 4: Global Cycles of Relative Changes of Sea Level, in Payton, C.E., ed., Seismic Stratigraphy-Applications to Hydrocarbon Exploration, Volume American Association of Petroleum Geologists Memoir 26, p. 49-212.

Van Wagoner, J.C., Posamentier, H.W., Mitchum, R.M., Vail, P.R., Sarg, J.F., Loutit, T.S., and Hardenbol, J., 1988, An overview of the fundamentals of sequence stratigraphy and key definitions: SEPM Special Publication, v. 42, p. 39-45.

Veevers, J., Powell, C.M., and Roots, S.R., 1991, Review of seafloor spreading around Australia: Australian Journal of Earth Sciences, v. 38, p. 373-389.

Wallace, M.W., Condilis, E., Powell, A., Redfearn, J., Auld, K., Wiltshire, M., Holdgate, G., and Gallagher, S., 2003, Geological Controls on Sonic Velocity in the Cenozoic Carbonates of the Northern Carnarvon Basin, Northwest Shelf, Western Australia: APPEA Journal, v. 43, p. 385-399.

Watts, A.B., and Ryan, W.B.F., 1976, Flexure of the lithosphere and continental margin basins: Tectonophysics, v. 36, p. 25-44.

Webster, M.A., and Petkovic, P., 2005, Australian Bathymetry and Topography Grid, Record 2005/12.

White, M.E., 1999, Reading the rocks: East Roseville, N.S.W., Kangaroo Press.

Zachos, J., Pagani, M., Sloan, L., Thomas, E., and Billups, K., 2001, Trends, Rhythms, and Aberrations in Global Climate 65 Ma to Present: Science, v. 292, p. 686.

Vita

Carla Maria Sanchez was born in Venezuela, as the daughter of Morelia and Carlos Sanchez. She attended school at Colegio Agustiniano Cristo Rey in Caracas. She enrolled in Universidad Simon Bolivar in 1995, where she obtained a B.E. degree in Geophysics. In 2001, Carla joined PDVSA as an Exploration Geophysicist. Later, in 2004, she enrolled at The University of Texas at Austin to pursue a M.Sc. degree in Geological Sciences. During her time as a Master student, she conducted research on quantitative seismic geomorphology of fluvio-deltaic systems from offshore Louisiana and was appointed as a Teaching Assistant for the Department of Geological Sciences and later as a Graduate Research Assistant for the Bureau of Economic Geology. Carla worked as a Geophysics Intern with Marathon Oil Company for the Sub-Saharan Exploration Team in 2006. She obtained her M.Sc. degree in 2006 and continued her graduate education at UT Austin as a Ph.D. Aspirant conducting research on the three-dimensional architecture of a mixed carbonate-siliciclastic margin from Northwest Australia. During her Ph.D., Carla worked as a Graduate Research Assistant for the UT Institute for Geophysics and as a Teaching Assistant for the Department of Geological Sciences. She also worked as Geoscience Intern for ConocoPhillips for the Subsurface Technology Group in 2008.

Permanent email: carlasphelps@gmail.com

This dissertation was typed by Carla Maria Sanchez.